Study of Jet Fires Geometry and Radiative Features

Adriana Palacios Rosas

A dissertation submitted in partial fulfilment of the requirements for the degree of Doctor of Philosophy in Chemical Engineering

Thesis supervisor:
Dr. Joaquim Casal Fàbrega

Centre for Technological Risk Studies
Department of Chemical Engineering
Universitat Politècnica de Catalunya

Barcelona, January 2011

To Derek

ACKNOWLEDGEMENTS

Over the duration of my Ph.D studies I have had the opportunity to tap into the knowledge and experience of a great number of persons who all contributed to this dissertation and my professional development in one way or another. Now is the time to thank each of them.

First and foremost I offer my sincerest gratitude to my supervisor Joaquim Casal, who has supported me throughout my thesis with his patience and knowledge whilst allowing me the room to work in my own way. His encouragement and effort make this thesis possible to be completed. He has also been invaluable on both an academic and a personal level, for which I am extremely grateful.

I gratefully acknowledge the funding sources that made my Ph.D work possible. I was funded by the Agència de Gestio d'Ajuts Universitaris i de Recerca of the Autonomous Government of Catalonia during the four years and I was honored to be a Roberto Rocca Fellow for my first year. My work was also supported by the Spanish Ministerio de Educación y Ciencia (projects No. CTQ2005-06231 and CTQ2008-02923) for which I wish to extend my gratitude.

Furthermore, my gratitude goes to Miguel Muñoz who considerably contributed to the completion of this dissertation. Thank you so much for sharing your knowledge with me.

I would also like to express my deep respect and appreciation to Derek Bradley not only for accepting me during my pleasant and fruitful stay at the University of Leeds but also for his excellent guidance and support; and even though in a different location, has always made himself available when I needed his help and input.

I would also like to thank and acknowledge the professors, colleagues and friends in CERTEC at UPC and in the Combustion Research Group at the University of Leeds. Thank you all so much for your constant support throughout the duration of my time in Barcelona and Leeds. In particular I would like to thank Josep Arnaldos who provided helpful comments on my work at different stages and several visiting students and engineers who made important contributions, especially in the early phases of this project. I also thank the staff of UPC Library, Montserrat Torres and Cristina Caba who provided outstanding help and support in my data collection effort.

I would also like to thank Joe Dolan, Richard Allan, Nathan Jones, Rachel Rotherham, Lucy West, Pamela Lomoro, Jian Fan, Markous Mansour, Tawfiq Al-Mughanam, Ahmed Eldein Hussin, Ahmed Khan, Isaias Ancalle, Gloria Penayo, Fabian Angulo, Oscar Suarez, Daniela Rivas, Alberto Tigre, Jose Garcia, Ma. Isabel Montoya and Hector Medina for their kindness, friendship and support.

Last, but by no means least, I want to express my gratitude to the most beautiful blessings in my life: my parents Felipe Palacios and Ma. Concepcion Rosas, for their constant love, encouragement and support in the pursuit of all my goals; and also to my loving, supportive and encouraging sister Erika who has been a priceless gift of God in my life. Thank you.

SUMMARY

The adverse effects of fires are usually confined to a smaller area than in the case of explosions and toxic releases; however, the affected area often contains other equipment that can be seriously damaged by the thermal flux and flame impingement, creating a domino effect, leading to a larger accident. Among the major fire accidents, jet fires are important since they have repeatedly been reported as being the first stage in severe accidents involving explosions, large fires, and serious damage to equipment because of thermal radiation and flame impingement. The present thesis is addressed to produce novel and useful information on the behaviour and modelling of jet fires for accurate risk assessment and better prevention and control of this major fire accident, occurred world-wide in industrial establishments and in the transportation of hazardous materials.

In the first chapter, a brief introduction on some general concepts about major accidents, major accidents involving fire and some of the main features of jet fires are described. The frequency of major accidents has also been analyzed through historical surveys, carried out on accidents registered in four European accident databases, concerning events occurred in fixed plants, seaports and/or in the transportation of hazardous materials over 95 countries. Some of the results of this chapter have been published (Darbra *et al.*, 2010).

In the second chapter, the literature review has shown that although jet fires have been theoretically and experimentally studied by several authors, there is still a lack of experimental research on large-scale hydrocarbon sonic exit velocity jet flames, and on adequate methodologies to estimate

their flame size, shape and radiative features. This is due to the fact that most of the work has been focused on subsonic flames, flares or small-scale jet fires, the conditions of which significantly differ from those found in real accidental jet fires, usually reaching much larger flames and sonic exit velocities. With the purpose of knowing deeply this type of accident, a series of experimental tests have been performed on relatively large-scale turbulent jet flames, in an outdoor fire-testing area, using LPG as a fuel. The experimental facility was built at the Can Padró Safety Training Centre (Catalonia, Spain), where a set of 20 experiments has been performed on sonic and subsonic exit velocity jet flames up to 10.3 m in length and 1.5 m in width, vertically released into still air, obtained with various exit diameters and mass flow rates ranging between 0.01 kg/s and 0.54 kg/s. The experimental facility, the instrumentation used (infrared and video cameras, a meteorological station, radiometers, a pressure transmitter, etc.), the test procedures and the test conditions are also described in this chapter.

Visible and infrared images, corresponding to the stationary state of the tests, allowed obtaining the main geometrical and radiative features of the flame: jet flame height, lift-off distance, flame width, jet flame shape, thermal radiation reaching a target, surface emissive power and emissivity of the flames.

In chapter three, based on the dimensional analysis of turbulent flames, the formulation of the most appropriate dimensionless groups has led to the obtention of a set of correlations for jet flame height and lift-off distance for propane flames under sonic and subsonic regimes, involving the orifice's Froude number and the orifice's Reynolds number. Also by dimensional analysis, a correlation for the total jet flame height (considered form the gas release point to the flame tip) to estimate the height of turbulent sonic jet hydrocarbon (CH_4 and C_3H_8) and hydrogen flames, involving chemical parameters such as the turbulent burning velocity, the turbulent karlovitz stretch factor, and also based on the considerations of turbulent flame structure, burning rates and non-ideal gaseous expansion of turbulent flames has been obtained. Comparisons between the present experimental data and the expressions suggested from other authors have also been carried out. The results of this chapter have been also published (Palacios *et al.*, 2009; Bradley *et al.*, 2010).

In chapter 4, the flame shape of sonic and subsonic exit velocities jet fires has been analyzed, considering the existence of flames over the region where a minimum given temperature (800 K) had been reached, and from

the jet flame width measurements from the registered images, at five heights: 10%, 30%, 50%, 70%, and 90% of the jet flame length (disregarding the lift-off length). The experimental results have been compared with the shapes proposed by other authors, leading to the suggestion of a cylinder, showing a constant flame-length-to-diameter ratio of 7, to describe the shape of vertical sonic and subsonic exit velocity jet flames. Following the previously mentioned dimensional analysis, an expression to correlate the jet flame diameter, normalized by the pipe diameter, at sonic and subsonic conditions, as a function of the orifice's Reynolds number has also been found. This contribution has also been published (Palacios and Casal, 2010).

Finally, in chapter 5 the main flame radiation features (incident radiant heat over a target, surface emissive power and emissivity of the flames) of jet fires have been analyzed. The radiative heat intensity, I, emitted from sonic and subsonic jet flames affecting certain targets (heat flux sensors) has been found to increase as the distance from the flame surface decreases, and as both the fuel mass flow rate and the jet flame length, respectively, increase. The surface emissive power of the jet flames, E_{HFT}, has been calculated based on the solid flame radiation model, assuming the flame shape to be a radiating cylinder (disregarding the lift-off length), and using the heat flux sensors measurements. The solid flame model has also been used for estimating the thermal radiation from jet fires by the treatment of infrared images of the flame, where the comparisons between experimental and estimated I values led to the determination of the emissivity of the flames, ε. An average value of $\varepsilon = 0.36$ has been obtained from the present experimental data. The infrared treatment also led to the obtention of a calculated surface emissive power, E_{IR}, later compared with E_{HFT}, showing a difference no greater than 14%. Both E_{IR} and E_{HFT} were found to increase with the jet flame length and mass flow rate. Comparisons with the experimental data on subsonic large-scale jet fires published by other authors and a widely used model have also been done in this chapter.

INDEX

1. INTRODUCTION

1.1. Risk and hazards

Certain plants or activities (process plants, storage of fuels, transportation of hazardous materials, etc.) can undergo severe accidents, usually called major accidents, which effects can reach distances beyond the plant or activity border, affecting external targets: human health, property, environment, etc.

Due essentially to the growth of the process industry and, consequently, of the associated transportation of hazardous materials, the frequency of occurrence of major accidents has increased in the last decades. Although the application of new regulations and risk planning policies in developed countries has certainly contributed to decrease the risk of the aforementioned activities, the real fact is that major accidents are still a significant risk. Thus, the effort made for years in the industrialized countries to improving the situation must be continued, as this is the only way to reach a “tolerable risk” situation.

Risk has evolved and changed with the industrialization of the modern society. The risk and the hazards to which a person is exposed today are significantly different from those to which our ancestors were exposed. New hazards have appeared, although the overall risk for a person living in a developed country has significantly decreased.

To manage risk, a definition allowing its qualification is required. The most usual one concerning a given event is the following one:

$$\text{Risk} = \text{frequency} \cdot \text{magnitude of consequences}$$

In this expression there are two different factors. On one hand, the frequency with which a hazard (hazard: “a condition or circumstance that has the potential for causing damage to people, property, or the environment”) will actuate on a given target. And, on the other hand, the severity of the consequences which will occur if the event takes place.

Although this definition of risk is quite clear, two problems arise from it if a value for the risk of a given accidental scenario must be established: the determination of the frequency of occurrence (how can the frequency of an event which very rarely occurs be established?) and, if the event occurs, the prediction of its effects and consequences (which will be the reach of the phenomenon? How many people will be killed or injured?). These two points are essential in risk analysis and, even though a lot of work has been done and a large number of researchers have published their contributions, there are still many gaps and a significant research effort to be performed in this field.

Both the estimation of frequencies and the evaluation of effects and consequences of accidents are still effectuated with a significant lack of accuracy. Research is still required to improve our knowledge on the main features of the most common major accidents which, too often, occur both in fixed installations and in the transportation of certain materials. Some of them are relatively well known nowadays, but the knowledge on some others has still large gaps which should be studied. A full knowledge of the features of major accidents is required to fight them and to avoid them or, in the worst case, to be able to take the measures to reduce and limit their consequences and severity.

The work described in this thesis is a contribution to the knowledge and prediction of the main features of jet fires, which have been the origin of severe accidental scenarios.

1.2. Major accidents

Major accidents have been defined by the Council Directive 96/82/EC on the Control of Major Accident Hazards Directive (1997) as “an occurrence such as a major emission, fire, or explosion resulting from uncontrolled developments in the course of the operation of any establishment (this latter defined as the whole area under the control of an operator where dangerous substances are present in one or more installations, including common or related infrastructures or activities), and leading to serious danger to human

health and/or the environment, immediate or delayed, inside or outside the establishment, and involving one or more dangerous substances".

Major accidents involve the release, usually instantaneous or in a relatively short period of time, of significant amounts of energy or hazardous materials. Among the most probable dangerous phenomena associated to these events the following ones can be cited: a) thermal (thermal radiation, flame impingement), b) mechanical (pressure wave, ejection of fragments) and c) chemical (release of toxic materials).

The occurrence of major accidents is often associated to the loss of containment of a hazardous material or of energy. Once the release takes place, depending on the condition of the material, on the type and dynamics of release and on the meteorological conditions, diverse possibilities exist. These have been shown in Fig. 1.1, trough a simplified schema modified from Casal (2008).

The released material can be a liquid, a vapour or gas or a mixture of gas and liquid (two-phase flow). This, together with the prevailing meteorological conditions, will determine the diverse sequences which will lead to the different accidental scenarios. These will imply finally a fire, an explosion (of a vessel or a flammable vapour cloud) or the atmospheric dispersion of a toxic cloud. It is important to note that an accident can also involve more than one of these phenomena simultaneously. There are also other possible consequences on the environment, such as for example soil or water pollution, not included in Fig. 1.1.

The release itself can be a major accident, as in the case of a pressurized vessel explosion (sometimes a Boling Liquid Expanding Vapour Explosion (BLEVE)). In other cases, the loss of containment can be originated by the collapse of a tank, the corrosion or breakage of a pipe, a safety valve, etc.

Once the loss of containment has taken place, the accidental sequence will depend on a) the condition of the released material: a liquid, a vapour or gas, or a mixture of liquid and gas phases; b) on the prevailing meteorological conditions at the site; and c) on the eventual existence of safety barriers as, for example, a dike, a foam blanketing system, etc. For example, if a gas is released and there is a strong wind, the gas will be quickly dispersed without any further consequences (except for the pollution of atmosphere). However, in normal meteorological conditions there is a range of hazardous situations: formation of a flammable or toxic (depending on the material) cloud, or ignition of a pool of flammable liquid, or ignition

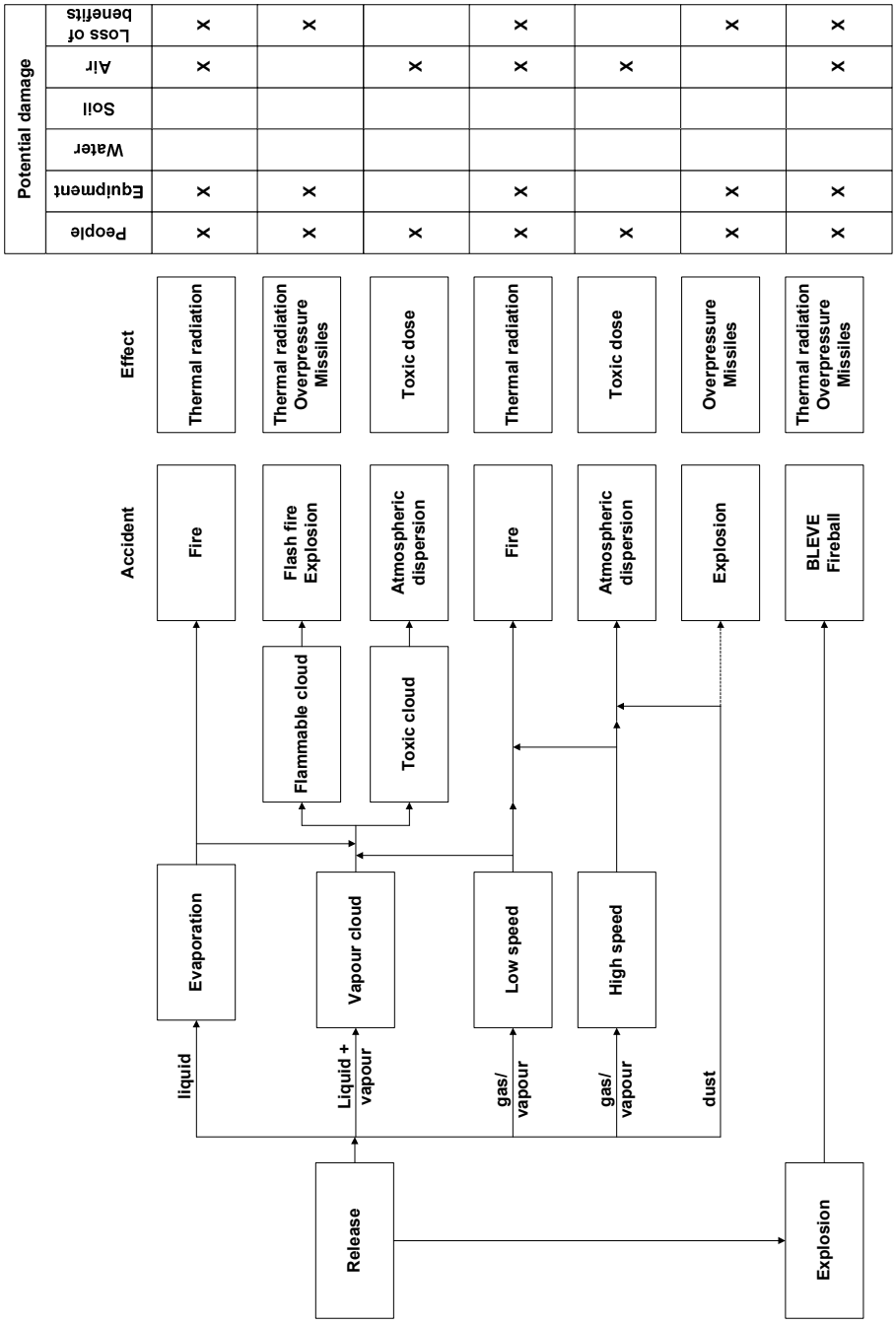

Figure 1.1. Major accidents: simplified schema (modified from Casal (2008)).

of a jet of flammable vapour/gas or two-phase flow released from a hole or a valve, etc.

The final dangerous phenomenon, already mentioned, can actuate in a quite different mode according to its features. Thus, an explosion will cover an approximately circular zone with its blast, while the associated missiles will imply a directional hazard. A toxic cloud will evolve towards a given direction, according to the wind. And the thermal radiation from a fire, although with a shorter reach, can easily affect other equipment (the same can happen with explosion missiles), thus enlarging the scale of the accident through the so-called “domino effect”.

To avoid these events, to control them or to predict their reach and effects (and, finally, their consequences), their main features must be known. Thus, the fire size and the thermal flux radiated from a fire must be known in order to establish whether a tank located at a given distance from the fire is or not at risk. Or the evaporation rate from a liquid pool should be calculated to predict the size and evolution of a toxic vapour cloud.

Therefore, the mathematical modeling of major accidents is an essential aspect in risk assessment. Mathematical models are available to describe explosions, fires and atmospheric dispersion of gases, but unfortunately many of them are not precise enough and often apply simplifying assumptions which lead to false results. Much research is still required in most of the blocks in Fig. 1.1.

1.3. Frequency of major accidents

The frequency of major accidents has been analyzed through historical surveys, carried out on accidents registered in four European accident databases, concerning events occurred in fixed plants, seaports and/or in the transportation of hazardous materials over 95 countries. These studies are briefly commented in the next paragraphs.

From the historical analysis based on a large sample of 5325 accidents, occurred both in fixed plants and in the transportation of hazardous materials, covering from the beginning of the twentieth century up to July 1992, Vílchez *et al.* (1995) found an increasing trend in the number of accidents as a function of time; the frequency of accidents as a function of time can be seen in Fig. 1.2. It can be observed that a significant increase was found in the period 1970-1990.

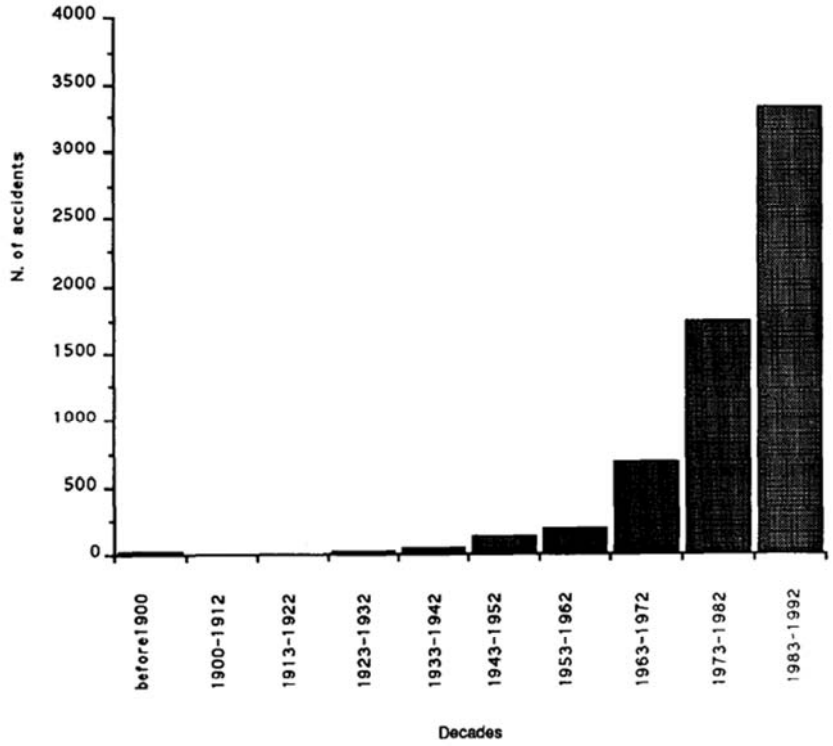

Figure 1.2. Distribution of the number of major accidents as a function of time (taken from Vílchez *et al.*, 1995).

Concerning the type of accident, these authors found release as the most frequent one, occurring in 51% of the cases, followed by fire (44%), explosion (36%) and toxic cloud (12.1%). It should be noted that two of these types of accident could exist in each accident; this is why the sum of the percentages is higher than 100.

Another survey developed by Planas-Cuchi *et al.* (1997) on 6099 accidents occurred in process plants and in the transportation of hazardous materials, from the beginning of the twentieth century up to the end of 1993, showed also the number of accidents to increase significantly as a function of time (Fig. 1.3).

Concerning the type of accident, these authors also found release as the highest percentage (52.15%), followed by fire (41.52%), explosion (34.83%) and gas cloud (11.18%). As previously noted, the sum of the

percentages is greater than 100, since a given accident can include two or more of the four mentioned types of accident.

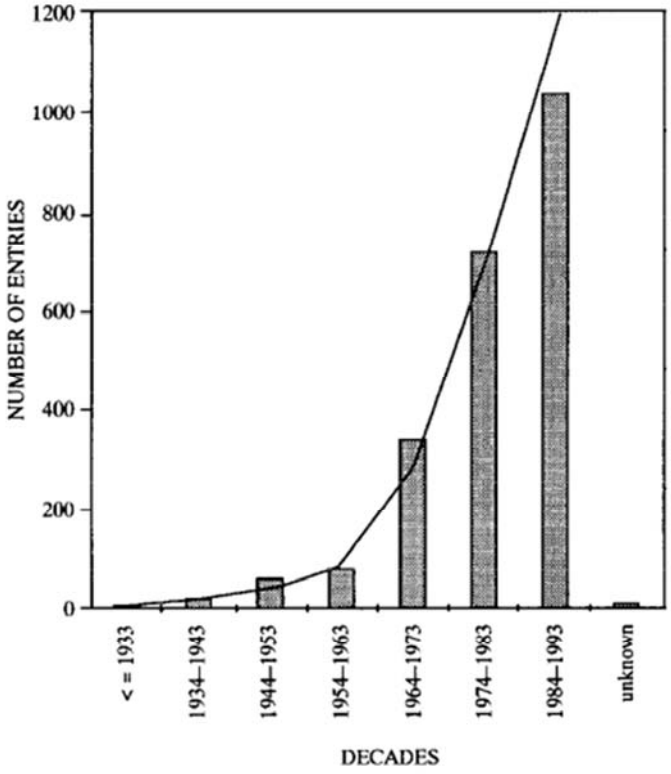

Figure 1.3. Distribution of major accidents as a function of time (taken from Planas-Cuchi *et al.*, 1997).

In 2004, Darbra and Casal carried out another historical analysis on 471 accidents occurred in seaports between the beginning of the twentieth century and October 2002. Their results show again a significant increase in the frequency of accidents over time (Fig. 1.4). From this plot it can be seen that the number of accidents increased dramatically: 83% of the accidents occurred during 1981-2002. Concerning the type of accident, these authors again found release as the most frequent accident (51%), followed by fire (29%), explosion (17%) and gas cloud (3%). It should be noted that 21% of the 471 total accidents were not classified into anyone of these four types of accidents.

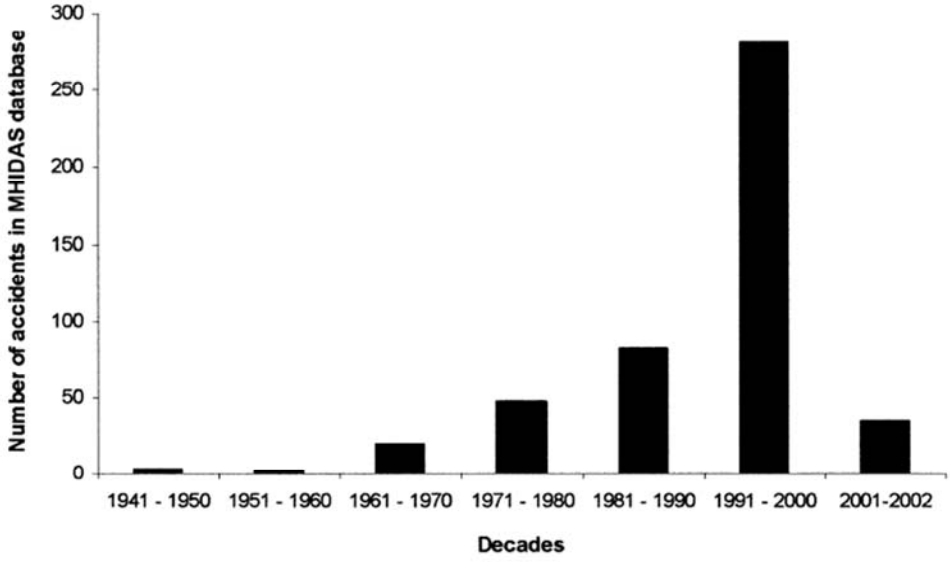

Figure 1.4. Distribution of major accidents occurred in seaports over time (taken from Darbra and Casal, 2004).

Another survey performed by Oggero *et al.* (2006) on 1932 accidents occurred in the transportation of hazardous substances by road and rail, from the beginning of the 20th century up to July 2004, has shown the same upward trend in the frequency of accidents over time, again with a gradual increase in the frequency of accidents over the second half of the twentieth century and a significant rise in the period 1981-2000. These authors found that the most frequent major accident was fire.

Ronza *et al.* (2003) carried out an historical analysis on 828 accidents, occurred in port areas, finding that 69% of the cases involved release, followed by fire (16%) and explosion (15%). These authors also constructed relative probability event trees to analyze the sequence of 108 accident scenarios in which a domino effect was observed, finding the most frequent sequences to be fire → explosion (4.4%), release → fire → explosion (0.9%) and release → gas cloud → explosion (0.3%).

Most of these surveys registered (Vílchez *et al.*, 1995; Planas-Cuchi *et al.*, 1997; Darbra and Casal, 2004; Oggero *et al.*, 2006) a significant progressive increase in the frequency of accidents with time, and in fact this has been a commonly accepted criterion among risk analysis researchers.

This trend could be attributed both to the improvement of access to information on accidents in recent years (whereas a large amount of information concerning accidents happening in the first decades of the twentieth century has probably been lost) and to the notable development of industrial activity in many countries, with the consequent increase in the transport of hazardous materials.

However, several recent surveys (Gomez-Mares *et al.*, 2008; Darbra *et al*., 2010 and Niemitz, 2010) seem to indicate that this widely accepted scenario could not be right any more. A historical analysis performed on 84 accidents involving a jet fire, identified since 1961, has been recently carried out by Gomez-Mares *et al.* (2008). These authors found that 25% of the total accidents occurred in the 1970s, decreasing by 8% in the 1980s, and since remained nearly constant. Thus, the aforementioned increasing trend in the number of accidents as a function of time was not observed here, at least during the last three decades.

More recently, Darbra *et al.* (2010), through a survey on 225 major accidents in process/storage plants and in the transportation of hazardous materials, involving domino effect and occurred after 1961, have found the number of accidents to increase from 1961 to the period 1970-1980, being stabilized afterwards during the 1980s and continuously decreasing later up to 2007 (Fig. 1.5).

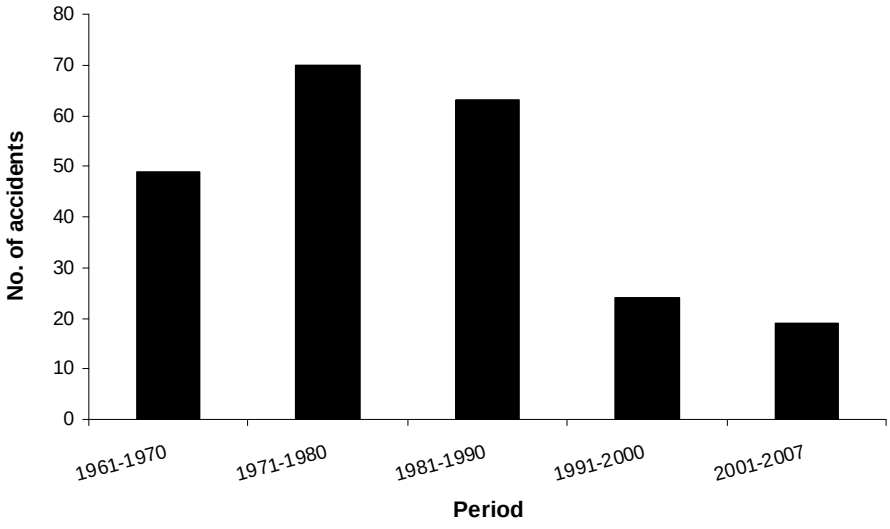

Figure 1.5. Distribution of accidents over time (taken from Darbra *et al.*, 2010).

This new trend has also been recently noted by another author (Niemitz, 2010); Niemitz analyzed the major accidents registered in the EU's major Accident Reporting System (MARS) between 1996 and 2004, and found also a lightly decreasing trend over the last decades (Fig. 1.6).

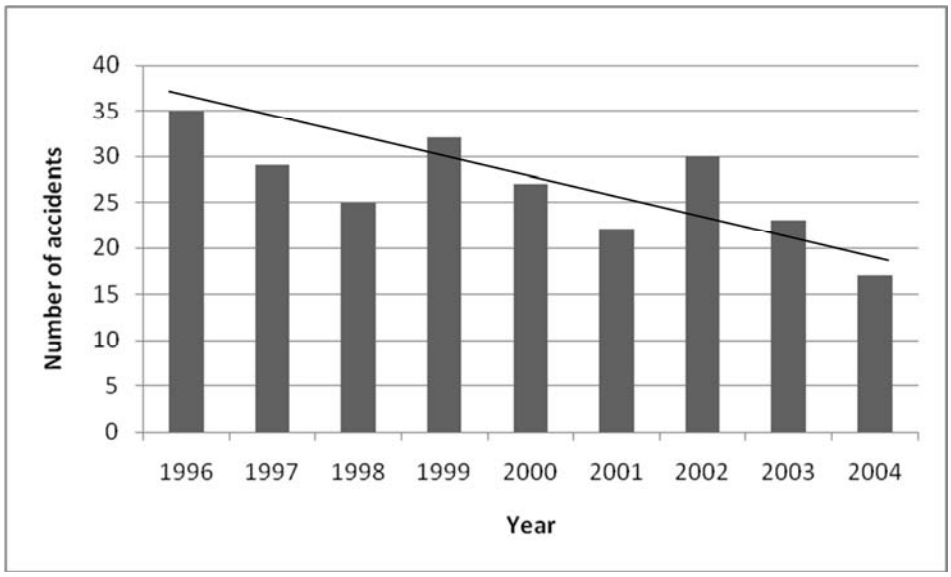

Figure 1.6. Trend of the frequency of major accidents in EU-15 (1996-2004) according to data registered in MARS (taken from Niemitz, 2010).

All these new surveys (Gomez-Mares *et al.*, 2008; Darbra *et al.*, 2010 and Niemitz, 2010) would therefore indicate stabilization, and even a decrease, in the frequency of major accidents, which would be a new and quite positive information. This decreasing accident rate could be explained by the general improvements in the safety culture measures applied to the chemical industry, by the implementation of strict new regulations (e.g. EU Directives), risk planning policies, stricter legislation and more effective operator training. However, the trend found by the above-mentioned studies is in some way surprising and should be monitored over the coming years, since major accidents are still a significant risk.

Concerning the material involved in the accidents, Gomez-Mares *et al.* (2008) found that 60% of the cases had involved LPG as a fuel. Similarly, Darbra *et al.* (2010) found that in 89% of the cases flammable materials have been involved, LPG being the most frequent one.

If release is not taken into account, most of the historical analyses on accidents have shown that fire accidents are the most frequent ones. It should be noted that in the surveys published by Ronza *et al.* (2003) and Darbra *et al.* (2010) the occurrence of explosions has a frequency close to that associated to fires. Thus, although the direct effects of fire accidents are restricted to relatively short distances as compared to other major accidents, they can often provoke a chain of events that ultimately amplifies the accident scenario, due to thermal radiation, flame engulfment and/or flame impingement on certain equipment. This is especially important in compact settings, such as those often found in process plants or offshore oil platforms that can lead to such dangerous situation.

1.4. Major accidents involving fire

Fire accidents can be classified into the following general categories (Casal, 2008):

Pool fire. Turbulent diffusion fire burning above a pool of vaporising flammable liquid (usually a hydrocarbon fuel). Pool fires can also be originated when a flammable, non-miscible liquid is spilled on water. Tank fires can be considered as a particular case.

Pool fires, once ignited, reach quickly a stationary state once pool surface has reached a constant value. The size of pool surface is determined by the eventual existence of a dike (often found in storage areas), by the slope of the ground or, for plain ground, by the equilibrium between the liquid release flow rate and the combustion rate, which established the maximum diameter that the pool can reach.

Once the stationary state has been reached, the thermal radiation emitted from the fire is practically constant and is a function of the type of fuel and of the combustion regime. Large fires are significantly turbulent and its shape is rather difficult to be defined. With liquid hydrocarbons such as raw oil, diesel oil or gasoline, combustion is rather bad; large amounts of black smoke (which sometimes can complicate the emergency intervention) are formed and the fire surface can be divided in two parts: the bright ones (flame) and the smoke ones. The surface emissive power is high for the bright flame surface, and has much lower values for the smoke-covered surface. Thus, to estimate with a better accuracy the average emissive power of the fire both contributions should be taken into account.

Figure 1.7. An outdoor pool fire. Pool diameter: 4 m; fuel: gasoline (taken from Chatris *et al.*, 2001).

Pool fires have been studied by a number of authors. Although many of them have dealt with rather small fires (Klassen *et al.*, 1992 and Choi *et al.*, 1994), which behaviour is not representative of real pool fires, some others (Mizner and Eyre, 1983; Gritzo *et al.*, 1998; Koseki, 1999; Chatris, 2001; Muñoz, 2005 and Ferrero, 2006) have worked with large scale fires, giving data and correlations which can be applied to real large scale accidental pool fires. Thus, the knowledge nowadays available on pool fires is relatively good and allows their mathematical modelling and the prediction of their effects with a fairly good accuracy (even though a series of gaps still exist).

Flash fire. Sudden and intense fire, originated by the ignition of a mixture of flammable gas/vapour and air. A pool fire will probably be originated from a flash fire, if the vapour comes from a liquid pool.

Flash fires have not been much studied and few mathematical models have been proposed (Eisenberg *et al.*, 1975; Raj and Emmons, 1975), because of several reasons. First of all, because of the difficulty associated to obtaining experimental data at a relatively large scale. Secondly, because their effects are: a) confined to a defined zone; concerning consequences on people, for example, it is often assumed that all people inside the flammable

cloud die, while those out of it undergo no consequences, and b) minor as compared to the mechanical ones (blast, missiles) if the flammable cloud has a large size enough to give rise to an explosion. As for the thermal effects on equipment, given the very short duration of the fire they are usually negligible.

Fireball. Sudden release and ignition of a large amount of flammable spray. It is usually associated with the explosion of a pressurized vessel containing a superheated flammable liquid. Large (but with a short duration) fireballs can also occur in tank fires in the event of a boilover.

Figure 1.8. A fireball originated by the explosion of a vessel containing ethylene.

Although the duration of a fireball is rather short (from a few seconds to up to one minute, depending on the mass of fuel involved), the associated thermal radiation is so intense that their consequences –specially on people– can be very severe over a relatively large area. Fireballs can occur with most flammable liquids, but the most commonly involved fuel is LPG. LPG fireballs are very bright and their surface emissive power can be three or even four times that of a pool fire. Furthermore, they can occur suddenly, without warning, and this is the reason why many persons (fire fighters amongst them) have died.

Even though there are few experimental results on large scale fireballs, there are available some data taken from real accidents. All these values have led to the development of several models which allow an approximate estimation of the thermal effects of a fireball, even though a number of uncertainties (as, for example, that concerning the mass of fuel which should be considered) are found when applying them to a given case.

Jet fire. Jet fires are originated by the loss of containment and ignition of a flammable gas/vapour or spray, released through a hole, a broken pipe, a flange, etc., or in process flares. Usually involving high heat fluxes, its direct effects are often confined to relatively shorter distances as compared to those associated to other types of fires (i.e. pool fires, flash fires or fireballs).

Figure 1.9. Two phase propane jet fires, obtained from vertical and horizontal releases.

Even though jet fires are relatively small, as compared with pool fires or fireballs, they have some specific features that increase significantly the hazard associated to them. Jet fires are usually originated from pressurized releases, i.e., from the ignition of highly turbulent fluid jets; this turbulence implies the entrainment into the jet of important amounts of air, and this

improves significantly the quality of combustion as compared with that found in a pool fire.

Due to this fact, the thermal energy released from a jet fire is very large. If the released fuel is a gas –for example, propane– then the flame is almost transparent; the emissive power is low and the thermal radiation is relatively small. If the released fluid is a spray –two phase flow– then the jet flames are much bright and the emissive power is high. Nevertheless, in both cases the thermal radiation intensity decreases quickly with distance, and the zone over which the effects are potentially dangerous is rather reduced.

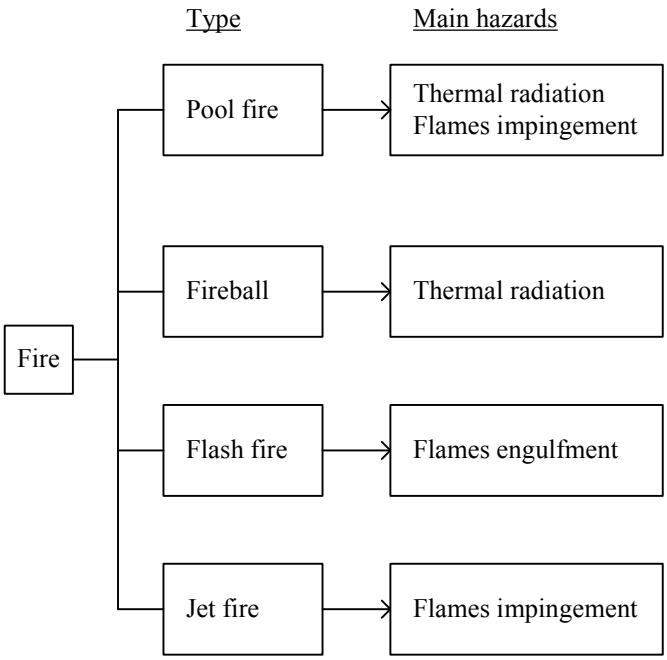

Figure 1.10. Main hazards associated to the diverse types of fire accidents.

However, as stated before, the overall heat released by a jet fire is locally very high. If a jet fire impinges on a given equipment (a pipe, a tank) the local effects will be extremely severe. Given the high density of equipment usually found in process plants, offshore oil platforms or even in certain storage areas, the probability of a jet fire impinging on some equipment is very high. In this case, a domino effect can be initiated, thus increasing the scale and the consequences of the accident.

Nevertheless, even though jet fires are important because of their potential consequences, they have not been much studied and the prediction of their behaviour and effects is still rather difficult.

The aforementioned diverse types of fire accidents lead to different scenarios from the point of view of the hazards implied. These hazards depend on the circumstances: features of the fire, duration, quality of combustion, etc. Fig. 1.10 shows a schematic summary of the hazards associated to each type of fire accident.

1.5. Jet fires

Jet flames can frequently be considered as the first stage of further major accidents, since the effects flame impingement and heat radiation on the near-by equipment can often provoke a chain of events that ultimately amplifies the severity of the accident. This is often referred to as the domino effect.

1.5.1. The behaviour of jet fires

Jet fires are characterized by a high momentum jet flame lifted above the mouth of the duct from which the fuel (often a gas) is flowing, generally at a relatively high pressure. Their behaviour is strongly influenced by the exit velocity.

Two dominant regimes can be found in jet flames: buoyancy and momentum. At high jet flow rates, the jet momentum dominates the mixing process. Thus, the momentum of the fuel vapour largely determines the behaviour of these types of flames. This will be typically the case of an accidental jet fire. Instead, at lower velocities, buoyancy effects become important in flames, due to the density differences that combustion generates (the density decreases from the density at the outlet orifice diameter to the density located at the top of the flame). This is often the case of flares, which are widely used in processing plants to dispose safely of flammable gases.

The jet exit velocity has a certain influence on some of the features of the fire (jet flame height, flame width and lift-off distance). This velocity will increase with the pressure inside the container or the pipe, usually reaching the sonic velocity, i.e. the velocity of sound in that gas. This represents the

choked condition; however, further increase in pressure will not modify the so-called critical velocity of the gas. Thus, two regimes can be found: subsonic flow and sonic exit velocities.

In the event of an accidental release of a gas, sonic exit velocity (i.e. the velocity of sound in the gas at exit gas conditions) is reached if the gas is (in a tank, a pipe, etc.) at a certain pressure above a minimum value. In fact, the sonic velocity is reached if the relationship shown in Eq. (1.1) is fulfilled; for most gases sonic velocity is reached if the pressure at the fuel source (P_{in}) is greater than 1.9 bar, which is common in many storage tanks and pipelines (Casal, 2008):

$$\frac{P_{out}}{P_{in}} \leq \left[\frac{2}{\gamma+1}\right]^{\frac{\gamma}{\gamma-1}} \tag{1.1}$$

It is important to note that stable jet flames are not always obtained from the ignition of flammable releases, since discharge conditions (exit velocity, outlet orifice diameter, concentration of fuel near the release source, etc.) can be such that provoke the self-extinction of the jet flames immediately after ignition.

This phenomenon, known as “blow-out”, is the result of an increase in the exit flow rate. This increase in the exit flow rate initially leads to the lifting of the flame, from the fuel source to a downstream further position; at this position, the burning velocity and the average velocity at the exit jet are equal; this distance defines the lift-off height. However, if the exit flow rate is still further increased, the flame could blow-out (depending on the outlet diameter) since this change in flow rate could not be maintained by the burning velocity. At these conditions, the flame is swept to a region in which the fuel concentration is out from the flammability limits range and is extinguished. This phenomenon is illustrated in Fig. 1.11 for a propane gas jet fire.

Blow-out has been studied only by a few authors; it is still badly known and its prediction is still rather difficult. The outlet orifice diameter seems to play a significant role, small diameters giving rise to blow-out. However, under blow-out conditions the jet fire can be sometimes maintained by applying continuously a pilot flame.

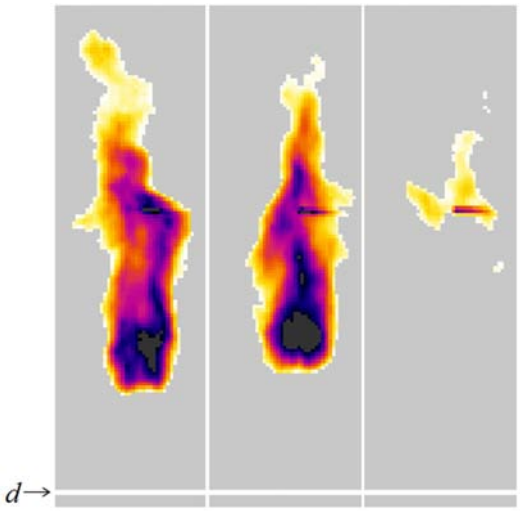

Figure 1.11. The blow-out phenomenon: infrared images of sonic jet flames issuing from a 10 mm outlet orifice. The time interval between the successive infrared images is 0.25 s. The height at which the outlet orifice diameter (*d*) was located is shown by a bottom horizontal line. The isotherm of 800 K was used to define the jet flame boundary.

Diverse factors, such as the fuel release orientation, flow composition (gas/liquid), and the presence or absence of cross winds during the attainment of flames (Fig. 1.12) also affect the features of the jet flames.

Concerning the orientation of jet fires, horizontal flames differ from vertical flames, since after following a straight distance (essentially horizontal) due to their initial high momentum, horizontal flames start turning upwards as a result of the buoyancy forces (vertical and horizontal jet fires can be seen in Fig. 1.9). If there is a significant cross wind, the jet fire becomes inclined. Finally, the condition of the fuel –gas o two-phase flow– has a strong influence on the quality of the combustion and, therefore, on the thermal properties of the flames: due to the existence of liquid droplets, the amount of fuel entering the jet is much higher than in the case of gas and, as a result, the combustion is poorer. This is the reason why a large amount of soot is formed; due to this high temperature soot, the flame (that in the case of a gas fuel is almost transparent) becomes much more brighty and the thermal radiation emitted is much stronger. Furthermore, for a given operating scenario (release pressure, outlet diameter) the jet fire size increases significantly if the fuel changes from gas to two-phase flow.

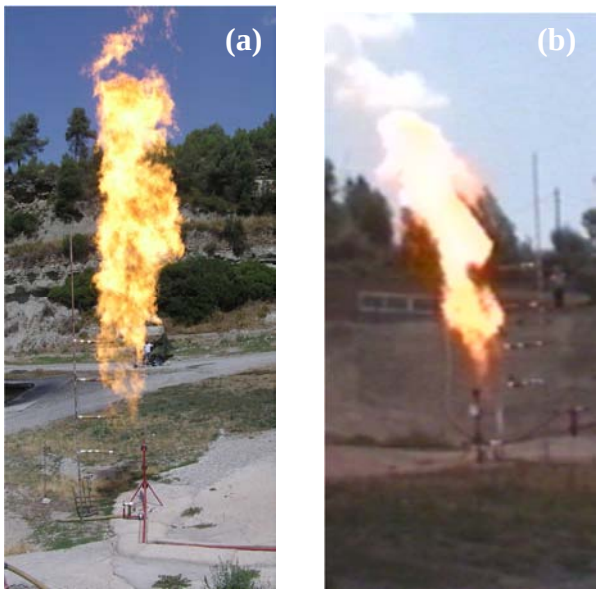

Figure 1.12. Two-phase flow vertical jet fires: (a) wind speed = 0.9 m/s, *d* = 43.1 mm and (b) jet flame influenced by cross winds, wind speed = 3.1 m/s, *d* = 35 mm.

1.5.2. Jet fires and the domino effect

A historical survey recently carried out by Gomez-Mares *et al.* (2008) reported that one of two jet fire events registered in accident databases originated at least another event with severe effects, often an explosion, due to the domino effect (see an example in Fig. 1.13). According to the results obtained by these authors, in 56% of the cases (over 84 cases, obtained from four European data bases) an explosion took place; in 27% of the cases another type of fire was generated, and in 26% of them a vapour cloud occurred; the percentage is not 100%, since more than one of these three events can occur in the same accident.

This is one of the reasons why jet fires can be so important from the point of view of risk analysis. In fact, as compared with pool fires, jet fires are commonly much smaller and the thermal radiation emitted by them is relatively reduced and important only at very short distances (it decreases very quickly as the distance from the flames increases). However, jet fires often occur in rather compact process or storage plants and the probability of flame impingement on another equipment –with the associated domino effect– is rather high.

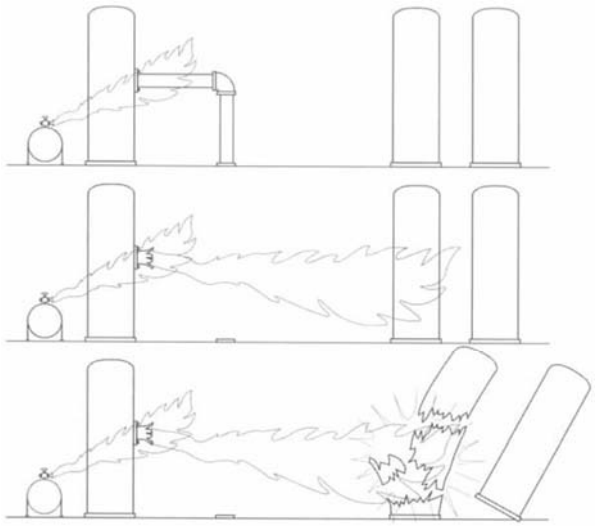

Figure 1.13. An illustration of the domino effect based on a real case (taken from Casal, 2008).

1.5.3. Flames impingement

The consequences for equipment are particularly severe if flames impingement occurs. One such scenario is jet flames impingement on a storage vessel, resulting from an ignited release from a leaking flange, failed pipework, etc. Fire impingement on vessels containing pressure liquefied gases may give raise to the failure of the vessel, leading to a Boling Liquid Expanding Vapour Explosion (BLEVE). If the gas is flammable, this can result in the formation of very large fireballs. For example, Roberts *et al.* (2000) performed a series of large-scale tests as a part of the Commission of the European Community (CEC) Science and Technology for Environmental Protection (STEP) Programme. In this study, four unprotected vessels, containing different amounts of propane (20%, 41%, 60% and 85% of the overall capacity) up to 2 tonne and setting to relieve at 18.3 bar of either propane or butane, were engulfed in a jet fire until they failed.

The jet fire consisted of ignited, flashing, liquid propane at a flow rate of about 1.8 kg/s from a nozzle equivalent to a 12.7 mm diameter hole. The results showed that the liquefied petroleum gas storage vessels, located at approximately 4.5 m of the release source, failed within 5 minutes of commencing jet-fire impingement, originating a fireball.

However, the time to failure from the beginning of the emergency (from the start of fire impingement) is somewhat unpredictable in a real case. In fact, it depends on diverse circumstances: the existence and behaviour of a thermal insulation layer, whether the flames impingement takes place above or under the tank liquid level (i.e. whether the impinged tank wall is or not in contact with the liquid fuel), etc. This is why the time to explosion can vary from a few minutes (69 seconds in the first BLEVES at the San Juanico (Mexico) accident (Pietersen and Cendejas, 1985)) up to several hours.

1.5.4. Jet fire's current knowledge

The prediction of jet flame size and shape, in the event of a subsonic or sonic jet fire, is quite important, since they are closely related to the possibility that jet flame impinge on other equipment, giving rise to a domino effect. To assess the risk of such a situation, it is essential to be able to predict the size and shape of a possible jet fire. Therefore, a set of expressions allowing the calculation of these features would be of great interest.

Jet flames have been studied both experimentally and theoretically. Nevertheless, the current knowledge on the main geometrical features (e.g. jet flame height, flame width and lift-off distance) of jet fires is still rather poor, and the accurate prediction of these features is still a problem. Most of the research performed up to now has been focused on relatively small-scale jet flames, subsonic jet fires and flares, which features are quite different from those of real accidental sonic jet flames.

Diverse authors, from experimental and theoretical studies, have proposed several mathematical models to estimate the shape of jet flames. For example, a cylindrical shape to describe the flame shape of subsonic jet flames, and a frustum of a cone to describe flares under the influence of cross winds have been suggested. Few experimental works concerning sonic jet fires have been published; in the small amount of published research, the jet flame size has been mostly analyzed for hydrogen jet flames, so the shape of hydrocarbon sonic jet flames is not yet well known.

As already mentioned, a reduced number of experimental studies on sonic jet flames have been carried out. Thus, there is a lack of experimental research into large-scale sonic jet flames and of methods that could be used to estimate the size and shape of such flames.

1.6. Objectives

The present PhD thesis describes diverse new methodologies to predict the effects of subsonic and sonic jet fires, both from an experimental study on relatively large-scale jet flames, and from the mathematical modelling of the main geometrical features of the flame: jet flame size and shape.

To address this main target, the following specific objectives have been carried out:

- Design and building of an experimental set-up to obtain relatively large subsonic and sonic jet flames.
- Carrying out a series of outdoor large jet-fire experiments under sonic and subsonic conditions.
- Obtention, identification and analysis of the main geometrical and radiative features of experimental jet flames: jet flame height, jet flame width, lift-off distance, incident radiant heat over a target, surface emissive power and emissivity of the flames.
- Mathematical modelling of the jet fire size (flame length, width and lift-off distance) and shape.
- Obtention of a set of expressions allowing the prediction of jet fire size (flame length, width and lift-off distance).
- Suggestion of a jet flame shape embracing subsonic and sonic regimes.
- Analysis of the main radiative features of experimental jet flames.

2. EXPERIMENTAL SET-UP

The experimental tests performed on large-scale turbulent jet flames issuing vertically, in an outdoor fire-testing area, are described in this chapter. The experimental facility, the instrumentation used, the test procedures and the test conditions are discussed in a detailed way.

2.1. The experimental facility

The experimental facility used in this study was built at the Can Padró Safety Training Centre, located in Sant Vincenç de Castellet (near Barcelona) in Catalonia, Spain.

Shown in Fig. 2.1 is the topographic map of the experimental field, where the diverse zones covered by the Can Padró Safety Training Centre are marked. These zones embrace three widely separated areas: the offices and services area, the driving circuit area and the fire fighting training centre (fire field). The experimental set-up was located in the fire field, in a zone reserved to CERTEC operations.

The scope of the project was to study relatively large jet fires –up to 10.3 m length of visible flame– using LPG as a fuel. A previous literature survey was effectuated to analyse the experimental work effectuated on this field by diverse authors. This survey showed that a relatively reduced number of researchers had worked experimentally with jet fires. Furthermore, some of those who had published experimental work had operated with rather small jet fires and/or at subsonic velocities; this means that their results were far from real accidental jet fires, which usually are much larger and are

originated from sonic velocity gas. Very few authors have published experimental data concerning large scale jet fires.

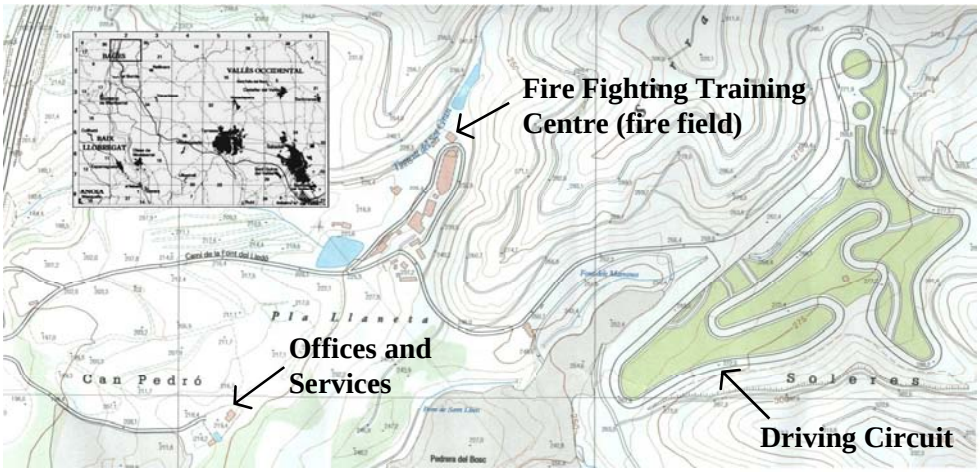

Figure 2.1. A topographic map of the experimental field.

2.2. Previous experimental studies

Jet flames have been theoretically and experimentally studied by several authors. Regarding experimental studies, some of them have dealt with flares, which are widely used in processing plants to dispose safely of flammable gases (Brzustowski *et al.*, 1975; API RP521, 1982; McMurray, 1982; Cook *et al.*, 1987a; Cook *et al.*, 1987b; Cook *et al.*, 1987c; Chamberlain, 1987; API RP521, 1997), and with non-premixed flames in cross-winds (Brzustowki *et al.*, 1975; Gollahalli *et al.*, 1975; Becker and Liang, 1981; Kalghatgi, 1983; Verheij and Duijm, 1991).

Jet fires have also been experimentally studied to determine the effectiveness of passive fire protection materials (HSE, 1993; HSE, 1996a; HSE, 1996b; HSE, 1997), the efficiency of water spray protection against jet fires impingement (HSE, 2000); and jet flame impingement effects (Cowley and Pritchard, 1990; Crespo *et al.*, 1994; HSE, 1999; Roberts *et al.*, 2000).

Regarding the phase flow, jet fires have been mostly obtained with a single phase (i.e. gas or liquid flow) or with two-phase flow (Hirst, 1984; Hustad and Sonju, 1985; Cowley and Tam, 1988; Gore *et al.*, 1989; Cowley and Pritchard, 1990).

Although a number of experimental works have been performed, there is still a lack of experimental research on large-scale hydrocarbon sonic exit velocity jet flames, and adequate methodologies to estimate the flame size and shape.

The present experimental study has been focused on gas jet fires issuing into still air at atmospheric pressure and temperature. This type of jet fires had been previously studied by several authors. Table 2.1 shows experimental studies concerning jet flames released in the absence of cross winds, obtained at small-scale under subsonic, sonic and/or supersonic conditions. Those concerning small-scale subsonic jet flames correspond to jet flames obtained with more than one fuel; this was the criterion with which subsonic small-scale works were selected.

A few number of experimental studies concerning large-scale gas jet fires released into still air have been found. These are shown in Table 2.2. Most of these studies concern on either subsonic jet fires or hydrogen jet flames. This lack of research on large-scale sonic hydrocarbon jet fires is the reason why they are still poorly understood.

From the literature survey, the interest of working with LPG was also shown: according to Gómez-Mares *et al.* (2008), most of the jet fire events registered in four European accident databases (60% of the cases) had involved LPG as a fuel.

Table 2.1. Experimental work on gas jet fires released in the absence of cross winds, corresponding to small-scale subsonic, sonic and/or supersonic jet flames

Authors	Fuel	*d* (mm)	Flow	Flame type
Hawthorne *et al.* (1949)	Acetylene, carbon monoxide, city gas, hydrogen, propane, mixtures of CO_2-city gas and H_2-propane	3–8	Subsonic	Vertical turbulent small-scale flames, up to 1 m in length.[a]

Baev *et al.* (1974)	Hydrogen	1–16.65	Subsonic, sonic and supersonic	75 experiments concerning vertical jet flames, obtained with outflow velocities up to 2600 m/s, Mach numbers ranging from 0.25 to 3.08, and flame heights ranging between 0.08 and 3.12 m.
Becker and Liang (1978)	Acetylene, carbon monoxide, ethane, ethylene, hydrogen, methane, propane	0.69–4.57	Subsonic, sonic and supersonic[b]	Some experiments were also obtained with nonstabilized flames using a burner consisting simply of a length of glass capillary tubing with *d* of 1.04 mm, 1.19 mm and 2.81 mm.
Becker and Liang (1981)	Acetylene, carbon monoxide, ethane, ethylene, hydrogen, methane, propane	0.69–4.57	Subsonic and sonic	Turbulent jet flames vertically released in cross-wind and vertical jet flames with the impartation of rotating entrainment air, have also been obtained in this experimental study on laboratory-scale flames horizontally released into still air.

Kalghatgi (1984)	Ethylene, hydrogen, methane and propane	1.08–10.1	Sonic and subsonic	Ethylene, methane and propane vertical jet flames were limited to subsonic flow; while hydrogen jet flames of up to 1.7 m in length were obtained at sonic and subsonic conditions.
Santos and Costa (2005)	Ethylene and propane	5–8	Subsonic	Vertical turbulent jet flames up to 1.7 m in length. The ranges of jet exit velocities and Reynolds and Froude numbers were 5–137 m/s, $8.97 \cdot 10^3 – 8.39 \cdot 10^4$, and $3.15 \cdot 10^2 – 3.85 \cdot 10^5$, respectively.[a]
Imamura *et al.* (2008)	Hydrogen	1–4	Sonic	Horizontal sonic flames up to 1.8 m in length.

[a] Flame height, defined as the distance from the base of the lifted flame to the flame tip.

[b] Data from other studies have been considered.

Table 2.2. Experimental work on gas jet fires released in the absence of cross winds, based on large-scale experimental jet flames

Authors	Fuel	Aperture (mm)	Flame Type	Notes
Sonju and Hustad (1984)	CH_4 and C_3H_8	10–80	Vertical subsonic flames up to 8 m in length.	–

Gore *et al.* (1986)	Natural gas[a]	76 and 102	Vertical sonic flames up to 25 m in length.	Burner exit Reynolds numbers were roughly $3 \cdot 10^6$. Four of total seven jet flames, included in this table, were obtained with maximum ambient wind speeds of 0.9 m/s. The other three jet flames, not included in this table, were obtained with ambient wind speeds ranging between 0.9 and 2.1 m/s.
McCaffrey and Evans (1986)	CH_4	38–102	Vertical subsonic and supersonics flames up to 23.5 m in length.	–
Sugawa and Sakai (1997)	C_3H_8	6.5–27.6	Vertical subsonic flames up to 8 m in length.	–
Schefer *et al.* (2006)	H_2	7.94	Vertical sonic flames up to 5.6 m in length.	Initial storage pressures up to 17.2 MPa. Subsonic laboratory-scale vertical hydrogen jet flames were also obtained with a 1.91 mm orifice exit diameter.
Schefer *et al.* (2007)	H_2	5.08	Vertical sonic flames up to 10.7 m in length.	Storage pressures up to 41.3 MPa. Subsonic laboratory-scale hydrogen and methane jet flames vertically released were also obtained with a 1.91 mm orifice exit diameter.

Mogi and Horiguchi (2009)	H_2	0.1–4	Horizontal subsonic and sonic flames up to 6.5 m in length.	Stable jet flames were obtained with *d* ranging between 0.4 and 4 mm. Release pressures ranged from 0.11 to 40.1 MPa. Flames up to 1.4 m length were also obtained through slit nozzles with a cross-sectional area equal to that of a circular nozzle *d* = 1 mm.

[a] Methane: roughly 95% in volume.

2.3. Measurement and calculation of the mass flow rate

The analysis of the aforementioned communications gave the range over which the values of certain variables (fuel flow-rate, jet exit hole, flames size) should be located in order to achieve experimental results which were significant and representative of real large jet fires. This analysis gave also a clear idea on the main difficulties of the experimental work to be performed. For example, an aspect which represents a real difficulty and which had been solved in different ways by the researchers was the measurement of fuel flow rate; this was seen from the very first moment as a problem to be solved. Hirst (1984) studied liquid and two-phase propane jet fires; this author measured the mass discharge rate of the fuel storage vessel mounted on a weighbridge to determine the jet fire fuel flow. McCaffrey and Evans (1986), working with methane jet fires, used a perforated plate to measure the fuel flow rate. Kalghatgi (1981) studied the blow-out phenomenon on jet fires of acetylene, butane, ethylene, hydrogen and methane, measuring the flow rate with a rotameter for low flow rates, and either a water or a mercury manometer was used for high flow rates. Cook *et al.* (1987a), working with natural gas flares, measured flow rate with a Pitot tube.

In the present study, the fuel flow rate was originally planned to be measured in its liquid phase, using an in-line ultrasonic flow meter, located at a few meters downstream the tank release. A non-invasive portable ultrasonic flowmeter of liquid, through clamp-on liquid sensors method, was tested. It should be noted that a non-invasive sensor was considered, since it would minimise the installation time and would not require the modification of the gas feeding pipe, described in section 2.4. The equipment was

supplied by two Spanish companies: LanaSarrate and Matelco. Fig. 2.2 shows it: portable ultrasonic flowmeter of liquid flow; Fluxus® ADM6725-02500686 model.

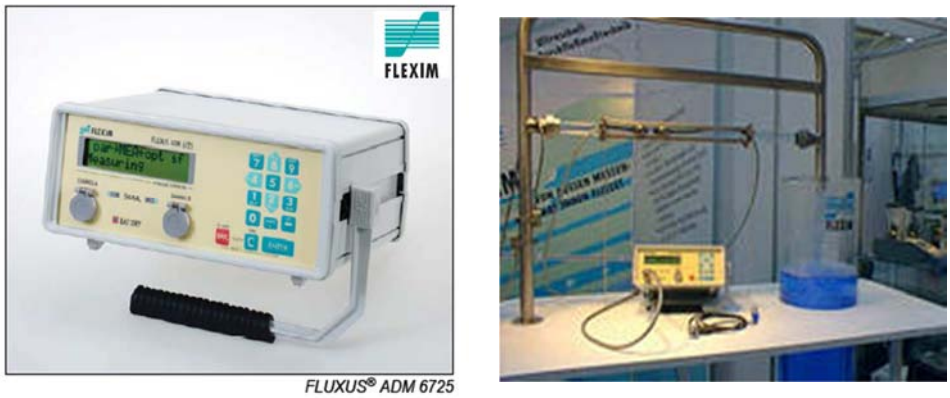

Figure 2.2. Portable non-invasive ultrasonic flowmeter of liquid flow; Fluxus® ADM6725-02500686 model.

The measuring principle of an ultrasonic flowmeter of liquid flow is based on the transit time difference principle. Ultrasonic signals are emitted by a transducer installed on one side of a pipe, reflected on the opposite side and received by a second transducer. These signals are emitted alternatively in flow direction and against it (Fig. 2.3-a). As the medium in which the signals propagate is flowing, the transit time of the ultrasonic signals in flow direction is shorter than against the flow direction. The transit time difference Δt is measured and allows determining the average flow velocity (Fig. 2.3-b). A flow profile correction is then performed in order to obtain the area average of the flow velocity, which is proportional to the volume flow. It is important to highlight that if the gaseous or solid content of the medium increases occasionally during measurement, this method can not be applied.

During the tests, the ultrasonic flowmeter was located on the pipeline at approximately 1 or 2 meters away from the storage vessel (Fig. 2.4), so as to guarantee the existence of liquid phase with a maximum permissible of 10% of gas phase in the pipeline. Although some data were collected during the tests, the ultrasonic flowmeter could not be stabilized, because of the sporadic existence of a two-phase flow of propane. Due to this difficulty,

found with both equipments, the possibility of measuring the fuel flow in its gas-phase was next considered.

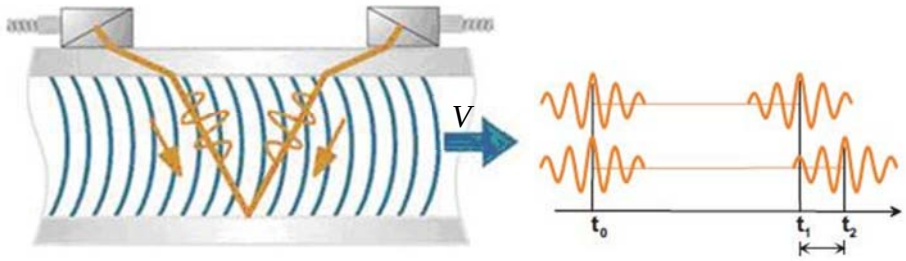

(a) (b)

Figure 2.3. Non-invasive ultrasonic flowmeter: (a) path of the ultrasonic signal. (b) transit time difference Δt.

Another ultrasonic flowmeter of gas flow, supplied by two companies (Katronic and Krohne, respectively) was considered for measuring the gas flow in the pipeline. According to the technicians of Katronic, the only suitable instrument for propane, due to their limitation in the range of gas applications measurements, was an ultrasonic flowmeter of liquids. Due to the early difficulties regarding ultrasonic flowmeter of liquids, this option was dismissed. The use of an ultrasonic gas flowmeter supplied by Krohne (OPTISONIC 7060 model) was also considered; however, according to the technicians of Krohne, due to the high density of the propane, this type of instrument could not be used in the present application. This was confirmed by the information reported in a study developed by Butler and Royle (2001), in which the flow of LPG was originally planned to be determined using an in-line ultrasonic flow meter. However, it was highlighted that this device did not work properly due to the density of propane. Thus, these authors measured the mass flow rate by measuring the change of the liquid level in the vessels (two 2 ton LPG storage vessels) and used along with the discharge time to calculate the mass flow rate.

Thus, the ultrasonic flowmeter of gas flow was dismissed, since the accuracy of the measurement could not be guaranteed.

A thermal gas mass flowmeter in an insertion style model was also considered and studied as another possibility for the fuel flow measurement.

Spanish and British companies (Eldridge and Endress+Hauser) were contacted to analyse this option. However, according to the first company, this type of instruments was suitable for a homogeneous gas phase flow only and the measurements could be affected by the presence of two-phase flow. The answer of the Endress+Hauser company confirmed this problem, noting that this kind of equipment could be only used in a homogeneous gas phase. Thus, due to the sporadic existence of two-phase flow during some of the present carried out tests, this instrument was dismissed.

Finally, the possibility of a quantometer to measure the gas flow was analysed. The consulted companies were Kromschroeder and Contagas. However, according to the answer obtained from the experts of these companies, a homogeneous gas phase flow should be guaranteed, and several modifications in the present installation should be required; these modifications concerned the increase of the diameter of the pipeline from DN40 to DN100 (i.e. from 43.1 mm to 107.1 mm of internal diameter). Due to these facts, this option was dismissed.

Several experimental studies on jet flames have used a theoretical estimation of the mass flow rate, by performing pressure and temperature measurements at the gas exit, assuming that the jet is expanded isentropically to atmospheric pressure and applying the adequate thermodynamic expressions. Some of them are briefly described.

In Kalghatgi's (1981) experimental study on blow-out phenomenon, for high flow rates, the pressure in the settling chamber was measured using either a water or a mercury manometer. This pressure was taken to be the stagnation pressure. The stagnation temperature was assumed to be equal to the ambient temperature, which was taken as 290 K.

In Gore's *et al.* (1986) experimental study, pressures and temperatures just upstream of the restriction orifice outlet were measured continuously. A metering orifice plate was used.

McCaffrey and Evans (1986) used a flange-tap orifice meter for measuring the methane flow rate.

Schefer *et al.* (2007) performed an experimental study on high-pressure vertical hydrogen jet flames (pressures up to 40.1 MPa), in which both the stagnation chamber pressure and temperature were measured. The temperature was measured with a K-type thermocouple, while the pressure was measured using a piezoresistive pressure transducer.

In Imamura's *et al.* (2008) experimental study on horizontal hydrogen jet flames, a strain-gauge-type pressure transducer was installed near the nozzle, while the ambient air temperature was measured by a K-type thermocouple. The temperature upstream of the vent orifice was assumed to be the temperature of the ambient air.

From this literature survey it was decided to obtain the mass flow rate from pressure and temperature measurements, as a function of pressure drop over the outlet orifice and assuming that the jet is expanded isentropically to atmospheric pressure (see Appendix I). The required variables for this calculation are the pressure in the pipe just upstream of the orifice and the temperature at the orifice exit; these were measured with an electronic pressure transmitter located at 0.05 m of the release fuel source and an uncoated K-type thermocouple located at the orifice jet exit. These instruments are described in section 2.4.

2.4. The experimental set-up

The experimental installation with which jet fires were obtained under sonic and subsonic conditions, concerned:

a. A 4 m^3 pressurized vessel located on an upper site. The fuel was liquefied propane with a composition of 97% propane (volume), 1.5% butane and 1.5% of other gases such as hydrogen, methane and nitrogen (Fig. 2.4).

Figure 2.4. View of the pressurized vessel containing liquefied propane (approximate conditions: temperature, 25ºC; equilibrium vapour pressure, 9.5 bar).

b. The liquefied propane flowed through a non-insulated pipe (approximately 50 m length) up to the jet fire location (Fig. 2.5); along this path it was vaporized.

c. The fuel was released through a vertically orientated pipe (Fig. 2.5), where interchangeable nozzles, ranging from 2 mm to 43.1 mm, could be installed. The last orifice diameter represented a full rupture of the pipeline (full open pipe, without any nozzle).

Figure 2.5. The release pipe.

The vertical pipe exit was located upward with the fuel outlet at a height of 0.5 m above ground level. Sonic and subsonic gas jet fires were obtained by using six nozzles with circular round orifices; the orifice exit diameters of 10, 12.75, 15, 20, 30 and 43.1 mm were used and studied. The blow-out phenomenon (self extinction of the jet flames immediately after ignition) was observed with the smallest nozzles ranging from 2 mm to 10 mm.

2.5. Instrumentation

The pressure of the fuel gas was measured in each test; the measurement was effectuated at 0.05 m upstream of the outlet orifice, using an electronic pressure transmitter (Barksdale, type UPA5). This was taken as the upstream stagnation pressure of the flow.

The temperature at the exit orifice diameter was continuously measured using an uncoated K-type thermocouple located at the jet outlet orifice. The jet velocity at the outlet orifice and the mass flow rate for both sonic and subsonic regimes could then be calculated assuming isentropic expansion between the stagnation point and the orifice jet exit by applying the appropriate thermodynamic relationships (see Appendix I).

A scheme of the nozzles arrangement and the location of the pressure transmitter and the uncoated K-type thermocouple can be seen in Fig. 2.6. Photographs of the electronic pressure transmitter equipment are shown in Fig. 2.7. Its main features are described in Table 2.3.

Table 2.3. Features of the electronic pressure transmitter

	Electronic Pressure Transmitter
Brand	Barksdale
Model	UPA 5 (0434-011)
Pressure range	0 – 10 bar
Output signal	4 – 20 mA/2-wire
Supply	12 – 36 V DC
Mechanical connection	G14" external thread
Permissible medium temperature	from -25ºC to 125ºC
Permissible electronic temperature	from -25ºC to 85ºC[a]

[a] The equipment was isolated with rock-wool during the experimental tests.

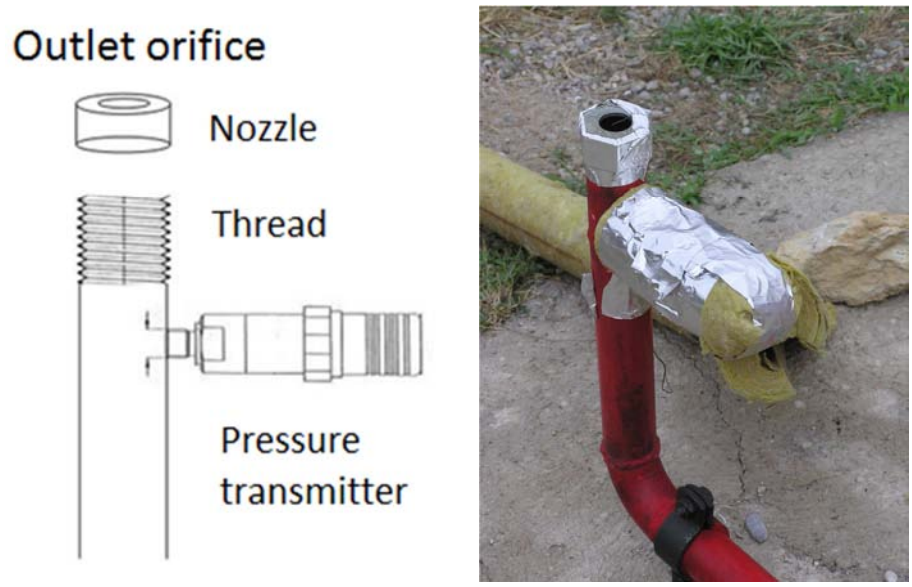

Figure 2.6. Pressure measurement equipment (electronic pressure transmitter) located 0.05 m upstream the outlet orifice and temperature measurement equipment at the nozzle jet exit (uncoated K-type thermocouple (nickel-chromium/nickel-aluminium)).

Figure 2.7. Electronic pressure transmitter (Barksdale, type UPA5).

The jet flame axial temperature distribution was measured using a set of thermocouples along the jet flame centreline. Three B-type and one S-type uncoated thermocouples (0.35 mm diameter) were used; higher temperatures (~ 1800 K) can be measured with these type of thermocouples (Table 2.4).

The four thermocouples were arranged on a mast at different heights above ground level, as shown in Fig. 2.8, in an attempt to cover all the flame regions, taking into account the lift-off of the jet flame (i.e. the centreline distance from the gas release point to the start of the detached and stabilized flame). The thermocouples were supported on a series of metallic bars, and insulated with rock-wool. These bars showed excellent mechanical strength at high temperatures (up to 1900 K) and good resistance to thermal shock. During the tests, the positions of the thermocouples were changed as required according to flame length. These are discussed in a later section concerning the experimental tests (see Table 2.7).

Figure 2.8. The temperature measurement equipment: a set of three thermocouples B-type and one S-type measuring the temperature distribution on the jet flame axis.

An additional K-type thermocouple was placed at the jet outlet. Some features of the diverse thermocouples used in the present study are shown in Table 2.4.

Table 2.4. Features of the thermocouples used in the present study

	Thermocouple	Thermocouple	Thermocouple
Type	K	S	B
Composition	Nickel – Chromium vs. Nickel – Aluminium	Platinum-10% Rhodium vs. Platinum	Platinum-30% Rhodium vs. Platinum-6% Rhodium
Maximum temperature range	from -200ºC to 1250ºC	from 0ºC to 1450ºC	from 0ºC to 1700ºC

The radiative heat intensity from jet flames was measured with three heat flow sensors (Schmidt-Boelter type) located at different distances from the jet flame axis; these positions were varied during the experiments. These are discussed in a later section concerning the experimental tests (see Table 2.8). They were 64 series transducers of the MEDTHERM Schmidt-Boelter thermopile type sensor, supplied by the Pamir Electronics Corporation. In this type of sensor, heat flux is absorbed at the sensor surface and is transferred to an integral heat sink that remains at a different temperature than the sensor surface. The difference in temperature between two selected points along the path of the heat flow from the sensor to the sink is a function of the heat being transferred, and a function of the net absorbed heat flux. At these two points, the transducers have thermopiles to form a differential thermoelectric circuit, thus providing a self-generated emf at the output leads that is directly proportional to the heat transfer rate.

In this work, the heat flow sensors (Fig. 2.9) had two transducers 64-2-16 model, measuring the total heat (convection plus radiation), and a heat radiometer/transducer 64-20T-20R(S)-20898 model, measuring total heat and radiation apart. The two heat flux transducers were identified as HTF-1 and HTF-2, and the heat flux transducer and radiometer was named as HFTR: HFTR(T) for the measures of total heat and HFTR(R) for the measures of radiation. The features of these heat flow sensors are shown in Table 2.5.

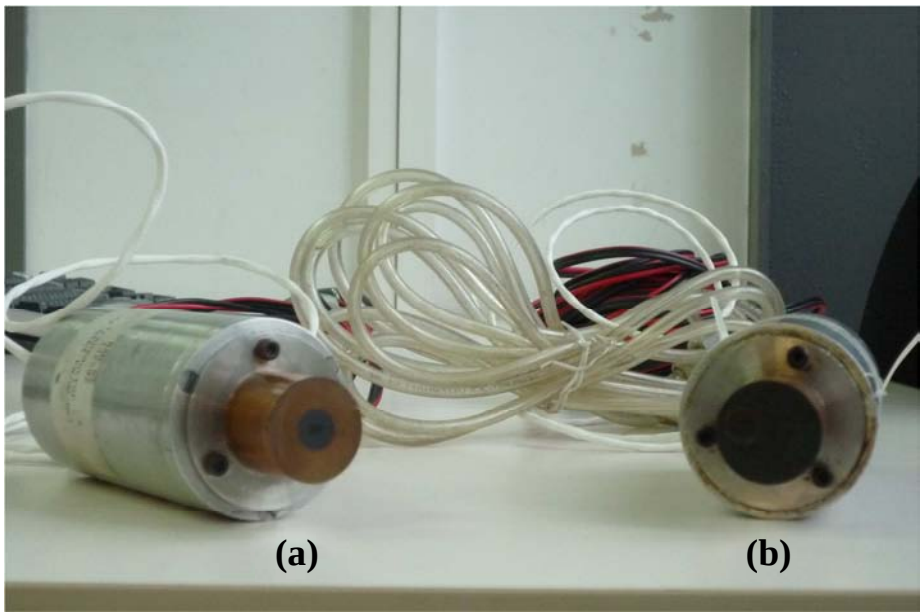

Figure 2.9. Views of: (a) heat flux transducer 64-2-16 model; (b) heat flux transducer and radiometer 64-20T-20R(S)-20898 model.

Table 2.5. Features of the heat flow sensors used in this work

	Model: 64-2-16	Model: 64-20T-20R(S)-20898
Measurement range	0 – 23 kW/m^2 (0 – 2 $BTU \cdot ft^{-2} \cdot s^{-1}$)	0 – 227 kW/m^2 (0 – 20 $BTU \cdot ft^{-2} \cdot s^{-1}$)
Output signal	Linear output, 0 – 12 mV	Linear output, 0 – 15 mV
Maximum allowable operating body temperature	200 ºC	200 ºC
Repeatability	± 0.5%	± 0.5%
Calibration expanded uncertainty	± 3% for ranges to 250 $BTU \cdot ft^{-2} \cdot s^{-1}$, coverage factor k = 2, for approximate 95% confidence level	± 3% for ranges to 250 $BTU \cdot ft^{-2} \cdot s^{-1}$, coverage factor k = 2, for approximate 95% confidence level

Sensor absorptance	0.94 nominal, from 0.3 to 15 μm	0.94 nominal, from 0.3 to 15 μm
Lead wire	24 AWG stranded copper twisted pair. Teflon insulation over each, braided copper shield. Teflon jacket overall 36" standard length with stripped ends	24 AWG stranded copper twisted pair. Teflon insulation over each, braided copper shield. Teflon jacket overall 36" standard length with stripped ends
Time constants	50 – 100 BTU·ft^{-2}·s^{-1}: 120 ms	50 – 100 BTU·ft^{-2}·s^{-1}: 120 ms
	2 – 30 BTU·ft^{-2}·s^{-1}: 250 ms	2 – 30 BTU·ft^{-2}·s^{-1}: 250 ms
	0.2 – 1 BTU·ft^{-2}·s^{-1}: 350 ms	0.2 – 1 BTU·ft^{-2}·s^{-1}: 350 ms
Sensor type	Medtherm Schmidt-Boelter thermopile	Medtherm Schmidt-Boelter thermopile
Nominal impedance	Less than 1000 Ω (250 Ω nominal)	Less than 1000 Ω (250 Ω nominal)
Responsivity (kW·m^2)/mV	HTF-1: 1.9715 kW·m^2/mV and HTF-2: 2.0464 kW·m^2/mV	HFTR(R): 15.18 kW·m^2/mV and HFTR(T): 15.29 kW·m^2/mV
Radiometer	–	Sapphire window; angle of view of 180º; transmittance (for a wavelength from 0.2 to 4 μm and a thickness of 0.5 mm)

During the tests, the nearest heat flow sensor (the heat radiometer/transducer 64-20T-20R(S)-20898 model) to the jet flame was supplied with a water cooling system (Fig. 2.10).

Figure. 2.10. Heat flux sensor: heat flux transducer and radiometer 64-20T-20R(S)-20898 model, with a water cooling system.

The experiments were also filmed with two video cameras registering visible light (VHS) and an infrared thermographic camera (Flir Systems, AGEMA 570), since the transparency of the flames can sometimes make it very difficult to analyse the geometrical parameters obtained with a common video camera.

These visible and infrared images allowed the study, analysis and determination of the main geometrical features of the flames (flame size and shape). Twenty five digital images per second were obtained from the video cameras, which resolutions were 320 x 240 pixels and 384 x 288 pixels, respectively; while four images per second were obtained form the IR camera. The visible cameras were located orthogonally to the flame, and one of them was located next to the infrared thermographic camera. This latter type of camera has a focal plane array (FPA) detector of 320 x 240 pixels, which is sensitive to radiation at a certain wavelength. The spectral range of the model used in this study was 7.5-13 μm, and the field of vision was 24º horizontal x 18º vertical. A photograph of the infrared camera is shown in Fig. 2.11.

Figure 2.11.View of the infrared thermographic camera (Flir Systems, AGEMA 570).

A meteorological weather station (Davis Instruments, GroWeather) continuously recorded the following meteorological conditions: wind direction, wind speed, ambient temperature, relative humidity and solar radiation. These variables are important because they may directly or indirectly affect both the jet flame and the measurement instruments. A view of the meteorological weather station used in the present study is shown in Fig. 2.12.

Figure 2.12. A view of the meteorological weather station (Davis Instruments, GroWeather).

A scheme of the experimental set-up is shown in Fig. 2.13: fuel feeding system, thermocouples mast, video and infrared thermographic cameras, radiometers and detail of the gas outlet arrangement.

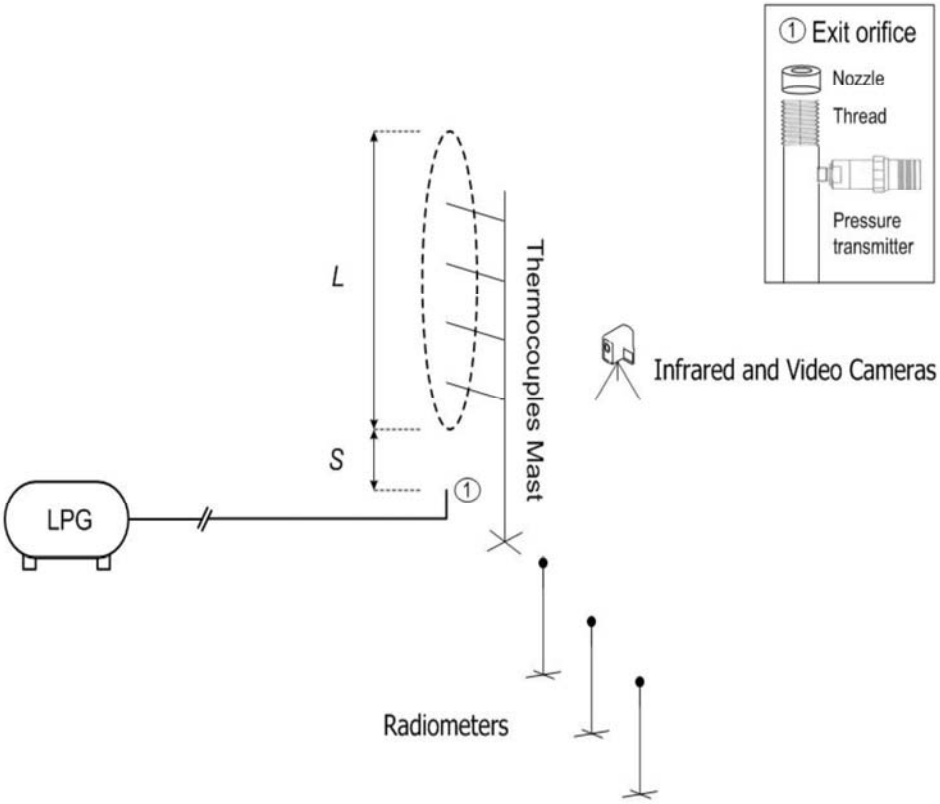

Figure 2.13. Experimental set-up.

2.6. Experimental data collection

The experimental data were collected and registered in real time by using a FieldPoint device hardware. It consisted of a FP-1001 communication module (RS-485, 115 kb·s^{-1}), three connection terminals FP-TB-1 and three input/output (I/O) modules. An RS-485 communication port was used to connect the I/O modules to the FP-1001 module, which was connected to the computer and to the power supply. The FP-TB-1 terminal connection bases were used to support the I/O modules, to guarantee a constant power

supply, and to serve as an internal communication system between the I/O and FP-1001 modules. Two of the I/O modules were FP-TC-120 modules. The thermocouples and radiometers were connected to each one of these FP-TC-120 modules and the measurements were stored by the computer. The other I/O module was of type FP-AI-110 and was used to collect the information generated by the electronic pressure transmitter (Fig. 2.14).

Figure 2.14. FieldPoint module used for data collection.

Two laptops were used to collect the data from the different equipments. They recorded the measurement and controlled the devices operation. It is important to note that the instruments provided four measurements per second. The IR camera and the FieldPoint were connected to one of the computers, through PCMCIA and RS-485 connections, respectively; the meteorological station was connected to the second computer by a RS-232 connection. Furthermore, the two laptops were linked via a network in order to synchronize the data collection. The FireAll software, created (Muñoz, 2005) and modified at CERTEC was installed on the computers to manage the operation of each one of the devices used in the tests. This software was used to synchronize the point at which the computers start recording measurements, to synchronize the measurements, and to make the data

easier to analyse by generating separate files for each experiment, letting further possible processing and analysis of the data. These devices and their connection are shown in Fig. 2.15.

The software FireAll also allowed the data being registered at the same time in both laptops, and the registration of notes during the tests; in that way, the ignition of the jet flame, the start of two-phase flow (occurred in some tests), the end of the jet flame, etc., could be registered.

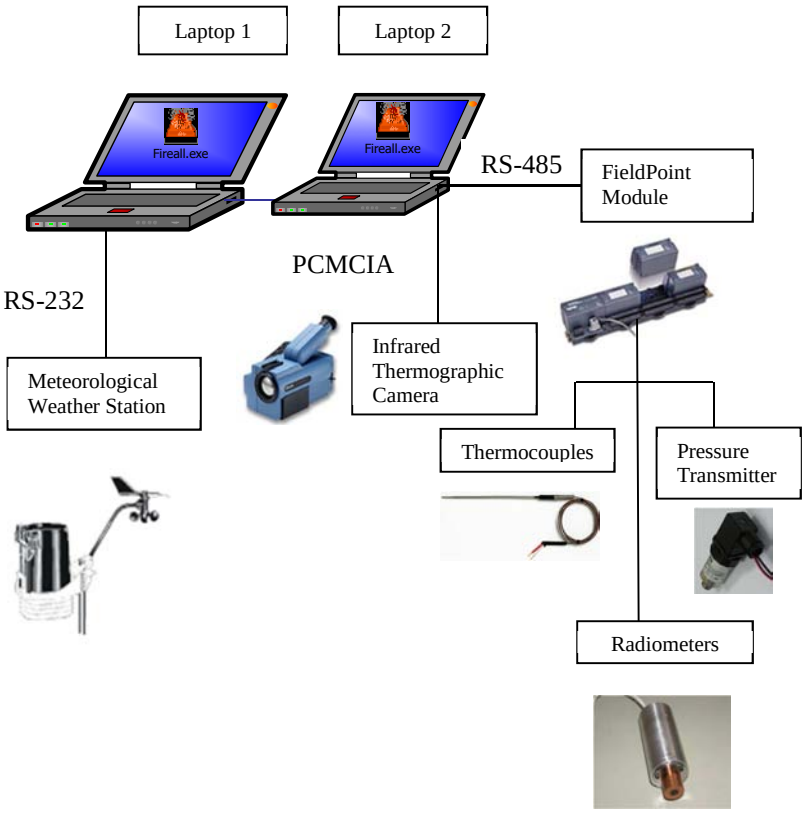

Figure 2.15. Measurement devices and their communications interfaces.

2.7. Experimental tests

Twenty large-scale vertical jet fire experiments were carried out, of which only the gas jet flames in the absence of cross winds were selected and analyzed. The geometrical and thermal jet flame features (flame size,

shape, radiative heat intensity from jet flames, jet flame axial temperatures, etc.) showed to be a function of the fuel condition: gas phase and two-phase flow jet flames (Fig. 2.16).

Figure 2.16. Visible images of vertical jet flames of propane obtained with: gas phase and d = 12.75 mm (left); two-phase flow and d = 43.1 mm (right).

The features of jet flames fed by gas or by a gas-liquid mixture were found to be significantly different. The jet fires fed by gas experienced a very good combustion and the flames were almost transparent. Instead, the flames fed by a two-phase flow mixture were yellow and very luminous, emitting a higher thermal radiation intensity (Fig 2.16); this was due to the poor combustion. The jet flame length is also increased significantly when the flow changed from gas to gas-liquid mixture; the variation found during one of the carried out tests can be seen in Fig. 2.17.

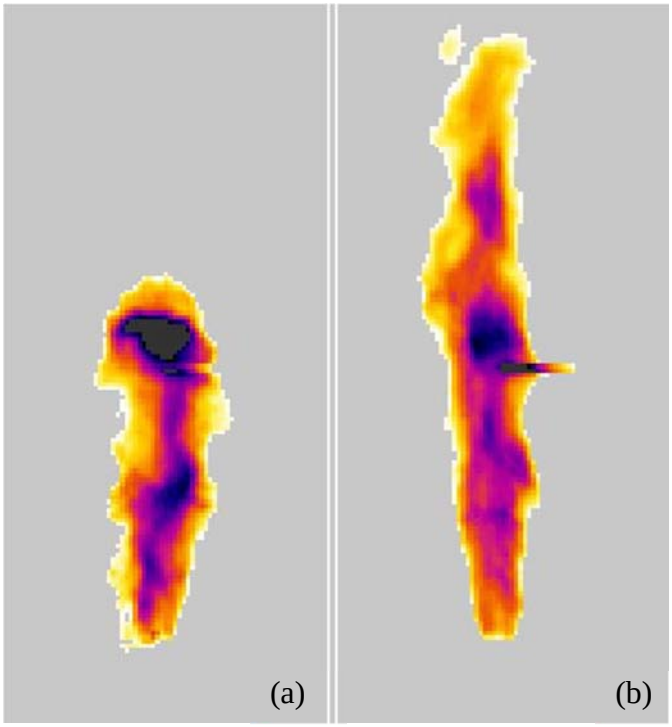

Figure 2.17. Infrared images of jet flames obtained with a 10 mm outlet diameter: (a) gas flow, total flame height (*H*) 2.6 m, thermal radiation intensity (*I*) 1.5 kW/m^2; (b) two-phase flow, H = 4.6 m, I = 2.2 kW/m^2 (right). The flame length (*H*) was measured from the fuel source to the flame tip along the centreline of the jet flame. The position of outlet orifice is shown by the bottom of the figure. The isotherm of 800 K defines the jet flame contour. *I* values concern the measurements obtained with the heat flux sensor located at a 2.8 m radial distance from the jet flame axis and 1 m above the ground.

2.7.1. Test procedure

Preliminary tests were developed to characterize the release, identify the best position for the equipment, adjust the instrumentation and test the operation of the diverse system items.

The tests carried out were very weather dependant; they were undertaken on days when the local weather forecast, obtained from the Meteorological Service of Catalonia, predicted acceptable weather conditions and local observations supported the predictions. Cloud cover presented no difficulties in undertaking tests, but trials were not undertaken with precipitation of any kind.

The time required for the test procedure was around two hours, as follows:

Before the test:

(a) The fire extinction system used during the development of the experimental tests was placed. It consisted of two firemen near to the experimental set-up, with hoses so as to extinguish the fire and/or protect the person who ignited the fire; a 25 mm hose with a diffusing mouth and a person who continuously controlled the supply or deprive of the fuel, by opening or closing the valve from which the fuel was released (this valve was located in an intermediate point between the experimental release point and the storage vessel, located in an upper site).

(b) The thermocouples mast was placed in position in the field. The four thermocouples (3 B-type and a S-type thermocouples) were supported on a series of metallic bars at different heights above ground level (4 positions were possible), insulated with rock-wool, and arranged on the mast. This arrangement is shown in Fig. 2.9. This distribution was chosen in an attempt to cover all the flame regions, taking into account the lift-off of the jet flame.

(c) An additional K-type thermocouple was placed at the jet outlet.

(d) The pressure transmitter was placed in position in the gas pipe. The pressure transmitter was located at 0.05 m from the jet outlet orifice and insulated with rock-wool.

(e) The heat flux sensors were placed in position in the field. The water cooling system for one of this heat flux sensors (the one located nearest to the jet flame: the heat radiometer/transducer 64-20T-20R(S)-20898 model) was also placed.

(f) The meteorological station was placed in position in the field.

(g) Infrared and video cameras in the field (the positions of the cameras during the different tests can be seen in Table 2.6) were set to record mode.

(h) The following devices: heat flux sensors, thermocouples and the pressure transmitter were connected to the Field Point module.

(i) The Field Point module and the infrared camera were connected to one of the two laptops.

(j) The meteorological station was connected to a second different laptop.

(k) The two laptops were linked via a network.

(l) Verification of the connection between the diverse equipments (thermocouples, heat flux sensors, pressure transmitter, and a laptop) to the Field Point module. The connections between the Field Point module and one of the laptops, between the infrared camera and this laptop, the connection between the meteorological station and the second laptop, and the connection between both laptops were also verified.

(m) The diverse devices (thermocouples, heat flux sensors, water cooling system for one of the heat flux sensor, pressure transmitter, meteorological station, video recording equipments and fire extinction system) and the data collection system (Field Point module and two laptops) were checked.

(n) Testing and verification of the data collection from the above-mentioned equipments.

(o) Registering of the positions of the equipments in the experimental data sheets.

(p) The ignition source (a torch) was put in place; the torch consisted of a burning rag on a long pole.

(q) Notification of the equipments being ready for the accomplishment of the tests.

The positions of the cameras, thermocouples and heat flux sensors during the different tests are shown in Tables 2.6, 2.7 and 2.8, respectively.

Accomplishment of the tests:

(a) The test site was evacuated of personnel and confirmed as empty of people, with the exception of the people, protected with fire fighting clothing (the two firemen, the person who ignited the jet flames and the one who controlled the release fuel flow), involved during the development of the experimental tests.

(b) The ignition source was lit.

(c) The data-collection system was started.

(d) The data collection programme FireAll was left to run to completion.

(e) The video recording equipments (infrared and video cameras) were started.

(f) The manually operated valves in the propane supply line were opened.

(g) The propane flowed through the pipeline, being released from the pressurized vessel up to the outlet.

(h) Downstream the fuel release point, the propane-jet flow at the outlet nozzle was ignited by the ignition source.

(i) The propane flow rate was increased by opening the main manually operated release valve.

(j) The jet flame reached stationary state. The transient state lasted approximately 0.8-1.5 s.

(k) The flow rate was checked and manually increased by opening the valve. Thus, the tests covered a wide range of mass flow rates and jet exit velocities. Each test lasted between one and five minutes.

(l) Most of the times, a post test investigation, some minutes after the flame had been extinguished and the pipeline had been defrosted, was carried out. During some tests, the pipeline was frozen (Fig. 2.18) due to the existence of two-phase flow.

Figure 2.18. View of the frozen pipe due to the existence of two-phase flow.

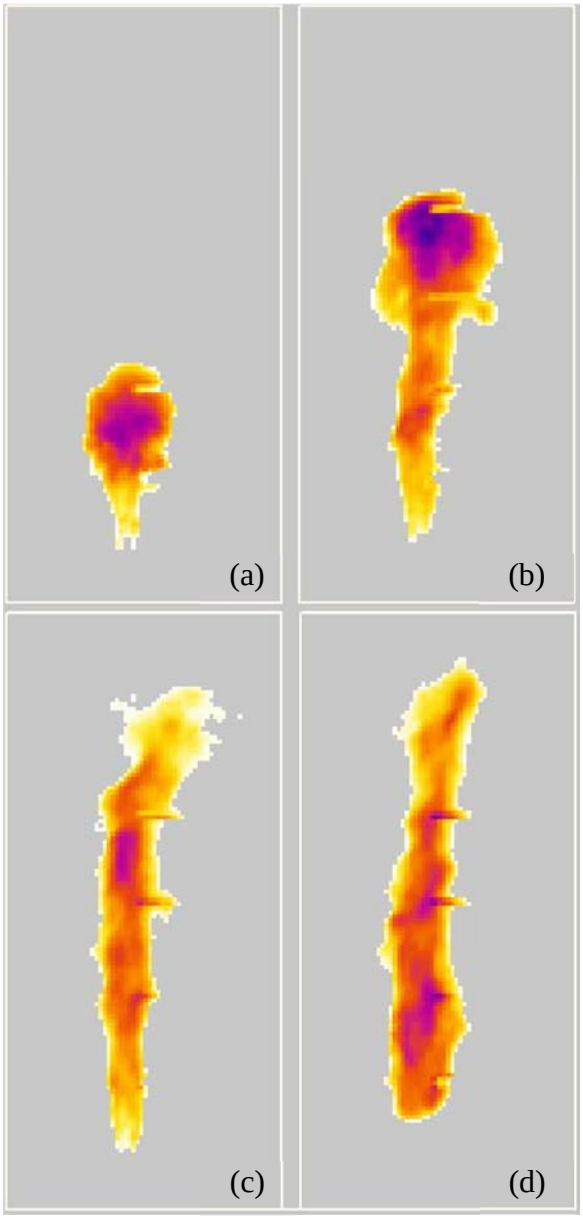

Figure 2.19. Successive infrared images of a vertical sonic jet fire of propane at different times. The jet flame shown in (a) corresponds to a time very close to the initial flame ignition. The time interval between the successive infrared images is 0.25 s. The jet exit diameter (d) is 12.75 mm. The position of outlet orifice shown by the bottom horizontal line. The isotherm of 800 K defines the jet flame contour.

Figure 2.19 shows typical single-frame infrared images of jet flames (sonic flow, d = 12.75 mm) at various times from the starting of the test (ignition of the jet). Fig. 2.19-a corresponds to a time very close to the initial flame ignition, and the flame is still very short. Figs. 2.19-b and (c), which are images taken at slightly later times (i.e. 0.25 and 0.5 s after Fig. 2.19-a, respectively). The final image, Fig. 2.19-d, corresponds to a time of 1 s where the fully developed flame has reached the steady state, stabilizing at a certain distance (lift-off distance) from the jet exit.

End of test and one hour after test:

(a) The propane flow was manually stopped by closing the fuel release valve, extinguishing the jet flame.

(b) At the end of the last test, once it was safe to do so, all the equipment were uninstalled.

Photographs were taken before, during and after the tests.

2.7.2. Test conditions

Twenty open field experiments on turbulent vertical sonic and subsonic jet flames were carried out. These are listed in Table 2.6; the distances at which the video cameras registering visible light (VHS) and the infrared thermographic camera (IR) were located away from the jet exit are also included.

The experimental tests were named with the following nomenclature: a) Jet Fire Test (JFT) followed by b) test number, including 3 digits (e.g. 001); the tests performed in the same day had the same test number; and c) experiment number, including two digits (e.g. 01). The tests performed in the same day followed a sequence, indicated by the experiment number. For example the second experiment done in the fourth day of tests was named JFT-004-02.

Table 2.6. Experimental tests performed on vertical jet flames of propane

No. Test	Test name	*d* (mm)	IR camera (m)	Video camera 1 (m)	Video camera 2 (m)
1	JFT-005-01	25.5	30.3	30.3	31
2	JFT-005-02	25.5	30.3	30.3	31
3	JFT-005-03	25.5	30.3	30.3	31
4	JFT-005-04	10	30.3	30.3	31
5	JFT-005-05	10	30.3	30.3	31
6	JFT-005-06	20	30.3	30.3	31
7	JFT-005-07	20	30.3	30.3	31
8	JFT-005-08	20	30.3	30.3	31
9	JFT-005-09	20	30.3	30	31
10	JFT-005-010	20	30.3	30	31
11	JFT-005-011	15	30.3	30	31
12	JFT-005-012	15	30.3	30	31
13	JFT-006-01	12.75	34	34	–
14	JFT-006-02	12.75	34	34	–
15	JFT-006-03	30	34	34	–
16	JFT-006-04	35	34	34	–
17	JFT-006-05	43.1	34	34	–
18	JFT-006-06	43.1	34	34	–
19	JFT-006-07	20	34	34	–
20	JFT-006-08	43.1	34	34	–

The positions of the thermocouples above ground level are listed in Table 2.7. The different types of thermocouples were named as TB-1, TB-2 and TB-3 for the three B-type thermocouples, respectively; and the S-type and K-type thermocouples were named as TS and TK, respectively.

Table 2.7. Distances and positions at which the thermocouples were located in the experimental field during the tests

Test name	*d* (mm)	TB-1 (m)	TB-2 (m)	TB-3 (m)	TS (m)	TK (m)
JFT-005-01	25.5	–	–	3.7	–	0.5
JFT-005-02	25.5	–	–	3.7	–	0.5
JFT-005-03	25.5	–	–	3.7	–	0.5
JFT-005-04	10	–	–	3.7	–	0.5
JFT-005-05	10	–	–	3.7	–	0.5
JFT-005-06	20	–	–	3.7	–	0.5
JFT-005-07	20	–	–	3.7	–	0.5
JFT-005-08	20	–	–	3.7	–	0.5
JFT-005-09	20	–	–	3.7	–	0.5
JFT-005-010	20	–	–	3.7	–	0.5
JFT-005-011	15	–	–	3.7	–	0.5
JFT-005-012	15	–	–	3.7	–	0.5
JFT-006-01	12.75	1.8	2.7	3.6	4.5	0.5
JFT-006-02	12.75	1.8	2.7	3.6	4.5	0.5
JFT-006-03	30	1.8	2.7	3.6	4.5	0.5
JFT-006-04	35	1.8	2.7	3.6	4.5	0.5
JFT-006-05	43.1	1.8	2.7	3.6	4.5	0.5
JFT-006-06	43.1	1.8	2.7	3.6	4.5	0.5
JFT-006-07	20	1.8	2.7	3.6	4.5	0.5
JFT-006-08	43.1	1.8	2.7	3.6	4.5	0.5

The positions of the heat flux sensors (x = distance between the release source and the equipment and z = distance above ground level) used are listed in Table 2.8. The two heat flux transducers were identified as HTF-1 and HTF-2, and the heat flux transducer and radiometer was named as HFTR.

Table 2.8. Distances and positions at which the heat flow sensors were located in the experimental field during the tests

Test name	*d* (mm)	HFTR [*x*] (m)	HFTR [*z*] (m)	HFT-1 [*x*] (m)	HFT-1 [*z*] (m)	HFT-2 [*x*] (m)	HFT-2 [*z*] (m)
JFT-005-01	25.5	2.8	1	5.1	1.5	10	1.5
JFT-005-02	25.5	2.8	1	5.1	1.5	10	1.5
JFT-005-03	25.5	2.8	1	5.1	1.5	10	1.5
JFT-005-04	10	2.8	1	5.1	1.5	10	1.5
JFT-005-05	10	2.8	1	5.1	1.5	10	1.5
JFT-005-06	20	2.8	1	5.1	1.5	10	1.5
JFT-005-07	20	2.8	1	5.1	1.5	10	1.5
JFT-005-08	20	2.8	1	5.1	1.5	10	1.5
JFT-005-09	20	2.8	1	5.1	1.5	10	1.5
JFT-005-010	20	2.8	1	5.1	1.5	10	1.5
JFT-005-011	15	2.8	1	5.1	1.5	10	1.5
JFT-005-012	15	2.8	1	5.1	1.5	10	1.5
JFT-006-01	12.75	1.1	0.9	5	1.5	3	1.5
JFT-006-02	12.75	1.1	0.9	5	1.5	3	1.5
JFT-006-03	30	1.1	0.9	5	1.5	3	1.5
JFT-006-04	35	1.1	0.9	5	1.5	3	1.5
JFT-006-05	43.1	1.1	0.9	5	1.5	3	1.5
JFT-006-06	43.1	1.1	0.9	5	1.5	3	1.5
JFT-006-07	20	1.1	0.9	5	1.5	3	1.5
JFT-006-08	43.1	1.1	0.9	5	1.5	3	1.5

The information regarding the position of the equipment (thermocouples, heat flux sensors, video and infrared cameras, etc.) in the field, and other data regarding the release orientation, the outlet orifice diameter, etc., were registered in experimental test data sheets.

Only the tests in which the jet flame was released in the absence of cross winds were considered. Thus, a total of eleven tests were selected and analysed. The present experimental results to be reported were obtained with six circular nozzles having diameters of 10, 12.75, 15, 20, 30 and 43.1 mm. The conditions at which these eleven tests were performed are listed in Table 2.9.

Table 2.9. Range of values in the selected experimental tests

Mass flow rate (m), $kg \cdot s^{-1}$	Reynolds number	Stagnation pressure (P_{in}), bar	Jet exit velocity, $m \cdot s^{-1}$	Ambient temperature, K	Relative humidity, %
0.01 – 0.54	$7 \cdot 10^4 – 4 \cdot 10^6$	1.02 – 6.43	24 – 256	302 – 305	44 – 50

From Table 2.9 it can be noted that the entire jet flames were on the turbulent regime. Both subsonic and sonic jet fires were obtained.

2.8. Safety measures

In order to reduce the diverse risks originated by the development of the jet fire experiments, a “Safety Plan” was followed. It was taken and modified from the previous safety plan applied in the outdoor pool fire tests carried out by Chatris (2001), Muñoz (2005) and Ferrero (2006). The protection measures were mainly focused to decrease the risk provoked by the thermal radiation reaching the experimental facility, the measuring equipment, and the people involved in the performed tests.

The main measures of protection applied to the experimental facility and to the measuring equipment consisted on the insulation of those instruments, cables or equipment that were in the operational range of the jet flame, this latter considered as a thermal radiation level higher than 3 $kW \cdot m^{-2}$, such as in the experimental studies of Muñoz (2005) and Ferrero (2006). The video cameras, the infrared thermographic camera, and the data collection system were located enough far away (~ 30 m; see Table 2.6) from the jet flames to diminish the radiation heat effects.

Other measures of protection followed during the development of the experimental tests consisted on:

(a) Available methods to extinguish the fire during the development of jet flames: (a.1) First of all, during all the tests a person was always placed next to the valves that controlled the flow exit of the fuel. In an emergency case, these valves could be manually closed, stopping the fuel flow.

(a.2) Two firemen were placed near the experimental set-up ready with hoses so as to extinguish the fire and/or protect the person who ignited the fire. It should be noted that no accident was caused during the ignition of the tests. In the cases where blow-out phenomenon occurred, the fuel flow was manually stopped. These firemen wore fire-fighting clothes.

(a.3) And finally, a 25 mm hose with a diffusing mouth could allow, in a necessary case, the extinction of the fire.

(b) The storage vessel was located in an upper site, far away from the release fuel point. It was provided with the required safety instruments.

(c) The person who ignited the jet flame wore fire-fighting clothes.

(d) All the people involved in the tests were always placed at a minimum safety distance of 30 m from the fuel release point to prevent any accident. This previously estimated distance was enough to protect the people, according to the bearable radiation limit for a person of 5 $kW \cdot m^{-2}$ (American Petroleum Institute Recommended Practice 521, 1997).

3. FLAME SIZE

A better understanding of jet flame size is essential to increase the accuracy in the prediction of the effects of jet fires. This subject has been addressed by several authors through both experimental and theoretical approaches, in which a number of correlations for jet flame size have been suggested. Nevertheless, the prediction of the flame size is still subjected to a significant error since most of the work has been focused on small-scale jet fires or subsonic flames; as mentioned earlier, these conditions significantly differ from those found in real accidental jet fires, where larger flames and sonic exit velocities are usually found.

Therefore, an effort has been done to obtain experimental data on large flames at these conditions.

3.1. Jet flame length

The prediction of jet flame length –or, better, the jet flame reach– is of practical interest for fire safety and process design, as it determines the zone over which there can be impingement of the jet flames on other equipment. Thus, various correlations have been proposed by diverse authors for predicting the length of vertical jet fires in the absence of cross winds. Most of these expressions have been obtained from the analysis of the variation of jet fire length as a function of certain operating variables (outlet orifice diameter, jet exit velocity, mass flow rate, heat of combustion, etc.). These previous relevant studies are discussed in view of our findings, being categorized according to whether or not they involve physicochemical parameters.

3.1.1. Correlations without any chemical parameters

Over the buoyancy-dominated jet regime, the prediction of jet flame height by Eq. (3.1) has been suggested from several experimental and theoretical studies (see Table 3.1). This expression relates the jet flame height (H) normalized by the outlet orifice diameter (d) to the Froude number (Fr):

$$\frac{H}{d} = a \cdot Fr^{n} \tag{3.1}$$

Table 3.1 summarizes the information about the type of fuel, the recommended values for the constants a and n, and the Froude number range over which each expression can be applied according to the different authors.

From the information contained in this table, it can be seen that the length of jet flames in the transition from buoyancy to momentum-controlled jet regime is related to the type of fuel.

Beyond the buoyancy-dominated jet regime, at high flow rates, when higher jet velocities are reached, momentum-dominated jet regime essentially becomes the essential mechanism. In this regime, the dimensionless flame height (H/d) has been found for some authors to be independent of Fr, reaching the H/d ratio a constant value which depends on the type of fuel.

In Table 3.2 the recommended values for the dimensionless flame height and the type of fuel, based on experimental and theoretical studies, are shown.

This table shows that the suggested values can be successfully applied to each gas separately, but could not embrace more than one fuel. It should be noted that the theoretical study of Bagster and Schubach (1996) concerns only jet flames in the buoyancy-dominated regime. In McCaffrey's (1989) experimental study, jet flames in the momentum-dominated regime were obtained; however, the three data points obtained in this region could not give support to a constant H/d value for the momentum-dominated regime.

Table 3.1. Values of *a*, *n* and *Fr* ranges of applicability of Eq. (3.1)

Author	Fuel	*Fr* range	*a*	*n*
Shevyakov and Komov (1977)	Hydrogen	Up to $1\cdot10^5$	14	0.2
		From $1\cdot10^5$ to $2\cdot10^6$	24	0.14
Suris *et al*. (1977)	Methane[a]	Up to $3\cdot10^4$	29	0.2
	Methane[b]		27	0.2
	Methane[c]		28	0.23
	Propane[a]		40	0.2
	Propane[c]		36	0.23
	Hydrogen[b]		14	0.2
	Hydrogen[c]		14	0.23
Sonju and Hustad (1984)	Methane	Up to $1\cdot10^5$	21	0.2
	Propane		27	
Hustad and Sonju (1986)	Methane[d]	Up to $1\cdot10^5$	21	0.2
	Propane[d,e]		27	
McCaffrey (1989)[f]	Methane	Up to $3\cdot10^4$	28	0.2
Rokke *et al*. (1994)[g]	Propane	Up to $1\cdot10^5$	33	0.2
Bagster and Schubach (1996)	Methane[h]	Up to $1\cdot10^5$	23	0.2
Santos (2003)[i]	Methane	Up to $1\cdot10^4$	26	0.2
Santos and Costa (2005)[i]	Propane	Up to $2\cdot10^4$	36	0.2
	Ethylene	Up to $8.2\cdot10^4$	24	
Kiran and Mishra (2007)[i]	LPG[j]	Up to $4.5\cdot10^4$	30	0.2
Molkov (2009)	Hydrogen[k]	Up to $1\cdot10^5$	15.8	0.2
		From $1\cdot10^5$ to $2\cdot10^6$	37.5	0.13

[a] Results obtained by Seeger and Werthenbach (1970).
[b] Results obtained by Komov *et al*. (1973). [c] Results obtained by Hess (1964).
[d] Results obtained with circular and rectangular nozzles.
[e] This expression also correlates data on horizontal jet flames.
[f] For other fuels *a* is suggested to vary with the square root of the density ratio (ρ_e/ρ_∞).
[g] Results obtained with a propane mass fraction (Y_f) equal to 1.
[h] Results based on the experimental methane data of Sonju and Hustad (1984).
[i] The value of *H* was measured from the base of the flame to the flame tip.
[j] Fuel composition: 72% butane and 28% propane.
[k] Applying linear regression analysis to the Shevyakov and Komov correlation (1977).

Table 3.2. Values of the ratio *H/d* of turbulent jet flames

Author	Fuel	*H/d*
Baev *et al.* (1974)	Hydrogen	190
Shevyakov and Komov (1977)	Hydrogen	220
Sonju and Hustad (1984)[a]	Propane	250
Hustad and Sonju (1986)[a]	Propane	260
Rokke *et al.* (1994)[b]	Propane	300
Costa *et al.* (2004)[c]	Methane	160
Santos and Costa (2005)[c]	Ethyelne	226
	Propane	242
Kiran and Mishra (2007)[c]	LPG	269
Molkov (2009)[d]	Hydrogen	230

[a] Experimental methane data were only obtained in the buoyancy-dominated regime.
[b] Extrapolation of the experimental data obtained in the buoyancy-dominated regime.
[c] The value of *H* was measured from the base of the flame to the flame tip.
[d] Applying linear regression analysis to the correlation of Shevyakov and Komov (1977).

It is important to highlight that this kind of correlation (Eq. (3.1)) is useful and suitable only for subsonic jet exit velocities. However, at sonic velocities, for a given value of *Fr* (i.e. for a constant sonic velocity of the gas at the outlet orifice) and an orifice outlet diameter, larger flame heights can still be obtained. This is due to the fact that for a given outlet diameter, flame height increases with mass flow rate, as a result of increase pressure. At these conditions, Eq. (3.1) can not be applied anymore.

The jet flame height has also been expressed as a function of the Reynolds number (*Re*). Baev *et al.* (1974) obtained subsonic and supersonic hydrogen jet flames with nozzle diameters ranging from 1 to 16.65 mm, Mach numbers from 0.25 to 3.08, and outflow velocities from 0 to 2600 $m \cdot s^{-1}$. The flame height divided by the orifice exit diameter was found to be practically constant for sonic releases at the momentum-controlled limit. Baev and Yasakov (1974) found the dimensionless flame height of laminar

flames to be proportional to the Reynolds number of the outflowing jet; however, in the turbulent regime the dimensionless flame height was a function of only the type of fuel, reaching a constant value for a given gas: 190 and 400 for hydrogen and propane jet flames, respectively. These authors (Baev and Yasakov, 1974; Baev *et al.*, 1974) have also found laminar jet flames over the buoyancy-dominated regime to be a function of $Fr^{1/3} \cdot Re^{2/3}$.

Shevyakov and Komov (1977), who performed an experimental study on hydrogen jet flames obtained with nine stainless steel tubular burners of diameters ranging between 1.45 and 51.7 mm, found a dependence of dimensionless flame height on Reynolds number, up to Re = 20,000. In the turbulent regime, the dimensionless flame height was found to increase with Re approaching a limit of 220-230 for high Reynolds numbers (Re > 20,000). These authors also found that for the same Re the dimensionless flame height decreased when the diameter increased. This is in good agreement with the results obtained by Baev and Yasakov (1974) and Baev *et al.* (1974).

Another study developed by McCaffrey and Evans (1986) analyzed very large vertical methane jet flames (up to about 20 m in length), obtained with orifice diameters ranging between 38 and 102 mm. These authors suggested the flame height to be 200 times the orifice exit diameter (d) for subsonic flames, and 200 times the value of the fictitious exit diameter resulting after the supersonic expansion to atmospheric pressure, for sonic jet fires.

The jet flame height has also been found to be a function of the mass flow rate (Steward, 1970; Kalghatgi, 1984; Turns and Myhr, 1991; Shell Shepherd Desktop Technical Guide, 2003; Schefer *et al.*, 2004; Mogi *et al.*, 2005; Schefer *et al.*, 2006; Schefer *et al.*, 2007; Imamura *et al.*, 2008; Mogi and Horiguchi, 2009 and Molkov, 2009). In some of these studies, flame height was shown to be proportional to the 0.4-0.53 power of the mass flow rate (Shell Shepherd Desktop Technical Guide, 2003; Mogi *et al.*, 2005; Imamura *et al.*, 2008 and Mogi and Horiguchi, 2009). However, the flame height has been found to be a function not only of the mass flow rate but also of the orifice exit diameter (Steward, 1970; Kalghatgi, 1984; Schefer *et al.*, 2004; Schefer *et al.*, 2006 and Molkov, 2009). Flame height was found to increase with mass flow rate (m) for a constant orifice exit diameter (d); and for a constant m, the flame length increased with d (Kalghatgi, 1984).

Similarly, other authors have found the jet flame length to depend on the release pressure (Iwasaka *et al.*, 1979; Odgaard, 1983; Mogi *et al.*, 2005;

Imamura *et al.*, 2008; Mogi and Horiguchi, 2009) which, for a given orifice diameter, is directly related to the fuel mass flow rate.

3.1.2. Correlations involving chemical parameters

Expressions of jet flame heights as a function of diverse physicochemical parameters have also been developed; these are discussed in the next paragraphs.

The flame lengths of vertical jets flames were predicted by Hawthorne *et al.* (1949) by means of an expression based on turbulent small-scale jet flames up to 1 m in length, obtained with a variety of fuels (acetylene, carbon monoxide, city gas, hydrogen, propane, mixtures of CO_2-city gas and H_2-propane) and with orifice exit diameters ranging from 3 to 8 mm. This expression gave the turbulent flame height as a function of fuel molecular weight, flame temperature, air requirement and molal expansion ratio due to combustion. These authors found the flame height to be proportional to *d*. They also found that for turbulent flames the gas flow rate had no influence on the height, a result in conflict with the findings of later works (Steward, 1970; Kalghatgi, 1984; Turns and Myhr, 1991; Shell Shepherd Desktop Technical Guide, 2003; Schefer *et al.*, 2004; Mogi *et al.*, 2005; Schefer *et al.*, 2006; Schefer *et al.*, 2007; Imamura *et al.*, 2008; Mogi and Horiguchi, 2009 and Molkov *et al.*, 2009).

From a theoretical study, Baron (1954) obtained an equation identical to that proposed by Hawthorne *et al.* (1949) to predict the turbulent jet flame height. The empirical constant proposed by Hawthorne *et al.*, 5.3, was theoretically found to be 5.2 (Baron, 1954). The theoretical expression suggested by Baron was later compared with a tracing of a photograph of a subsonic small-scale city-gas jet flame, obtained with a 1 mm burner tube diameter, taken during experimental work with city-gas and butane flames of up to 1.35 m in length (Wohl *et al.*, 1949(a)). Except for the ragged edges caused by flickering, eliminated in the development of the theory, the agreement was satisfactory. However, the features of the subsonic small-scale city gas jet flame are quite different from the ones usually found in real accidental jet fires (larger jet flame heights and sonic jet exit velocities).

Odgaard *et al.* (1983) suggested four methods for estimating the flame height, based on underexpanded methane gas jets expanding from reservoir conditions of 15 MPa and 50ºC (Forsth and Odgaard, 1982). Three of the proposed methods apply the expression suggested by Hawthorne *et al.*

(1949), replacing the orifice exit diameter by the diameter of the jet at the location where the gas expansion ceases. The first method replaced the orifice exit diameter by the Mach disk diameter. In the second method, the orifice exit diameter was replaced by the expanded diameter, assuming conservation of momentum and a sonic jet velocity from orifice exit up to the point where expansion to ambient pressure was fulfilled. In the third method, the orifice exit diameter was replaced by an expanded diameter. The ratio between the expanded diameter and the orifice exit diameter assumed isentropic expansion from the reservoir at a certain pressure up to the orifice exit, the gas behaving like an ideal gas and the velocity being equal to the velocity of sound at both the jet exit and where the expansion ceases. It should be noted that this expression was also suggested for other gases than methane, assuming ideal gas behaviour. The calculations of the fourth method were based on the assumption that the methane gas behaved as an ideal gas, expanding isentropically from the reservoir pressure (up to 15 MPa) to the ambient pressure, thus obtaining an apparent diameter at the point where the expansion ceases. This apparent diameter was obtained from the mass balance and from the maximum diameter of the flame, assuming the shape of the jet flame as an inverted cone.

Becker and Liang (1978) found that their experimental data on flame lengths, together with the results published by Baev and Yasakov (1974) and Baev *et al.* (1974), correlated over a range of operating conditions that extended from the natural to the forced convection limits. Appropriate dimensionless parameters included the Richardson number, which determined the transition between forced and natural convection, and a term that included the adiabatic combustion temperature and the mean product molecular weight for the burning of a stoichiometric mixture of fuel and air to full chemical equilibrium. By applying such non-dimensional parameters, Kalghatgi's (1984) experimental data on flame lengths of different gases (ethylene, hydrogen, methane and propane) were found to collapse onto a single curve. However, in the forced convective limit, the fitting constants determined by Kalghatgi (1984) differed from those obtained by Becker and Liang (1978). The jet flame heights obtained by Kalghatgi (1984) were found to be smaller than the flame heights published by Becker and Liang (1978); ideal gas behaviour was assumed in both studies.

McCaffrey (1988) correlated experimental dimensionless flame heights concerning pool fires and jet fires obtained by several authors with a dimensionless heat release rate (Q^*). This dimensionless heat release rate is a function of the total heat release rate in the flame (based on the product of

fuel flow rate by the lower heating value), burner diameter, temperature, density, specific heat at constant pressure of the ambient gas, and of the acceleration of gravity; Q^* had been earlier suggested by Zukoski *et al.* (1981), from an study on a new technique for measuring mass flow rates in a buoyant fire plume, concerning pool fires.

Sugawa and Sakai (1997), using experimental subsonic propane jet flames, also found that the jet flame height depended on the heat released by combustion. The jet flame height divided by the orifice exit diameter was correlated as a function of the 1/3 power of the dimensionless heat release rate.

Mogi and Horiguchi's (2009) experimental study on horizontal high-pressure hydrogen jet flames (release pressures of up to 40.1 MPa), also found a relationship between the dimensionless flame height (*H/d*) and the dimensionless heat release rate. These authors found the *H/d* ratio to be proportional to the 0.25 power of Q^*. However, when the orifice exit diameter (*d*) was replaced by a pseudo orifice diameter (d_{ps}), calculated from the expansion of the jet from the orifice exit to the atmosphere, the ratio of the jet flame height divided by the above-mentioned pseudo orifice diameter (H/d_{ps}) was found to be constant. For example, H/d_{ps} was found to be approximately 200 for hydrogen jet flames, showing the flame height to be proportional to d_{ps} regardless of the release pressure.

A simplified expression for predicting the flame height for partially premixed jet flames in the buoyancy-dominated regime was suggested by Rokke *et al.* (1994). It was based on an experimental study on turbulent subsonic propane/air jet flames, issuing vertically into still air at atmospheric pressure and temperature. The degree of partially premixing varied between a fuel mass fraction of 1 to 0.15. The tests covered six different orifice exit diameters ranging from 3.2 to 29.5 mm, with which jet flames of up to 2.5 m in length were obtained. These experimental results were correlated in the buoyancy-dominated regime ($Fr \leq 10^4$) with Eq. (3.2); the transition to the momentum-dominated regime was shown, as an extrapolation of the experimental results, at Froude numbers exceeding 10^5. It should be noted that this limit became smaller for partially premixed flames, as did the flame height.

$$\frac{H}{d} = 33 \cdot Y_f^{2/5} Fr^{1/5} \tag{3.2}$$

As mentioned above, a common way to present flame height data has been by means of the dimensionless ratio (*H*/*d*) plotted versus the Froude number. Some authors have suggested several expressions to estimate jet flame height by using a modified *Fr*. Steward (1970) correlated the *H/d* ratio, in the buoyancy-dominated regime, for several fuels with a mixing controlled burning rate parameter. This included such variables as the Froude number, the mass of air per mass of fuel for stoichiometric combustion, the jet density, the inverse volumetric expansion ratio.

In Schuller *et al.* (1983), the *H/d* ratio, modfified by the density ratio of gas to surrounding medium, was correlated with *Fr*. Subsonic propane and methane jet flames, obtained with circular and rectangular nozzles, were well correlated with Froude numbers of up to $3 \cdot 10^4$; for larger Froude numbers, the flame height was found to be less sensitive to *Fr*, but a small increase in *H/d* with *Fr* was still seen. It should be noted that the suggested expression for jet flame height was based on subsonic data, and it is not recommended for underexpanded jets (Schuller *et al.*, 1983).

Peters and Göttgens (1991) derived theoretical approximate solutions for buoyant turbulent jet diffusion flames, using the radially integrated continuity, momentum and mixture fraction equations and an additional equation for the half-width of the jet flame. Buoyancy was found to be the dominant mechanism for hydrocarbon jet flames issuing into still air, for Froude numbers less than $\sim 10^5$. It was experimentally verified with the subsonic methane and propane jet flames obtained by Sonju and Hustad (1984). For Froude numbers exceeding 10^5, momentum became the dominant mechanism, making the jet flame height independent of Froude number (the Froude number independent solution was approached for Froude numbers $> 10^6$). These authors used a modified Froude number taking into account the changeable density (the gas density at exit, stoichiometric and ambient conditions, respectively) and a correction factor for the mixing over the jet area.

Blake and McDonald (1993) found the *H/d* ratio for vertical turbulent jet flames to be a function of the density weighted Froude number, including chemical reaction and the flame to ambient density ratio, in the buoyancy-dominated regime. In the momentum-dominated regime, *H/d* exhibited an asymptotic value, specific for each fuel, independent on the density weighted Froude number.

The *H/d* ratio, modified by the air to fuel mass stoichiometric ratio and the ratio of fuel density at the nozzle to ambient gas density, was correlated with a modified Froude number for several fuels in the buoyancy-dominated regime (Delichatsios, 1993). This modified Froude number includes the flame temperature and the heat of combustion, as in Ricou and Spalding (1961). In the momentum-dominated regime, a constant value of the modified *H/d* ratio was attained that depended upon the fuel (Delichatsios, 1993). This expression was verified by comparison with some of the experimental data of Kalghatgi (1984), concerning methane, propane and hydrogen jet flames. Based on this experimental data, Delichatsios (1993) found the transition from buoyant to momentum-dominated jet flames to occur for a modified Froude number between 3 and 5, and for modified Froude numbers greater than about 5, an essentially constant flame height was found for hydrogen jet flames.

Heskestad (1999) introduced the gas release momentum, arising from the momentum generated in a purely buoyant flame. Flame heights were normalised by the flame heights of purely buoyant flames, with a dependence on a momentum parameter, the ratio of discharge momentum of the gas release to momentum generated by a purely buoyant flame. The jet flame length normalized by the pipe diameter in the buoyancy-dominate regime was correlated against a dimensionless group involving variables such as the Froude number, the heat of combustion of the source gas per unit mass, and the mass stoichiometric ratio. An expression for the constant flame height, in the momentum-dominated regime, dependent on the type of fuel was also obtained. This showed a primary dependence on the stoichiometry, gas density and heat of combustion.

The experimental studies of Schefer *et al.* (2004, 2006, 2007) on subsonic and sonic high-pressure hydrogen jets (initial stagnation pressures of approximately 15.5 MPa and storage pressures of up to 41.3 MPa) used flame temperature, heat of combustion and a “notional” nozzle diameter in dimensionless groups, as suggested in Delichatsios (1993), to predict jet flame height. The notional nozzle diameter is originated from the assumption of an isentropically expansion from the orifice jet exit under sonic velocity to atmospheric pressure. Schefer *et al.* (2004, 2006, 2007) obtained the notional nozzle diameter by using an entirely analogous approach to that of Birch *et al.* (1987), based on the conservation of mass and momentum, assuming no viscous forces and a uniform velocity profile across the notional nozzle cross section. However, Schefer *et al.* (2007) also

included the non-ideal behaviour of the gas at high pressures and this was done by using the Abel-Noble equation of state:

$$P = \frac{\rho \cdot R \cdot 10^3 \cdot T}{M_v(1-h\rho)} = \frac{Z \cdot \rho \cdot R \cdot 10^3 \cdot T}{M_v} \tag{3.3}$$

Molkov (2009), using more than 95 experimental hydrogen data obtained in a wide range of conditions (storage pressures of up to 41.3 MPa and orifice exit diameters ranging from 0.4 to 10.1 mm) from several experimental works (Kalghatgi, 1984; Mogi *et al.*, 2005; Schefer *et al.*, 2006; Schefer *et al.*, 2007 and Proust *et al.*, 2009), determined the flame height (*H*) of subsonic and sonic hydrogen jet flames; this author proposed the following expressions:

$$H = 76 \cdot (m \cdot d)^{0.347} \tag{3.4}$$

$$H = 116 \cdot (m \cdot d)^{0.347} \tag{3.5}$$

Equation (3.4) concerns the best fit line for all the experimental data, while Eq. (3.5) corresponds to an upper limit curve. This author also suggested the calculation of *H* for a given storage pressure and value of *d* by using a nomogram. Required parameters for this calculation were *d* and the fuel mass flow rate.

For high pressure sonic jets, when the ideal gas laws are not applicable, a system of nine equations, using the stagnation, choked and expansion conditions and invoking flame temperatures and specific heats, enabled *m* to be found. The non-ideal behaviour of the gas was allowed by the use of the Abel-Noble equation of state.

As can be seen from all this information, although jet fires have been studied by a number of authors, most of the research has focused on subsonic jet flames. However, very often accidental jet fires occur with gas being released at such a pressure that sonic flow at the outlet is achieved. The literature survey revealed a significant lack of research and

experimental work data on hydrocarbon sonic jet fires. Thus, a set of expressions allowing the calculation of sonic and subsonic hydrocarbon jet flame size was still needed. Finally, the literature survey has also clearly shown that a number of existing correlations to predict sonic jet flame height, whilst successful for each gas separately, could not embrace more than one fuel. Therefore, a single correlation for the height of sonic jet flames involving several fuels over a wide range of operating conditions (release pressures and pipe diameters) would be of great interest.

3.2. Lift-off distance

Another variable that influences the distance covered by a jet fire is the lift-off distance. At a sufficiently low jet exit velocity a turbulent jet diffusion flame is attached to the release point; however, by increasing the exit velocity, the flame will lift-off and stabilize itself further downstream within the jet. The lift-off distance concerns the centreline distance from the gas release point to the base of the stable lifted flame. This phenomenon occurs due to the fact that at the jet exit the average flow velocity exceeds the turbulent burning velocity; at a farther downstream position, the flame is stabilized at the position where equilibrium is reached between both velocities. The existence of a zone in which the fuel-air mixture is not between the flammability limits can also have an influence.

3.2.1. Previous studies

The stabilization of lifted jet flames has been consistently addressed. Wohl *et al.* (1949(b)) carried out an experimental study on subsonic butane-air flames burning from tubes and nozzles in laminar and turbulent flow, with butane concentrations ranging from lean mixtures to pure fuel gas, proposing that a lifted diffusion jet flame will exist when the mean velocity gradient at the burner rim exceeds a certain critical value, stabilizing itself at the position where both velocities become equal (i.e. the mean flow velocity and the burning velocity). The stability of butane-air flames and city gas-air flames which burn from a tube in an enclosing cylinder was also analyzed.

Vanquickenborne and Van Tiggelen (1966) carried out a study on the stabilization mechanism of lifted diffusion flames. Subsonic jet flames of methane, released through circular burners of 1.33 mm, 1.8 mm and 2.4 mm in diameter, were obtained. From the experimental data, it was suggested

that the base of a lifted diffusion flame anchors in a region where a stoichiometric composition is attained. An experimental relation between the turbulent burning velocity and the parameters of turbulence, by assuming that the turbulent burning velocity equals the gas flow velocity, was also proposed.

The prediction of lift-off distance is relevant because, together with the visible flame length, it determines the position of the flame and the distance over which there can be flame impingement on nearby equipment. The variation in lift-off height as a function of diverse variables, such as outlet diameter, jet exit velocity, laminar burning velocity, the Froude number and the Reynolds number at the outlet orifice, has been studied by several authors, both theoretically and experimentally.

The variation in the lift-off distance (S) with the jet exit velocity has been reported in several experimental studies (Annushkin and Sverdlov, 1979; Kalghatgi, 1984; Rokke *et al.*, 1994; Cha and Chung, 1996; Wu *et al.*, 2007 and Wu *et al.*, 2009). Some of the features of these studies are shown in Table 3.3.

In half of the works shown in Table 3.3 (Cha and Chung, 1996; Wu *et al.*, 2007 and Wu *et al.*, 2009), S was found to increase linearly with jet velocity. However, the rest of the studies (Annushkin and Sverdlov, 1979; Kalghatgi, 1984 and Rokke *et al.*, 1994) found S to increase linearly with the jet exit velocity, except near the lift-off limit (i.e. a nonlinear behaviour between S and jet velocity was found at the lowest values of jet exit velocity).

The expressions suggested by these studies are briefly commented. Annushkin and Sverdlov (1979), based on small-scale experimental results, suggested an expression for predicting the lift-off distance, invoking the discharge rate of the fuel and the Reynolds number, corresponding to the maximum turbulent burning rate.

Kalghatgi (1984) correlated sonic and subsonic lift-off distances up to 0.24 m in height for several gases, by using two dimensionless groups: the turbulence Reynolds number ($S \cdot S_L / \nu_{or}$) and the jet exit velocity divided by the maximum laminar burning velocity, modified by the 1.5 power of jet to air density ratio. However, although Kalghatgi's scaling law gave reasonable good agreement for different fuels, the hydrogen data deviates substantially from the predictions (Miake-Lye and Hammer, 1988; Rokke *et al.*, 1994).

The experimental work of Cha and Chung (1996) suggested an expression for predicting *S* only as a function of the jet exit velocity, being independent of the nozzle diameter and linearly proportional to the nozzle exit mean velocity. However, as discussed later, the dependence or independence of the lift-off distance on the orifice diameter seems to be uncertain.

Table 3.3. Experimental studies on lifted vertical jet flames

Author	Aperture (mm)	Release type	*S* up to (m)	Fuel	Notes
Annushkin and Sverdlov (1979)	0.55–16[a]	Subsonic, sonic and supersonic flows	0.22	hydrogen, methane, municipal natural gas and propane	–
Kalghatgi (1984)	1.08–10.1[b]	sonic and subsonic flows	0.24	ethylene, hydrogen, methane, propane	sonic flows were limited to hydrogen flames
Rokke *et al.* (1994)	3.2–29.5[b]	subsonic flows	0.32	propane	fuel mass fraction varied between 1 and 0.15
Cha and Chung (1996)	0.84–2.58[b]	subsonic flows	0.12	propane	confined jet flames were also obtained
Wu *et al.* (2007)	2[b]	sonic and subsonic flows	0.07	hydrogen, propane, hydrogen/argon, hydrogen/carbon dioxide and hydrogen/propane	–

Wu *et al.* (2009)	2[b]	sonic and subsonic flows	0.07	hydrogen, propane, hydrogen/argon, hydrogen/CO_2 hydrogen/methane hydrogen/propane	–

[a] Convergent nozzles.
[b] Circular nozzles.

Following Kalghatgi (1984), Wu *et al.* (2007, 2009) correlated lift-off heights with the dimensionless groups suggested by Kalghatgi (1984), changing in one of them the power concerning the ratio of densities from 1.5 to unity. Thus, again small-scale lift-off distances, under sonic and subsonic conditions and involving several fuels have been correlated.

The expression suggested by Rokke *et al.* (1994) will be discussed later in this section.

It can be seen therefore that the study of lift-off phenomenon has been developed essentially on subsonic flames and/or small-scale jet fires, conditions that significantly differ from those found in real accidental sonic jet fires.

The lift-off distance, normalised by the pipe diameter, has been correlated in several experimental studies (Peters and Williams, 1983; Sonju and Hustad, 1984; Costa *et al.*, 2004; Santos and Costa, 2005 and Kiran and Mishra, 2007), by relating the *S/d* ratio to the relationship between the pipe flow mean velocity and the pipe diameter by the following equation:

$$\frac{S}{d} = c \cdot \frac{V}{d} \tag{3.6}$$

where the constant (c) has the dimension of time. Different values have been proposed, based on experimental studies. The suggested values, together with some other features are shown in Table 3.4.

Table 3.4. Values for *c* (Eq. (3.6)) based on experimental data

Author	Fuel	Orifice diameter (mm)	*c* (s)
Peters and Williams (1983)	methane	4–12	0.0036
Sonju and Hustad (1984)	methane and propane	10–80	0.0036[a]
Rokke *et al.* (1994)	propane	0.84–2.58	0.0021[b]
Costa *et al.* (2004)	methane	5–8	0.0031
Santos and Costa (2005)	ethylene	5–8	0.0008
	propane		0.0026
Kiran and Mishra (2007)	LPG[c]	2.20	0.0018

[a] The experimental methane and propane *S/d* values plotted against *V/d* agreed quite well with the *c* value recommended by Peters and Williams (1983).
[b] Some of the *S/d* values together with the results obtained by other authors were plotted against the *V/d* ratio; however, the *c* value shown in this table was not obtained by the authors, it was obtained in the present study, correlating their experimental data on pure propane jet flames.
[c] Composition: 72% butane and 28% propane.

Eq. (3.6) can only be applied at subsonic conditions, since once the sonic velocity has been reached, larger lift-off distances can still be obtained (using a specific outlet diameter) if the gas pressure inside the pipeline continues to be increased. This is due to the increase in the gas density upstream the orifice which finally leads to a larger fuel mass flow rate.

The experimental study of McCaffrey and Evans (1986) on vertical methane jet diffusion flames, released from circular orifices ranging between 32 and 102 mm, has also correlated sonic and subsonic lift-off heights with an expression similar to Eq. (3.6), involving instead of the pipe flow mean velocity, the velocity when the gas expands fully to atmospheric

pressure. Although sonic lift-off distances up to 4.2 m in length were obtained, these authors concluded that the large scatter in their data in the sonic regime was not a characteristic of this type of flames, based on other flames produced at laboratory scale. As a result, it was suggested that far more systematic research on this phenomenon at sonic conditions should be carried out.

It should be also noted that Eq. (3.6) shows the lift-off distance to be independent of pipe diameter; however, the dependence or independence of the lift-off distance on the pipe diameter is still uncertain.

Schuller and co-authors (1983), based on an experimental study on subsonic jet fires of methane and propane, correlated the lift-off height normalized by the pipe diameter (*S/d*) with the 0.5 power of the Froude number (*Fr*); thus, showing *S* to depend on the outlet orifice diameter.

Broadwell's *et al.* (1984) studied essentially the blow-out behaviour; the lift-off height of turbulent diffusion flames was suggested to be a function of the pipe diameter, the fuel/air density ratio, the jet exit velocity, the laminar burning velocity and the thermal diffusivity of the air. However, the validity of this expression was not verified.

Donnerhack and Peters (1984) carried out an experimental study on vertical lifted subsonic methane jet diffusion flames undiluted and diluted with nitrogen. Undiluted flames were obtained with orifice diameters ranging between 2 mm and 10 mm; while diluted flames were released through a 4 mm orifice diameter. No correlation has been suggested for predicting lift-off distance. However, concerning undiluted jet flames, in the present study, the lift-off distances obtained by Donnerhack and Peters (1984) were plotted as a function of the jet exit velocity, showing a linear behaviour between *S* and the jet exit velocity, except for the data obtained with the smallest orifice diameters (i.e. 2 mm and 3 mm). It was also seen that in some cases, for the same jet exit velocity (e.g. around 40 m/s) higher lift-off distances were obtained as the pipe diameter was increased.

In McCaffrey (1989), subsonic methane diffusion flames were obtained with a 0.0292 m diameter pipe threaded reducer and a 0.0318 m diameter flat-edged orifice. The lift-off distance normalized by the pipe diameter was plotted against the Froude number (*Fr*), finding the *S/d* ratio to rise with *Fr* and obtaining higher lift-off values with the biggest outlet orifice (i.e. the 0.0318 m diameter flat-edged orifice). However, in McCaffrey (1989) the lift-off height was scaled with the jet exit velocity, being independent of

pipe diameter; in fact, it was cited that all the data were for essentially a single diameter (i.e. a 0.03 m orifice diameter). In the present study, when the lift-off distances obtained by McCaffrey (1989) were plotted against the jet exit velocity, for the same jet exit velocity, higher lift-off distances were shown to be obtained with the biggest orifice diameter. Thus, showing a dependence of S on d.

The experimental study of Lee *et al.* (1994) on subsonic jet flames of propane in an enclosure, showed the dependence of lift-off height in the turbulent regime on the pipe diameter, the level of dilution, and the jet exit velocity. This was shown by the correlation between the lift-off distance normalized by the pipe diameter and the ratio of the jet exit velocity to the mass fraction of the fuel.

Rokke's *et al.* (1994) experimental study on partially premixed subsonic propane/air flames, proposed a correlation for predicting the lift-off height. The suggested expression gives S as a function of the pipe diameter, the pipe flow mean velocity, the density ratio of jet fluid to air and the fuel mass fraction. This correlation was based on the previous expression suggested by Peters and Williams (1983).

Thus, it can be seen that the lift-off distance dependence on the orifice diameter, in both sonic and subsonic regimes, has not been solved yet.

A chemical parameter that has often been invoked in several theoretical and experimental studies (Broadwell *et al.*, 1984; Kalghatgi, 1984; Miake-Lye and Hammer, 1988; Pitts, 1989; Bradley *et al.*, 1998; Peters, 2000; Driscoll *et al.*, 2004; Wu *et al.*, 2007 and Wu *et al.*, 2009) to correlate the lift-off distance, is the laminar burning velocity. Some of these studies have already been mentioned, the rest of them are briefly commented in the next paragraphs.

Miake-Lye and Hammer (1988) suggested an expression for predicting the lift-off distance as a function of the mass fraction of fuel in air at stoichiometric conditions, the mass fraction of the fuel in the jet fluid, the jet exit velocity and the inverse of the chemical time given by the ratio of the thermal diffusivity for a stoichiometric mixture of fuel in air to the maximum laminar burning velocity. This expression was obtained from an experimental study on turbulent jet flames of ethylene and methane, released through a 3.8 mm orifice diameter, and on natural gas flames released through 3.8 mm, 6.3 mm and 7.9 mm orifice diameters. The suggested expression was compared with the experimental data of Kalghatgi

(1984) and Donnerhack and Peters (1984), noting from Miake-Lye and Hammer's (1988) predictions that the data concerning sonic and subsonic hydrogen jet flames obtained by Kalghatgi (1984) were not well predicted.

From a study on lift-off distances and blow-out phenomena, Pitts (1989) developed a calculation procedure, implemented in a computer program, to estimate lift-off height as a function of the jet exit velocity, the laminar burning velocity, the mass fraction of fuel-air mixture, the maximum laminar burning velocity, the time for chemical reaction and the time for turbulent mixing. The proposed model was tested with the predictions of the experimental data of Kalghatgi (1984). Accurately predictions for the subsonic jet flames of methane, propane and ethylene were obtained; instead, the sonic and subsonic hydrogen flames were overestimated. Pitts (1989) verified the expression suggested by Broadwell *et al.* (1984) for predicting lift-off height, finding that it did not accurately correlate experimental findings for lift-off heights.

In Bradley's *et al.* (1998) study on lift-off and blow-out phenomena, a model for non-premixed turbulent combustion has been developed and applied to subsonic undiluted methane jet flames, obtained experimentally by Donnerhack and Peters (1984). The computed lift-off heights normalized by the pipe diameter have been correlated with a dimensionless group involving the Reynolds number for the pipe flow and the ratio of the pipe flow mean velocity to the laminar burning velocity. The predicted lift-off heights showed this suitable model for subsonic regime, to be most accurate at higher flow rates and smaller pipe diameters.

Peters (2000), based on previous studies (Vanquickenborne and Van Tiggelen, 1966; Eickhoff *et al.*, 1984; Kalghatgi, 1984; Müller *et al.*, 1994, among many others), found the lift-off distance to be a function of the jet exit velocity, the maximum laminar burning velocity and the diffusion coefficient. However, as previously noted, the linear dependence of lift-off height on the jet exit velocity is suitable for subsonic flames, since once the sonic condition has been achieved, the fluid velocity cannot be further increased and remains constant at the speed of sound in that gas; while larger lift-off distances can still be obtained (using a specific outlet orifice diameter) if the gas pressure inside the pipeline continues to be increased.

The expression suggested by Driscoll and colleagues (2004) is based on an experimental study, concerning two subsonic small-scale lifted turbulent non-premixed flames (a 100% methane jet flame and a flame of 77% CH_4 and 23% N_2 by volume) with lift-off distances of 0.092 m for both cases,

released from a 5 mm circular tube. The lift-off height is proposed as a function of the laminar burning velocity, the stoichiometric mixture fraction, the jet exit velocity and the thermal diffusivity, similar to the expression proposed by Kalghatgi (1984).

Several other models have been proposed for predicting the lift-off distance. Müller *et al.* (1994) developed a model to predict flame propagation and lift-off height in turbulent jet diffusion flames. The propagation velocities in turbulent jets were obtained from experimental methane jet flames, vertically released through 4 mm, 6 mm and 8 mm cylindrical tubes. Propagation flame fronts and lift-off distances have also been simulated; concerning lift-off distances, the suggested model predicted with good accuracy the methane jet flames obtained by Donnerhack and Peters (1984), Kalghatgi (1984) and Miake-Lye and Hammer (1988), all of them obtained under subsonic conditions.

Another approach for estimating the lift-off distance of turbulent jet flames has been suggested by Chen *et al.* (2000). A flamelet model for partially premixed turbulent combustion was developed to simulate subsonic lifted turbulent jet fires, obtained with orifice diameters of 4 mm and 8 mm, using methane as a fuel, and propane jet flames released through a 6 mm outlet diameter. The predicted lift-off distances were compared with subsonic experimental data, obtained from several studies (Donnerhack and Peters, 1984; Kalghatgi, 1984; Miake-Lye and Hammer, 1988 and Rokke *et al.*, 1994). The calculated non-dimensional lift-off heights (*S/d*) were plotted as a function of the fuel exit velocity. The predicted lift-off heights concerning methane flames were shown to be in good agreement with the experimental data of Kalghatgi (1984), Miake-Lye and Hammer (1988) and Donnerhack and Peters (1984); while the simulations concerning propane flames agreed with Rokke's *et al.* (1994) data and overestimated Kalghatgi's (1984) measurements.

It can be seen that whether the lift-off distance, in either sonic or subsonic regimes, is dependent or not on the orifice diameter is still uncertain. Besides, most of the studies have been focused on the lift-off distance, but only at subsonic exit velocities and/or small-scale jet fires. Thus, research on large jet fires, and an equation allowing the estimation of flame lift-off distance in sonic conditions, which is the most common situation in accidental gas releases, would be of utmost interest, due to the lack of research on this phenomenon.

3.3. Experimental data

In the present study, vertical jet fires of propane issued from diverse outlet orifices, at atmospheric pressure in the absence of cross winds have been obtained under sonic and subsonic conditions. The results concerning the jet flame height obtained with these experimental turbulent flames of up to 10.3 m in length are discussed in this section.

The total jet flame height (Fig. 3.1) was determined by analyzing visible and infrared images once the stationary state was reached. This flame length was initially defined as the visible flame length (L), considered as the distance from the base of the lifted jet flame to the flame tip, plus lift-off distance (S), defined as the centreline distance from the gas release point to the base of the stable lifted jet flame.

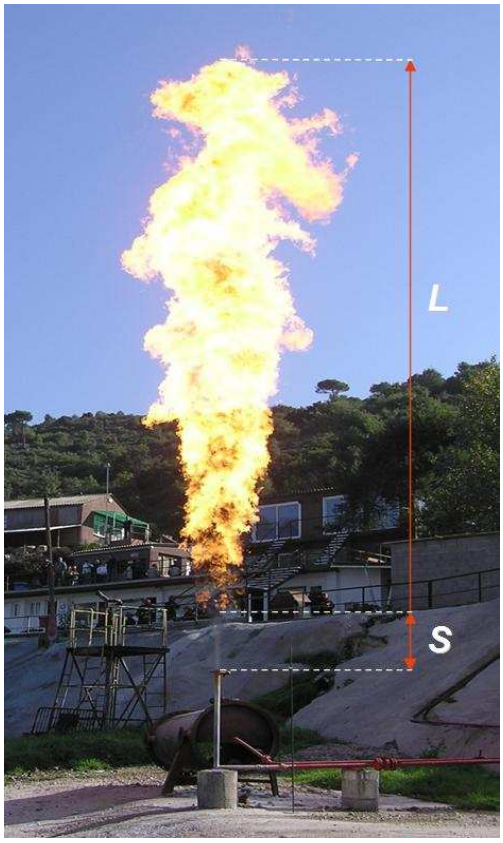

Figure 3.1. Vertical jet fire of propane showing total flame height as the visible flame length (L) plus the lift-off distance (S).

The ranges of data obtained in the present study are shown in Table 3.5. The data concern the following variables: visible jet flame height (L), lift-off distance (S), outlet orifice diameter (d), mass flow rate (m), jet exit velocity (V), stagnation pressure (P_{in}) and the dimensionless Froude number (Fr) and Reynolds number (Re).

Table 3.5. Experimental data concerning the propane jet fires

L (m)	S (m)	d (m)	m (kg/s)	V (m/s)	P_{in} (bar)	Fr (-)	Re (-)
2.57	0.61	0.01	0.07	246.92	3.33	$6.22\cdot10^{5}$	$1.2\cdot10^{6}$
2.78	0.61	0.01	0.10	244.28	4.65	$6.08\cdot10^{5}$	$1.7\cdot10^{6}$
2.74	0.65	0.01	0.11	244.72	5.07	$6.11\cdot10^{5}$	$1.8\cdot10^{6}$
2.89	0.68	0.01	0.11	244.08	5.27	$6.07\cdot10^{5}$	$1.9\cdot10^{6}$
2.92	0.82	0.01	0.11	243.82	5.45	$6.06\cdot10^{5}$	$2.0\cdot10^{6}$
2.95	0.78	0.01	0.12	243.65	5.60	$6.05\cdot10^{5}$	$2.1\cdot10^{6}$
1.48	0.13	0.01275	0.01	26.99	1.02	$6.60\cdot10^{3}$	$6.9\cdot10^{4}$
1.95	0.19	0.01275	0.01	66.90	1.05	$3.58\cdot10^{4}$	$1.7\cdot10^{5}$
2.90	0.33	0.01275	0.02	106.27	1.12	$9.03\cdot10^{4}$	$2.8\cdot10^{5}$
3.18	0.41	0.01275	0.03	148.41	1.23	$1.76\cdot10^{5}$	$3.9\cdot10^{5}$
2.93	0.41	0.01275	0.04	191.50	1.40	$2.93\cdot10^{5}$	$5.1\cdot10^{5}$
3.02	0.58	0.01275	0.05	234.14	1.63	$4.38\cdot10^{5}$	$6.3\cdot10^{5}$
3.18	0.62	0.01275	0.06	254.46	1.93	$5.18\cdot10^{5}$	$7.7\cdot10^{5}$
3.36	0.74	0.01275	0.07	254.49	2.25	$5.18\cdot10^{5}$	$8.9\cdot10^{5}$
3.01	0.75	0.01275	0.08	254.51	2.57	$5.18\cdot10^{5}$	$1.0\cdot10^{6}$
3.39	0.79	0.01275	0.09	254.49	2.83	$5.18\cdot10^{5}$	$9.5\cdot10^{5}$
3.25	0.91	0.01275	0.10	254.46	3.08	$5.18\cdot10^{5}$	$1.0\cdot10^{6}$
3.68	0.83	0.01275	0.11	254.43	3.32	$5.17\cdot10^{5}$	$1.3\cdot10^{6}$
3.40	0.83	0.01275	0.12	254.08	3.56	$5.16\cdot10^{5}$	$1.4\cdot10^{6}$
3.37	1.03	0.01275	0.13	253.91	3.82	$5.15\cdot10^{5}$	$1.5\cdot10^{6}$
3.73	0.87	0.01275	0.13	253.71	4.09	$5.15\cdot10^{5}$	$1.7\cdot10^{6}$

3.64	0.95	0.01275	0.14	253.49	4.34	$5.14\cdot10^{5}$	$1.8\cdot10^{6}$
3.86	1.04	0.01275	0.15	253.41	4.60	$5.13\cdot10^{5}$	$1.9\cdot10^{6}$
3.92	0.99	0.01275	0.16	253.29	4.86	$5.13\cdot10^{5}$	$2.0\cdot10^{6}$
3.72	0.95	0.01275	0.17	253.07	5.12	$5.12\cdot10^{5}$	$2.1\cdot10^{6}$
4.18	0.96	0.01275	0.18	252.92	5.42	$5.11\cdot10^{5}$	$2.2\cdot10^{6}$
4.23	0.99	0.01275	0.18	253.96	5.63	$5.16\cdot10^{5}$	$2.3\cdot10^{6}$
3.99	1.16	0.01275	0.19	252.87	5.72	$5.11\cdot10^{5}$	$2.4\cdot10^{6}$
3.95	1.03	0.01275	0.19	253.15	5.91	$5.12\cdot10^{5}$	$2.4\cdot10^{6}$
3.65	1.12	0.01275	0.19	252.75	5.91	$5.11\cdot10^{5}$	$2.5\cdot10^{6}$
3.95	1.04	0.01275	0.20	253.05	6.13	$5.12\cdot10^{5}$	$2.5\cdot10^{6}$
4.30	1.03	0.01275	0.20	252.48	6.15	$5.10\cdot10^{5}$	$2.6\cdot10^{6}$
4.64	1.12	0.01275	0.21	252.69	6.43	$5.11\cdot10^{5}$	$2.7\cdot10^{6}$
3.89	0.61	0.015	0.14	244.79	3.04	$4.07\cdot10^{5}$	$1.6\cdot10^{6}$
4.46	0.61	0.015	0.15	244.37	3.23	$4.06\cdot10^{5}$	$1.7\cdot10^{6}$
4.72	0.57	0.015	0.16	244.31	3.39	$4.06\cdot10^{5}$	$1.8\cdot10^{6}$
4.45	0.65	0.015	0.18	241.18	3.78	$3.95\cdot10^{5}$	$2.1\cdot10^{6}$
4.99	0.65	0.015	0.20	236.74	4.08	$3.81\cdot10^{5}$	$2.5\cdot10^{6}$
5.00	0.69	0.015	0.22	233.81	4.39	$3.72\cdot10^{5}$	$2.8\cdot10^{6}$
5.10	0.81	0.015	0.24	242.69	5.06	$4.00\cdot10^{5}$	$2.8\cdot10^{6}$
5.41	0.85	0.015	0.25	242.51	5.20	$4.00\cdot10^{5}$	$2.9\cdot10^{6}$
5.18	0.81	0.015	0.26	242.50	5.45	$4.00\cdot10^{5}$	$3.1\cdot10^{6}$
5.27	0.93	0.015	0.26	242.22	5.53	$3.99\cdot10^{5}$	$2.7\cdot10^{6}$
5.11	0.81	0.015	0.27	242.18	5.68	$3.99\cdot10^{5}$	$3.2\cdot10^{6}$
5.15	0.81	0.015	0.28	240.31	5.73	$3.92\cdot10^{5}$	$3.3\cdot10^{6}$
3.02	0.12	0.02	0.02	32.92	1.02	$5.52\cdot10^{3}$	$1.4\cdot10^{5}$
4.25	0.57	0.02	0.13	233.22	1.63	$2.77\cdot10^{5}$	$1.0\cdot10^{6}$
5.37	0.61	0.02	0.16	253.70	2.01	$3.28\cdot10^{5}$	$1.3\cdot10^{6}$
5.32	0.62	0.02	0.19	253.40	2.36	$3.27\cdot10^{5}$	$1.5\cdot10^{6}$
5.80	0.78	0.02	0.22	253.13	2.74	$3.27\cdot10^{5}$	$1.7\cdot10^{6}$

5.73	0.74	0.02	0.25	252.94	3.12	$3.26\cdot10^{5}$	$2.0\cdot10^{6}$
5.90	0.74	0.02	0.28	252.82	3.51	$3.26\cdot10^{5}$	$2.2\cdot10^{6}$
6.46	0.78	0.02	0.31	252.71	3.88	$3.25\cdot10^{5}$	$2.5\cdot10^{6}$
6.18	0.86	0.02	0.33	255.69	4.17	$3.33\cdot10^{5}$	$2.6\cdot10^{6}$
6.75	0.82	0.02	0.34	252.21	4.23	$3.24\cdot10^{5}$	$2.7\cdot10^{6}$
7.13	1.02	0.02	0.37	254.88	4.57	$3.31\cdot10^{5}$	$2.9\cdot10^{6}$
7.05	0.82	0.02	0.37	252.46	4.59	$3.25\cdot10^{5}$	$3.0\cdot10^{6}$
6.84	0.90	0.02	0.37	254.70	4.63	$3.31\cdot10^{5}$	$2.9\cdot10^{6}$
6.91	1.02	0.02	0.38	254.00	4.72	$3.29\cdot10^{5}$	$3.0\cdot10^{6}$
7.20	0.90	0.02	0.39	253.12	4.81	$3.27\cdot10^{5}$	$3.1\cdot10^{6}$
5.00	0.29	0.03	0.12	94.60	1.10	$3.04\cdot10^{4}$	$5.9\cdot10^{5}$
5.54	0.45	0.03	0.19	149.57	1.24	$7.60\cdot10^{4}$	$9.4\cdot10^{5}$
6.46	0.54	0.03	0.23	191.45	1.38	$1.25\cdot10^{5}$	$1.1\cdot10^{6}$
6.49	0.54	0.03	0.25	195.26	1.42	$1.30\cdot10^{5}$	$1.3\cdot10^{6}$
6.50	0.58	0.03	0.30	244.30	1.68	$2.03\cdot10^{5}$	$1.5\cdot10^{6}$
6.91	0.58	0.03	0.31	248.79	1.72	$2.10\cdot10^{5}$	$1.5\cdot10^{6}$
7.31	0.66	0.03	0.34	253.25	1.88	$2.18\cdot10^{5}$	$1.8\cdot10^{6}$
6.17	0.29	0.0431	0.07	23.86	1.02	$1.35\cdot10^{3}$	$2.6\cdot10^{5}$
7.83	0.46	0.0431	0.15	51.25	1.04	$6.21\cdot10^{3}$	$5.7\cdot10^{5}$
8.72	0.54	0.0431	0.31	101.27	1.13	$2.43\cdot10^{4}$	$1.2\cdot10^{6}$
9.20	0.74	0.0431	0.43	162.67	1.28	$6.26\cdot10^{4}$	$1.5\cdot10^{6}$
9.51	0.83	0.0431	0.47	153.75	1.29	$5.59\cdot10^{4}$	$1.9\cdot10^{6}$
9.55	0.79	0.0431	0.48	179.14	1.35	$7.59\cdot10^{4}$	$1.7\cdot10^{6}$
9.71	0.71	0.0431	0.50	165.46	1.34	$6.48\cdot10^{4}$	$2.0\cdot10^{6}$
9.68	0.79	0.0431	0.51	179.04	1.38	$7.58\cdot10^{4}$	$1.9\cdot10^{6}$
9.59	0.83	0.0431	0.54	195.19	1.44	$9.01\cdot10^{4}$	$2.0\cdot10^{6}$

The ranges of the values of the eight variables shown in Table 3.5 are given in Table 3.6.

Table 3.6. Ranges of L, S, d, m, V, P_{in}, Fr and Re values

Value	L (m)	S (m)	d (m)	m (kg/s)	V (m/s)	P_{in} (bar)	Fr (-)	Re (-)
Min.	1.48	0.12	0.01	0.01	23.86	1.02	$1.35 \cdot 10^3$	$6.9 \cdot 10^4$
Max.	9.71	1.16	0.0431	0.54	255.69	6.43	$6.22 \cdot 10^5$	$3.3 \cdot 10^6$

From Table 3.6 it can be seen that all the data concern turbulent jet flames, involving sonic and subsonic conditions.

3.4. Data processing

The main geometric parameters of jet flames (flame size and shape) are occasionally very difficult to analyse with a common video camera, since the flame can be sometimes transparent. In the present study, the visible light and infrared thermographic video recordings, obtained from two VHS cameras registering visible light and an infrared thermographic camera, were used to determine the jet flame size and shape.

In each test, a segment of infrared thermographic recordings corresponding to the stationary state was selected, digitalized, and divided into a sequence of digital images at four frames per second. In most of the tests, the same procedure was followed using a series of 25 digital images per second, which were obtained from the VHS films. The transient state lasted approximately 0.8-1.5 seconds. Two different software programs (i.e. ThermaCAM Researcher 2001® and Matlab R2007b®) and specially-developed ad-hoc algorithms were used for image processing.

It should be noted that at this stage L and S were obtained without applying any temperature criterion; the measurements performed in the visible and infrared images depended on the decision of the observer and the conditions of observation, such as the flame tip being taken to be the highest point to which the flickering tip reached. However, as a later stage, a criterion of temperature was applied to define the existence of jet flame, defining a new flame boundary.

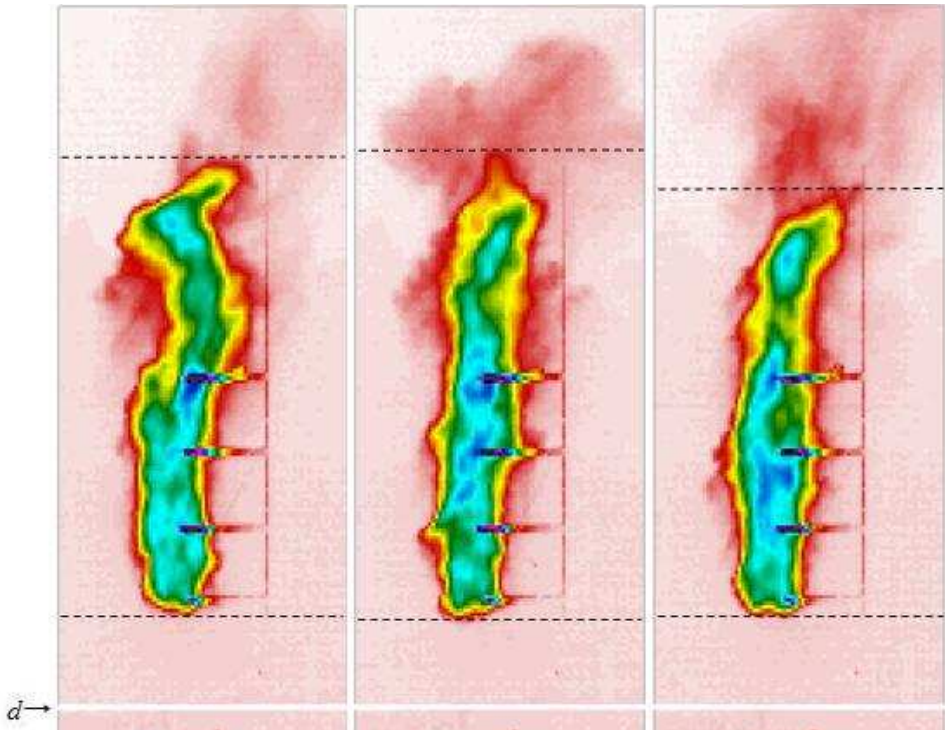

Figure 3.2. Successive infrared images of jet flames obtained with a 12.75 mm outlet diameter. The time interval between the successive infrared images was 0.25 s. The position of the outlet orifice diameter is shown by the bottom horizontal white line. The position of the base and tip of the flame is also shown by dotted lines, respectively. The flame length (*L*) was measured from the base of the flame to the tip, and the lift-off (*S*) from the outlet orifice to the base of the stable flame.

Examples of infrared images are shown in Fig. 3.2, where the lift-off distance, measured from the outlet orifice to the zone at which the detached jet flame started, is clearly shown.

The total flame length (*H*), considered from the pipe exit plane to the flame tip was also obtained from the visible images (Fig. 3.3), by applying an ad-hoc algorithm developed in Matlab R2007b®.

Figure 3.3. Visible image of a jet flame. Dotted lines shown pipe exit plane and flame tip, respectively.

Each visible image was exported to MATLAB R2007b® so as to obtain *H*. Fig. 3.4 shows the visible image (right), corresponding to that previously shown in Fig. 3.3, and an example of the transformation of the instantaneous visible image with the aforementioned algorithm, where the position of the flame tip and the outlet orifice are shown by top and bottom horizontal red lines, respectively (left). By applying colour and luminosity criteria, hot

gases and clouds were excluded from this one and from the rest of the images analyzed.

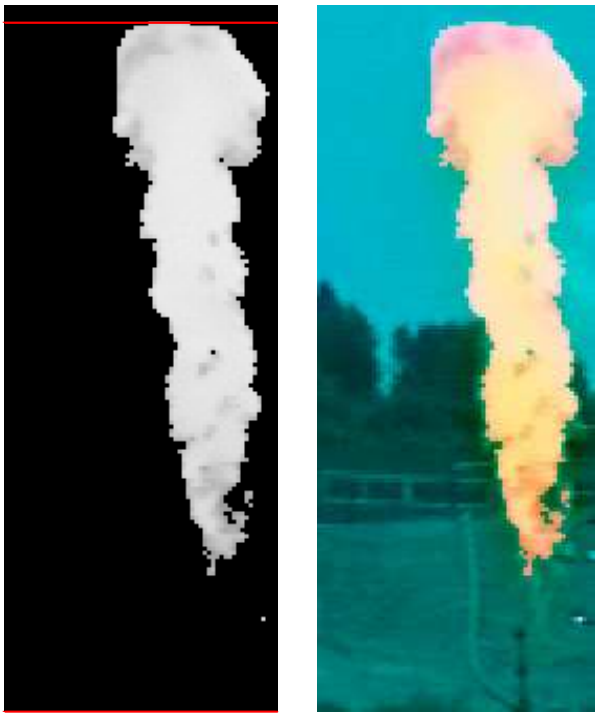

Figure 3.4. Jet flame: visible image corresponding to that previously shown in Fig. 3.3 (right); and an example of the transformation of the instantaneous visible image with the algorithm developed in MatlabR2007b ®; the position of flame tip and outlet orifice are shown by top and bottom horizontal red lines, respectively (left).

Diverse tests concerning color and luminosity in the images were done; some of them are illustrated by the following figures. Figs. 3.5 and 3.6 show the visible jet flame image previously shown in Fig. 3.3 by applying different values for the intensity of colour.

From Fig. 3.5, it can be seen that at low values of this variable, the flame tip cannot be detected.

Figure 3.5. Visible image (Fig. 3.3) (right) and using a lower value for the intensity of colour: the flame tip is not detected (left).

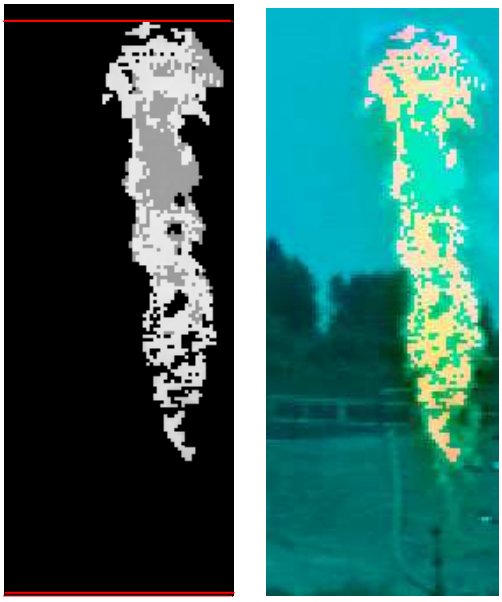

Figure 3.6. Visible image (Fig. 3.3) (right) and using a higher value for the intensity of colour: the jet flame height and area are underestimated (left).

At high intensities of colour, the flame tip was detected; however, the jet flame height and the area covered by the jet flame were underestimated (Fig. 3.6). Thus, an intermediate value was selected to define the jet flame height and surface for this and for the rest of the images.

Different values of luminosity were also tested. Figs. 3.7 and 3.8 show the visible jet flame image previously shown in Fig. 3.3 by applying diverse values of luminosity. It can be seen that at low values of this variable, the flame tip is overestimated and that the presence of clouds are considered as a part of the jet flame area (Fig. 3.7). Instead, at high values of luminosity, both the measured flame tip and the jet flame area are underestimated. Thus, again, an intermediate value had to be selected to define the jet flame height and surface.

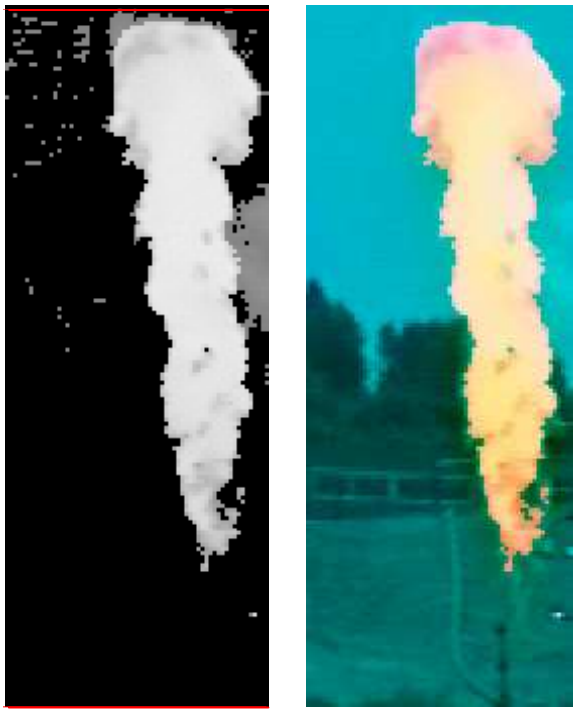

Figure 3.7. Jet flame: visible image (Fig. 3.3) (right) and the corresponding transformation (left). Due to a lower value for the luminosity than that used in Fig. 3.4, the jet flame tip is overestimated and clouds are considered as jet flame area.

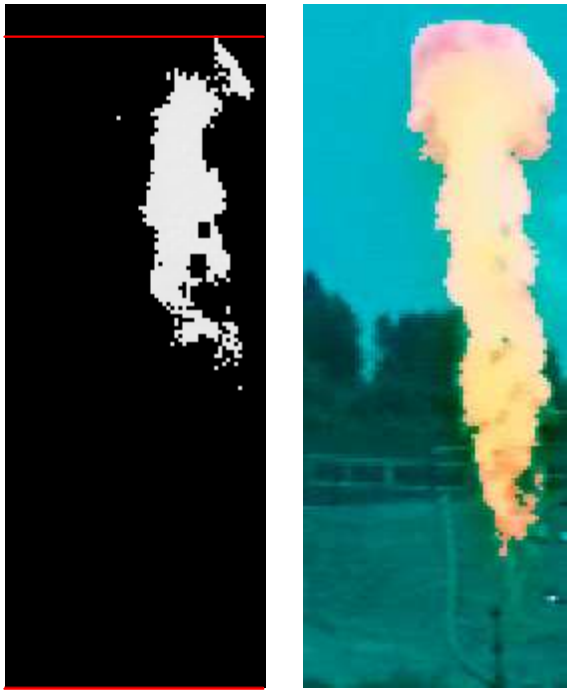

Figure 3.8. Jet flame: visible image (Fig. 3.3) (right) and the corresponding transformation (left). Due to a higher value for the luminosity than that used in Fig. 3.4, both the jet flame tip and jet flame area are underestimated.

As a later stage, the visible flame height from all the visible images was obtained as the difference between the total jet flame height and the lift-off distance, this latter variable obtained from the infrared images.

In some studies the reported experimental total flame lengths, visible flame lengths and lift-off distances correspond to time-averaged values (Sonju and Hustad, 1984; Santos and Costa, 2005; Kiran and Mishra, 2007). In the present study the reported average values for flame height and lift-off distance were obtained in accordance with the intermittency criterion developed by Zukoski *et al.* (1984). The intermittency (*i*) is defined as the fraction of time during which at least part of the flame lies above a horizontal plane located at an elevation *X* above the burner (Zukoski, 1995). *i* was defined as the fraction of time during which flame height and lift-off distance were at least higher than *L* and *S*, respectively. Therefore, the average flame height and lift-off distance values were defined as the length

and distance at which *i* reached a value of 0.5. However, the values for time-averaged jet flame heights and those obtained by the intermittency criterion were quite similar (3% of difference between them). Finally, it is important to highlight that the flame heights reported in Tables 3.5 and 3.6 correspond to the average value of *L* obtained from the infrared and visible images, applying the intermittency criterion, respectively.

3.5. Results

The experimental values for sonic and subsonic flame heights (*L)* have been plotted against the mass flow rate (*m)* in Fig. 3.9. The transition to sonic flow is marked with an arrow for each outlet diameter. Solid lines represent experimental data, while dashed lines correspond to an extrapolation of the experimental data. This extrapolation has been based on the experimental data obtained with the lowest mass flow rate values combined with the fact that they should meet the origin of coordinates. It is important to note that with an orifice diameter of 10 mm the flame had to be maintained with a permanent ignition source (i.e. a torch), otherwise, blow-out phenomenon (self-extinction of the jet fire immediately after ignition) occurred.

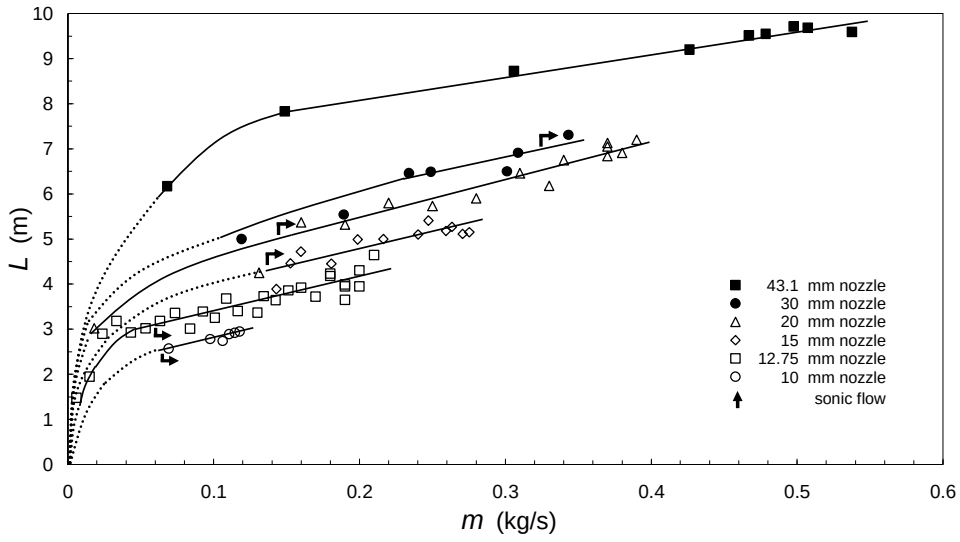

Figure 3.9. Sonic and subsonic flame height as a function of fuel mass flow rate, for the various orifice diameters.

This figure shows that for a given outlet diameter (*d*), flame height increases with *m*, and for a given mass flow rate, *L* increases with *d*. Thus, flame height was found to be a function of both mass flow rate and orifice exit diameter, for both sonic and subsonic conditions. Similar experimental results had been obtained by Kalghatgi (1984).

Then, a dimensional analysis was carried out, enabling the experimental results to be correlated. It is summarized in the Appendix II of this document; however, it is briefly commented in the following section.

3.5.1. Dimensional analysis

By applying the Buckingham's pi theorem, the dimensional analysis of the jet flame size has been carried out.

In the buoyancy-dominated jet regime, the jet flame length and the lift-off distance normalized by the pipe diameter, respectively, have been found to be a function of the orifice's Froude number (*Fr*) and the orifice's Reynolds number (*Re*). In the momentum-dominated jet regime, the *L/d* and *S/d* ratios, respectively, have been found to be a function of only the orifice's Reynolds number.

3.5.2. Assessment of empirical correlations

As already noted in the literature review, the jet flame length has been usually expressed as a function of the orifice's Froude number (Hess, 1964; Seeger and Werthenbach, 1970; Komov *et al.*, 1973; Baev *et al.*, 1974; Shevyakov and Komov, 1977; Suris *et al.*, 1977; Sonju and Hustad, 1984; Hustad and Sonju, 1986; McCaffrey, 1989; Rokke *et al.*, 1994; Bagster and Schubach, 1996; Santos, 2003; Costa *et al.*, 2004; Santos and Costa, 2005; Kiran and Mishra, 2007; Molkov, 2009). However in the momentum-dominated regime the jet flame length against *Fr* has been found to reach a constant value which depends on the fuel.

The jet flame length has also been correlated with a modified value of *Fr* (Steward, 1970; Schuller *et al.*, 1983; Peters and Göttgens, 1991; Blake and McDonald, 1993; Delichatsios, 1993; Heskestad, 1999; Schefer *et al.*, 2004, 2006, 2007). However, it should be noted that these correlations are useful and suitable only for subsonic releases, since once the sonic exit velocity is reached for a given value of *Fr* and an orifice outlet diameter, larger flame

lengths are still possible if the gas pressure inside the pipeline continues to increase.

Concerning the lift-off distance, the literature review has shown that subsonic exit velocity jet flames have been correlated against *Fr* (Schuller *et al.*, 1983; McCaffrey, 1989). However, as occurs with jet flame length, once the sonic condition has been achieved, the fluid velocity cannot be further increased and remains constant at the speed of sound in that gas; instead, larger lift-off distances can still be obtained (for an specific outlet orifice diameter) if the gas pressure inside the pipeline is increased. Thus, this kind of correlation is again restricted to subsonic conditions and cannot be applied to sonic exit velocities.

In the present study, according to this consideration and to the results obtained by the dimensional analysis, the jet flame height and lift-off distance, both normalized by the orifice exit diameter, have been correlated as a function of the orifice's Froude number (*Fr*) and the orifice's Reynolds number (*Re*).

3.5.2.1. Jet flame length

The dimensionless flame height (*L/d*) was plotted as a function of *Fr* (Fig. 3.10) showing as a common trend an increase in *L/d* with *Fr,* over all the subsonic range.

The relationship between the two dimensionless groups in the subsonic regime could be given by the following expression ($R^2 = 0.7$):

$$\frac{L}{d} = 61 \cdot Fr^{0.11} \tag{3.7}$$

However, for a given value of *Fr* in the sonic flow range (i.e. for a constant sonic velocity of the gas at the orifice) and an orifice outlet diameter, larger flame heights are still possible. This is due to the fact that jet flame height increases with mass flow, as a result of the increment in the gas density inside the pipeline, which can take place if the gas pressure inside the pipeline continues to increase. Thus, this variation in flame height corresponding to sonic flow could not be predicted in such a plot (Fig. 3.10).

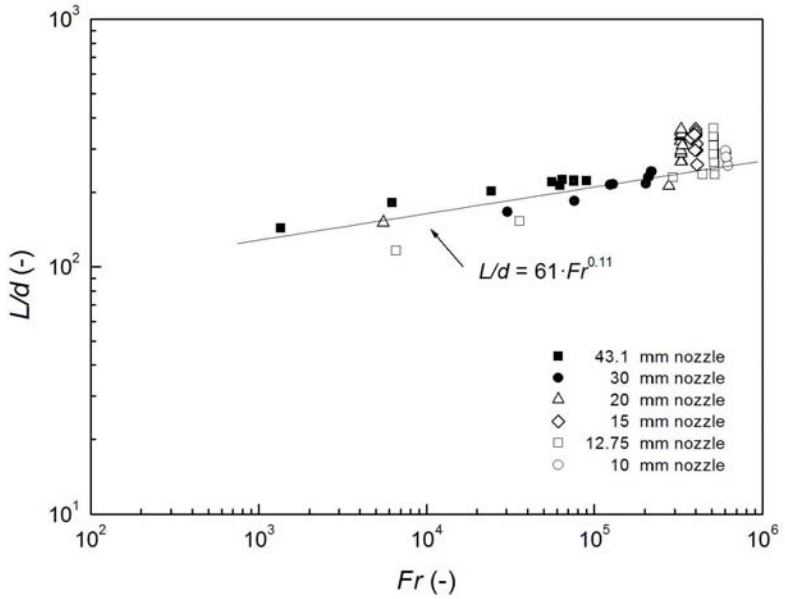

Figure 3.10. Variation of the normalized flame length as a function of the Froude number: experimental results (subsonic and sonic exit velocity) for the various orifice outlet diameters. Eq. (3.7) (subsonic data) is also shown.

The dimensional analysis carried out has shown that the jet flame length, over the buoyancy-dominated regime, is a function of the orifice's Froude number and the orifice's Reynolds number. Thus, as a later stage, the present subsonic exit velocity jet flames have been plotted against these dimensionless groups (Fig. 3.11).

The relationship between the two dimensionless groups can be expressed by the following expression (R^2 = 0.8):

$$\frac{L}{d} = 26 \cdot (Fr \cdot \mathrm{Re})^{0.08} \qquad (3.8)$$

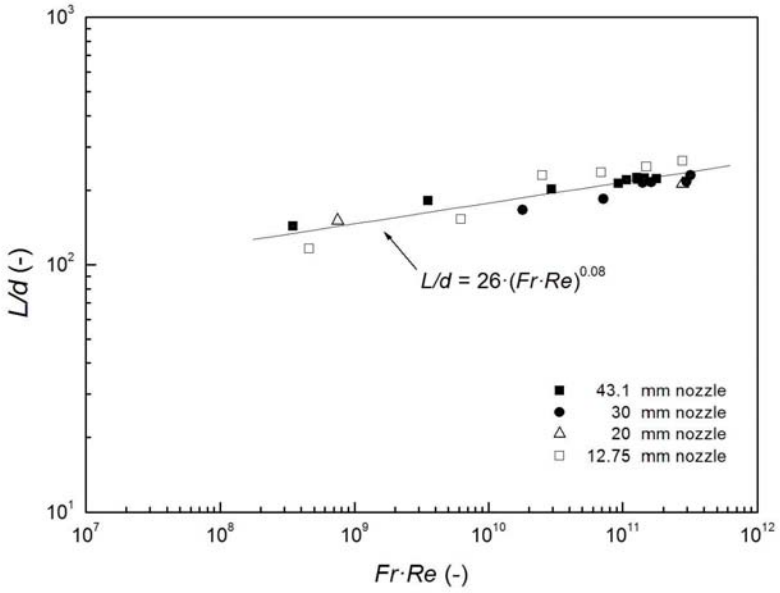

Figure 3.11. Variation in normalized flame length as a function of the Froude number times the Reynolds number: experimental results (subsonic exit velocity), for the various orifice outlet diameters. Eq. (3.8) is also shown.

From Fig. 3.11 it can be seen that the subsonic exit velocity jet flames are correlated in a better way by using the dimensionless grouping $Fr \cdot Re$ than using the kind of expression commonly suggested in several experimental and theoretically studies, where the jet flame height is correlated only with Fr. Other numerical exponents for Fr and Re were tested, finding the optimized exponents be equal to 0.08. As early mentioned, in the literature review, Baev and Yasakov (1974) and Baev *et al.* (1974) have found laminar jet flames over the buoyancy-dominated regime to be a function of $Fr^{1/3} \cdot Re^{2/3}$.

The dimensional analysis has shown that jet flames over the buoyancy-dominated regime are a function of both the orifice's Froude number and the orifice's Reynolds number, while at the momentum-dominated jet regime, the flame length is only a function of Re. However, in the present study when all sonic and subsonic exit velocity jet flames normalized by the

pipe diameter were correlated with the dimensionless group involving *Fr·Re* with optimised exponents, all data follow the same trend (R^2 = 0.81).

In an attempt to achieve a more straightforward expression suitable for predicting *L* in the two regimes (subsonic and sonic exit velocities), the *L/d* ratio was plotted against the orifice's Reynolds number (Fig. 3.12), revealing the same trend for all data. In this way, all the sonic and subsonic data could be correlated by the following expression (R^2 = 0.73):

$$\frac{L}{d} = 5.8 \cdot Re^{0.27} \tag{3.9}$$

It should also be noted that when the sonic exit velocity jet flames normalized by the pipe diameter were plotted against the orifice's Reynolds number, they were correlated with the 0.28 power of *Re* (R^2 = 0.78). However, from Fig. 3.12 it can be seen that all sonic and subsonic data can be expressed fairly accurately by Eq. (3.9).

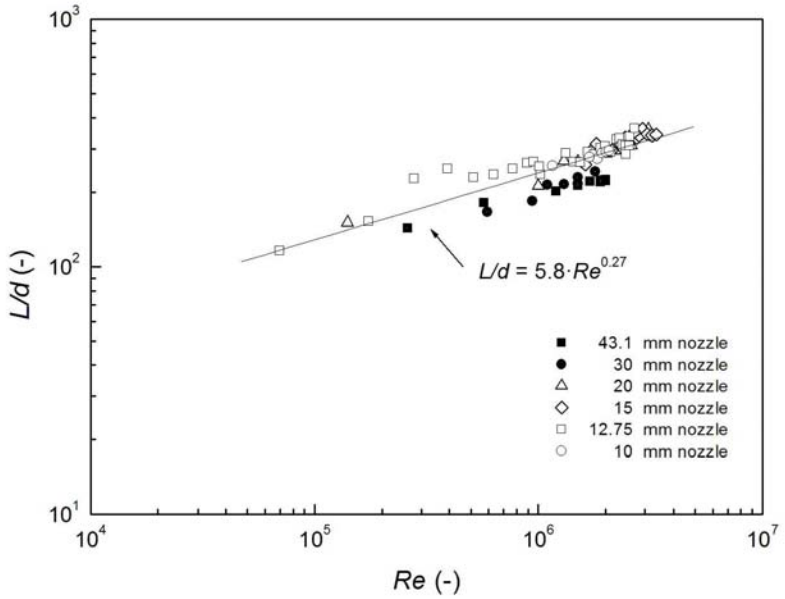

Figure 3.12. Variation in the sonic and subsonic normalized flame lengths as a function of the orifice's Reynolds number, for the different orifice outlet diameters. Eq. (3.9) is also shown.

Similar results were found by Shevyakov and Komov (1977) in an experimental study on hydrogen jet flames, with *Re* up to $2 \cdot 10^4$, where for a given *Re* the *L/d* ratio was shown to decrease as the outlet orifice diameter increased, such as in the present experimental data (jet flames obtained with *Re* up to $3.3 \cdot 10^6$). These authors suggested a constant value for the *L/d* ratio equal to ~220, from the extrapolation of their experimental data; however, it can be seen (Fig. 1 in Shevyakov and Komov, 1977) that the constant value would be rarely reached by their data obtained with the larger outlet orifice diameters.

Baev and Yasakov (1974) and Baev *et al.* (1974) have also found the flame length of a turbulent jet flame to reach a constant value, which depended on the type of fuel. However, in the present study the sonic and subsonic *L/d* ratios have been found to increase with *Re* (Fig. 3.12), showing that in the two regimes (sonic and subsonic) *L* is again a function of the mass flow rate and the orifice diameter, as *Re* is a function of these two variables.

3.5.2.2. Lift-off distance

The lift-off distance (*S*) was correlated with variables proposed in previous works and with the dimensionless groups obtained by the dimensional analysis.

As a first stage, the sonic and subsonic lift-off distances were plotted against the jet exit velocity (Fig. 3.13). The data for d = 10 mm were excluded, since these data were obtained by applying a constant ignition source (i.e. a torch), which prevented blow-out phenomenon to occur. As a result, the end of the lift-off distance corresponds to the height at which this torch was located.

Fig. 3.13 shows that the present subsonic lift-off distances increase with jet exit velocity. However, once the sonic condition is achieved (i.e. the velocity of sound in the gas at exit gas conditions), the fluid velocity cannot be further increased and remains constant at the speed of sound in that gas; however, as occurs with flame length, larger lift-off distances can still be obtained if the gas pressure inside the pipeline continues to be increased.

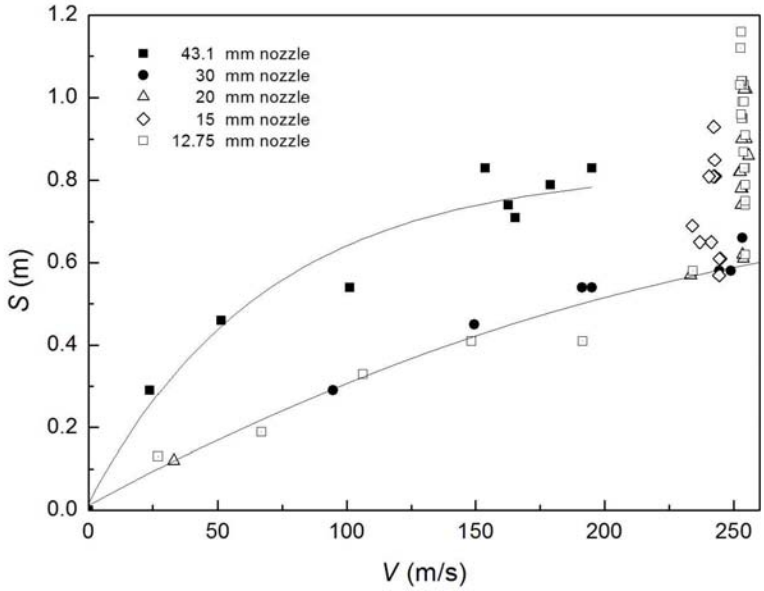

Figure 3.13. Variation in sonic and subsonic lift-off distances as a function of the jet exit velocity for various orifice outlet diameters.

Concerning subsonic data, it can also be seen from this figure that *S* linearly varies as a function of *V*, except for low values of *V* and the fact that the data should meet the origin of coordinates. A similar behavior has been found by Annushkin and Sverdlov (1979), Kalghatgi (1984) and Rokke *et al*. (1994), where *S* was found to increase linearly with the jet exit velocity, except at the lowest values of the jet exit velocity. It is also shown by Fig. 3.13 that the largest orifice diameter (43.1 mm) gives significantly higher values for *S* than the smaller orifice diameters (from 12.75 mm to 30 mm); subsonic values for the latter follow a common trend; a similar behaviour was found with the data of Donnerhack and Peters (1984) and McCaffrey (1989). Thus, it can be seen that lift-off distance at subsonic conditions is a function of two variables: orifice diameter and jet exit velocity; and that the data corresponding to sonic flow are not significant in such a plot.

As a later stage, the present sonic and subsonic lift-off distances normalized by the pipe diameter (*S*/*d*) were plotted as a function of *Fr* (Fig. 3.14).

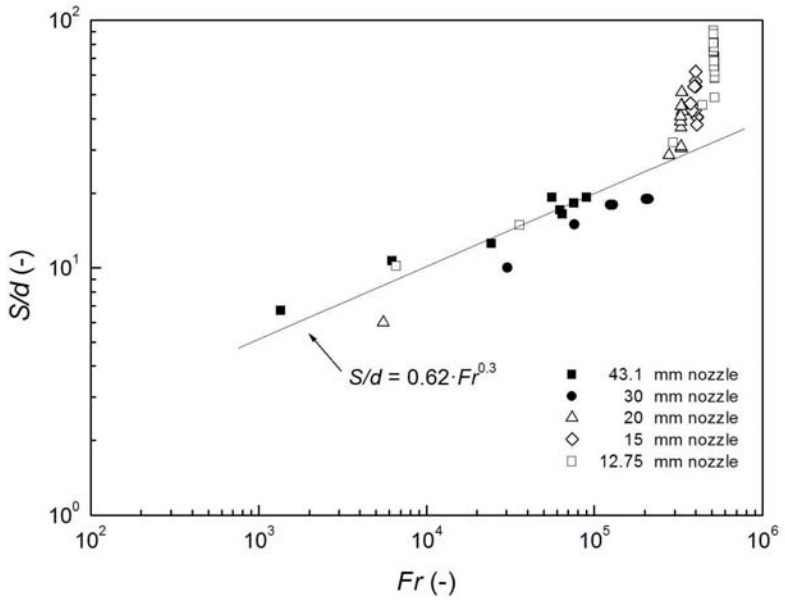

Figure 3.14. Variation in the subsonic and sonic lift-off distances normalized by the pipe diameter as a function of the Froude number for various values of *d*. Eq. 3.10 (subsonic data) is also shown.

The subsonic experimental data could be correlated fairly accurately using a single expression (R^2 = 0.82), which again shows the dependence of the lift-off distance on both orifice diameter and jet exit velocity at subsonic conditions:

$$\frac{S}{d} = 0.62 \cdot Fr^{0.3} \tag{3.10}$$

This expression is relatively similar to that obtained by Schuller *et al.* (1983) for subsonic jet flames of methane and propane, released through orifice diameters ranging between 10 mm and 80 mm. However, these expressions are restricted to subsonic flow conditions and cannot be applied to sonic flow, as lineal gas velocity does not increase any more once the

sonic flow has been reached (even though mass flow rate could be increased if pressure was increased).

The experimental subsonic and sonic lift-off distances normalized by the pipe diameter have been plotted against the fuel mass flow rate (Fig. 3.15).

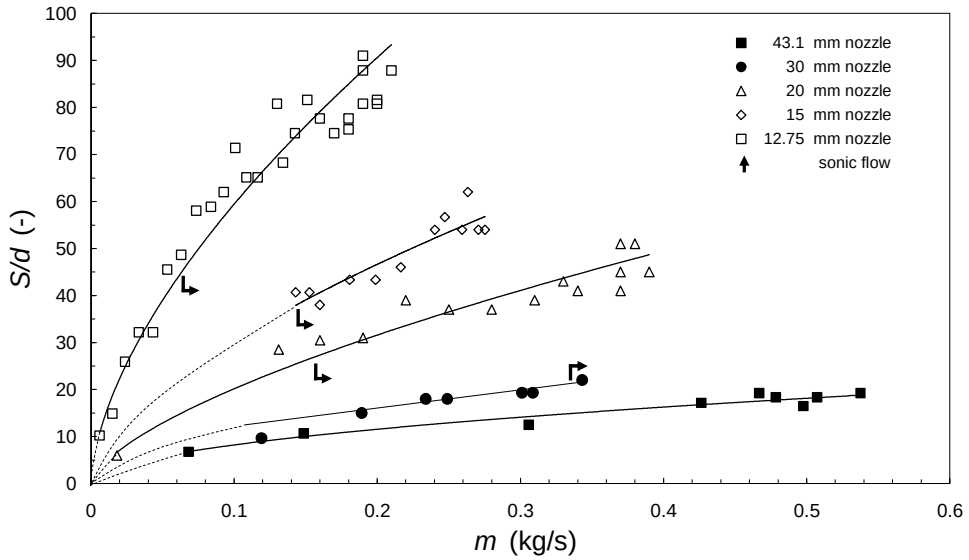

Figure 3.15. Variation in the sonic and subsonic lift-off distances normalized by the pipe diameter with fuel mass flow rate, for various orifice outlet diameters.

The solid lines represent data from the present study, while the dashed lines are an extrapolation following the trend of the data obtained with the lowest *m* values combined with the fact that they should meet the origin of coordinates. In this figure it is clear that for a specified diameter *d*, *S/d* increases with mass flow rate; furthermore, the trend of the results does not change when the flow changes from subsonic to sonic. Thus, the dependence of lift-off distance upon the mass flow rate and orifice diameter for the two regimes can be established again.

It is also important to note that when the present subsonic and sonic lift-off distances were plotted against the fuel mass flow rate in a log-log plot, the trend of the results was the same when the flow changed from subsonic to sonic. Furthermore, for a specific pipe diameter, the lift-off distance increased with the mass flow rate under sonic and subsonic regimes; and although the data seemed to probably collapse into a single curve, a

dependence upon the orifice diameter for the two regimes could also be established. Thus, once again, the lift-off distance in both the sonic and subsonic regimes has been found to be a function of both variables *m* and *d*.

Regarding subsonic exit velocity jet flames, the lift-off distance normalized by the pipe diameter has been plotted against the dimensionless numbers *Fr*·*Re*, finding the best fit relationship when the numerical exponent for the orifice's Reynolds number tends to zero. For example, when the numerical exponents for *Re* and *Fr* are both equal to 0.18 an expression with a correlation coefficient (R^2) equal to 0.41 has been obtained. When the exponents become 0.12 and 0.24 for *Re* and *Fr*, respectively, R^2 is equal to 0.57 and finally when the exponents are respectively, 0.06 and 0.28 for *Re* and *Fr*, respectively, $R^2 = 0.68$. Thus, the best correlation for subsonic exit velocity lift-off distances has been found when the data are correlated only against *Fr* (Fig. 3.16, $R^2 = 0.82$). However, this expression is suitable only for subsonic conditions, since once the sonic regime is reached, the jet exit velocity remains the same and higher lift-off distances can be obtained as the release pressure is increased.

Following the results obtained with the dimensional analysis, the sonic exit velocity lift-off distance normalized by the pipe diameter has been plotted against the orifice's Reynolds number (Fig. 3.16). The results have shown that it is not possible to obtain any correlation for sonic data, and that for a given value of *Re* the *S/d* ratio decreases as the orifice outlet diameter rises, a similar behaviour to that already found for the jet flame length.

As a later stage, the sonic and subsonic lift-off distances normalized by the pipe diameter have been plotted against *Re*; however, as for sonic data, any common trend has been found at both sonic and subsonic conditions.

In an attempt to find an expression for the lift-off distance suitable for subsonic and sonic velocities, *S* has been plotted against the orifice's Reynolds number for all data (Fig. 3.17), revealing the same trend. The relationship between *S* and *Re* can be expressed by the following equation ($R^2 = 0.63$):

$$S = 6 \times 10^{-4} \cdot Re^{0.5} \tag{3.11}$$

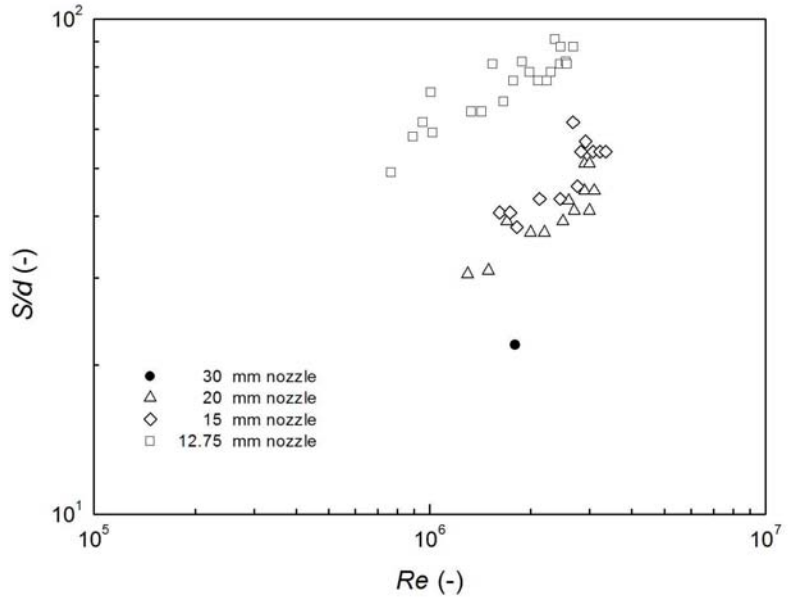

Figure 3.16. Variation of sonic lift-off distance normalized by the pipe diameter as a function of the orifice's Reynolds number, for various orifice outlet diameters.

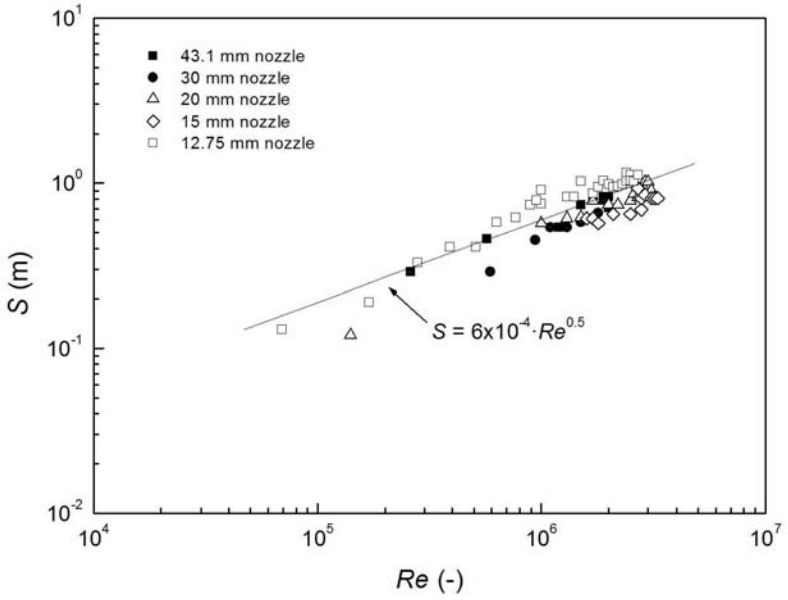

Figure 3.17. Lift-off distance (sonic and subsonic exit conditions) as a function of the orifice's Reynolds number, for various orifice outlet diameters. Eq. (3.11) is also shown.

This expression (Eq. (3.10)) can be used to estimate the lift-off distance as a function of the Reynolds number, for sonic and subsonic regimes, and propane as a fuel. Fig. 3.17 also shows that sonic and subsonic *S* values are a function of the mass flow rate (*m*) and the orifice diameter (*d*) as *Re* is a function of the two variables, *m* and *d*.

3.6. A new definition of flame boundary

A problem which is found when analyzing the flame reach is the exact definition of where the flame does end, i.e. to establish the actual envelope of the flame.

Several criteria have been used by diverse authors to establish flame length, such as the height at which enough air has been entrained to achieve stoichiometric combustion (e.g. the height at which 400% excess air is entrained (Steward, 1970)), the length at which the axial temperature is equal to 600 ºC (Odgaard, 1983), or the assumption that the end of the flame may be identified with the point on the axis of maximum concentration at which the fuel gas is diluted to its lower flammability limit (Brzustowski, 1973); flame length and shape have also been defined by the locus of all points characterized by the stoichiometric concentrations (Hawthorne *et al.*, 1949). These quite different criteria give a clear idea of the difficulty in defining the boundary of the flame.

In this study, as a later stage, the jet flame was analyzed as a radiative source of heat to the surroundings. Thus, the criterion selected to define the jet flame surface (a rather ambiguous concept) consisted in considering the existence of flame where a minimum given temperature had been reached. After testing several different temperatures to define the jet flame surface based on observations of visible and infrared flame images, a temperature of 800 K was selected.

At a temperature $\geq$ 1000 K, the jet flame surface covered by the flame in the IR image did not correspond to the image of the visible flame (Fig. 3.18 (d)); the area covered by the flame was smaller than that corresponding to the visible image. Similar results were obtained at a temperature $\geq$ 900 K. At a temperature $\geq$ 500 K, however, the area covered by the jet flame was larger than that covered by the visible image (Fig. 3.18 (b)). Similar results were obtained at a temperature $\geq$ 600 K and $\geq$ 700 K. At a temperature $\geq$ 800 K (Fig. 3.18 (c)), it was found that both the visible and infrared jet flame images overlapped with a fairly good agreement.

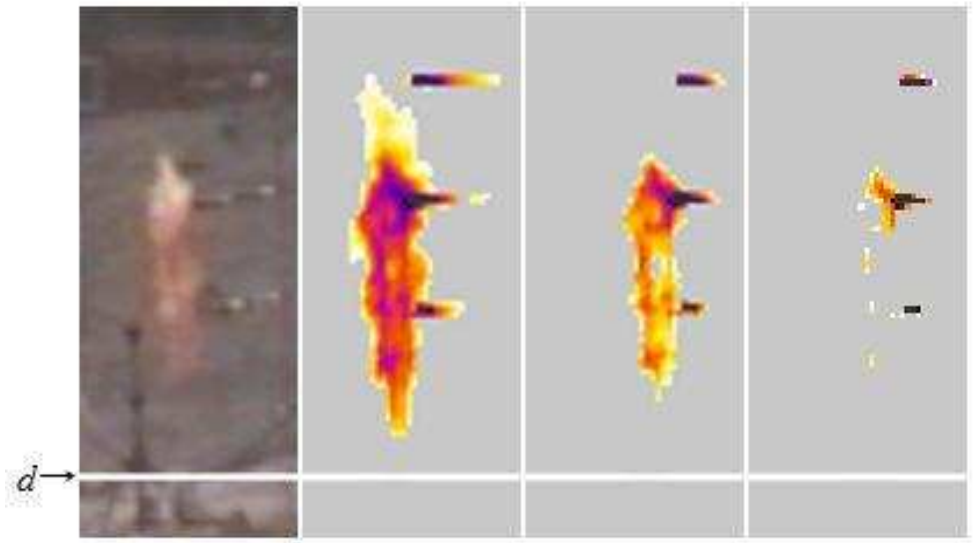

Figure 3.18. The criterion applied to define the flame boundary on a vertical jet fire: (a) the visible image; (b) the infrared image with a temperature of 500 K defining the jet flame contour; (c) the flame with a 800 K temperature contour; (d) the flame with a 1000 K temperature contour. Position of outlet orifice diameter (*d*) shown by the bottom horizontal white line.

Siegel and Howell (1992) reported that light first becomes visible from a heated object in darkened surroundings at 798 K. This value is known as the Draper point (Draper, 1847) and is defined as the temperature at which radiation emitted by a heated black body in darkened surroundings becomes visible to the human eye. This is consistent with our findings at a temperature of 800 K, which was therefore selected to define the jet flame boundary in the infrared images.

The values of the jet flame heights, obtained from the analysis of both the visible and infrared images (L) without taking into account any temperature criterion, and those obtained by the overlapping of visible and infrared images (L_{IR}), defining the jet flame envelope by the isotherm of 800 K, are shown in Table 3.7, together with the L/L_{IR} ratios and the pipe diameters from which each jet flame height has been obtained.

Table 3.7. Experimental data concerning jet flame height

d (m)	L (m)	L_{IR} (m)	L/L_{IR} (-)
0.01	2.57	2.46	1.04
0.01	2.78	3.63	0.77
0.01	2.74	3.36	0.82
0.01	2.89	3.63	0.80
0.01	2.92	3.43	0.85
0.01	2.95	3.35	0.88
0.01275	1.48	0.80	1.85
0.01275	1.95	1.51	1.29
0.01275	2.90	2.45	1.18
0.01275	3.18	3.03	1.05
0.01275	2.93	2.78	1.05
0.01275	3.02	3.39	0.89
0.01275	3.18	3.62	0.88
0.01275	3.36	4.06	0.83
0.01275	3.01	4.02	0.75
0.01275	3.39	4.10	0.83
0.01275	3.25	4.45	0.73
0.01275	3.68	4.40	0.84
0.01275	3.40	4.81	0.71
0.01275	3.37	4.40	0.77
0.01275	3.73	5.03	0.74
0.01275	3.64	5.17	0.70
0.01275	3.86	5.07	0.76
0.01275	3.92	4.71	0.83
0.01275	3.72	4.58	0.81
0.01275	4.18	5.14	0.81

0.01275	4.23	5.49	0.77
0.01275	3.99	4.80	0.83
0.01275	3.95	5.39	0.73
0.01275	3.65	5.16	0.71
0.01275	3.95	5.43	0.73
0.01275	4.30	5.16	0.83
0.01275	4.64	5.46	0.85
0.015	3.89	4.66	0.83
0.015	4.46	4.71	0.95
0.015	4.72	5.42	0.87
0.015	4.45	5.42	0.82
0.015	4.99	5.78	0.86
0.015	5.00	6.52	0.77
0.015	5.10	5.72	0.89
0.015	5.41	6.10	0.89
0.015	5.18	5.82	0.89
0.015	5.27	6.07	0.87
0.015	5.11	6.23	0.82
0.015	5.15	6.37	0.81
0.02	3.02	2.18	1.39
0.02	4.25	4.56	0.93
0.02	5.37	5.89	0.91
0.02	5.32	5.81	0.92
0.02	5.80	6.47	0.90
0.02	5.73	6.38	0.90
0.02	5.90	6.98	0.85
0.02	6.46	7.08	0.91
0.02	6.18	6.94	0.89
0.02	6.75	7.41	0.91

0.02	7.13	7.28	0.98
0.02	7.05	7.22	0.98
0.02	6.84	7.20	0.95
0.02	6.91	7.09	0.97
0.02	7.20	7.25	0.99
0.03	5.00	5.00	1.00
0.03	5.54	5.78	0.96
0.03	6.46	7.45	0.87
0.03	6.49	6.71	0.97
0.03	6.50	7.06	0.92
0.03	6.91	7.42	0.93
0.03	7.31	7.54	0.97
0.0431	6.17	7.60	0.81
0.0431	7.83	9.27	0.84
0.0431	8.72	9.78	0.89
0.0431	9.20	10.07	0.91
0.0431	9.51	10.13	0.94
0.0431	9.55	10.19	0.94
0.0431	9.71	10.31	0.94
0.0431	9.68	10.30	0.94
0.0431	9.59	10.14	0.95

It should be noted that the L_{IR} values correspond to time-averaged values; that the average ratio of L/L_{IR} was found to be 0.9, with minimum and maximum values of 0.7 and 1.85, respectively; and that by applying this temperature criterion, the values of L_{IR} obtained were generally somewhat higher than those previously obtained for L (14% higher, based on the average value obtained from the cases where L_{IR} was higher than L (i.e. in 91% of all the cases)).

Schefer *et al.* (2004 and 2006) compared infrared (IR), visible (VIS) and ultraviolet (UV) flame lengths, finding that the longest flame lengths were

those based on IR emissions and that the average values for L_{VIS}/L_{IR} were approximately 0.88.

The sonic and subsonic radiant jet flame lengths (L_{IR}) were again correlated as a function of orifice's Reynolds number (Fig. 3.19).

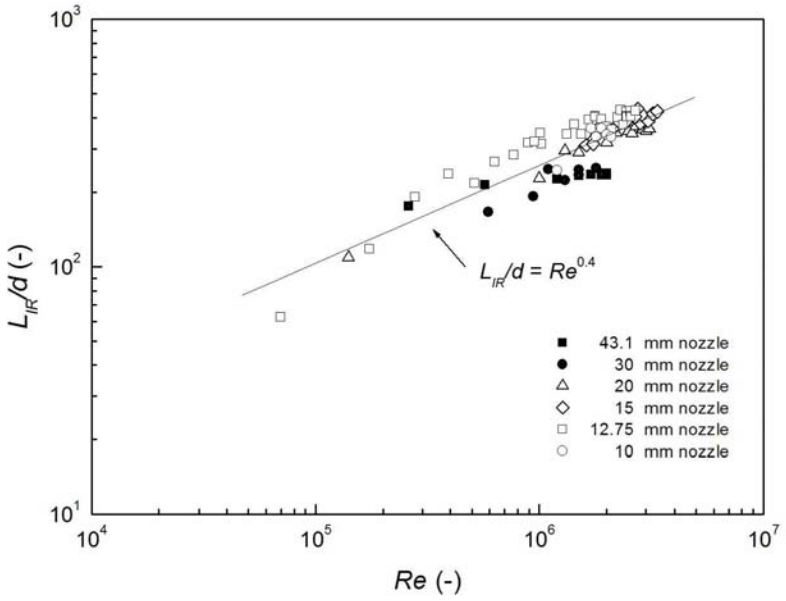

Figure 3.19. Variation in the sonic and subsonic normalized radiant jet flame lengths as a function of the orifice's Reynolds number, for the different orifice outlet diameters. Eq. (3.12) is also shown.

The relationship between the radiant jet flame length normalized by the pipe diameter and the orifice's Reynolds number could be expressed as a function of the 0.4 power of *Re* (R^2 = 0.7):

$$\frac{L_{IR}}{d} = Re^{0.4} \qquad (3.12)$$

When applying this new criterion, the jet flame height was shown to be again a function of *Re*, as in our previous findings (Eq. (3.9)) in which no

temperature criterion was used. Thus, this expression (Eq. (3.12)) can be used to estimate the jet flame height as a function of the Reynolds number, for sonic and subsonic regimes, and propane as a fuel. Since lift-off distances were obtained only from infrared images, the proposed expressions for this variable remain the same.

3.7. Prediction of jet flame height for diverse fuels

The treatment of flame length and lift-off data presented in the previous sections is restricted to propane flames (propane was the only fuel used in the experimental work). However, it was found that an expression for the height of sonic exit velocity jet flames embracing more than one fuel and accounting for the non-ideal behaviour of the gas was still needed, due to the lack of research in this area.

This is why an additional effort was also done to obtain a single correlation for the length of sonic exit velocity jet flames for several fuels over a wide range of pressures and pipe diameters, with allowance for the non-ideal behaviour of the gas.

3.7.1. Experimental data used

The jet flame data have been taken from six sources (Kalghatgi, 1984; McCaffrey and Evans, 1986; Schefer *et al.*, 2007; Imamura *et al.*, 2008; Mogi and Horiguchi, 2009), including the present study. Some of the features of these experimental studies concerning sonic exit velocity jet flames, measured from the pipe exit plane to the flame tip, are shown in Table 3.8.

It can be seen from this table that these data involve three different fuels: hydrogen, methane and propane, obtained over a wide range of pressures and pipe diameters in vertical and/or horizontal orientations.

3.7.2. Dimensionless groups

The formulation of the most appropriate dimensionless groups was based on previous studies involving chemical parameters such as the turbulent burning velocity, the turbulent karlovitz stretch factor, and also on the

considerations of turbulent flame structure and burning rates (Kalghatgi, 1984; Bradley *et al.*, 1998 and Bradley *et al.*, 2008).

Table 3.8. Range of values of experimental data used

Authors	Fuel	Orientation	d (mm)	P_{in} (MPa)	H (m)
Kalghatgi (1984)	Hydrogen	Vertical	1.08–5.03	up to 0.9	up to 1.3
McCaffrey and Evans (1986)	Methane	Vertical	38–102	up to 3.5	up to 23.5
Schefer *et al.* (2007)	Hydrogen	Vertical	5.08	up to 41.3	up to 10.4
Imamura *et al.* (2008)	Hydrogen	Horizontal	1–4	up to 3.4	up to 1.8
Mogi and Horiguchi (2009)	Hydrogen	Horizontal	0.4–4	up to 40.1	up to 6.2
Present study	Propane	Vertical	12.75–30	up to 0.6	up to 7.5

At high flow rates the intense mixing between fuel jet and ambient air at the base of the flame and the associated quenching there of any incipient flame, creates pre-mixtures with subsequent turbulent combustion in premixed flamelets. The flame surface density, Σ, can be expressed in terms of the mean reaction progress variable, $\bar{c}$, which ranges from 0 to 1, by $k \cdot \bar{c}(1-\bar{c})$, where k is a constant inversely proportional to the integral length scale of turbulence, L_s. The total wrinkled flame area over the entire volume of the reacting flow field multiplied by the laminar burning velocity (S_L) and a dimensionless factor, I_o, to allow for the effect of flame stretch rate on S_L, is equal to the product of the turbulent flame mean cross section area, A, and the turbulent burning velocity (S_T).

At high flow rates in a given burner there is evidence that an increase in S_T with increasing turbulence is achieved more by an increase in the volume

filled by flame, and hence in the present case in the jet flame height *H*, than by any change in *k* and Σ (Bradley *et al.*, 2009). It is as if there is a limiting flame surface density and that any increase in the burning rate must be achieved by an increase in the volume of the flame brush. If the mean flame surface density through the flame brush is $\overline{\Sigma}$, then $S_T \cdot A \sim \overline{\Sigma} \cdot A \cdot H \cdot I_o \cdot S_L$. As Σ is proportional to *k*, which is inversely proportional to L_s, then *H/L* is a function of S_T/S_L, provided I_o has a similar value for all mixtures at the maximum value of S_L.

The expressions for S_T/S_L proposed by Bradley *et al.* (2008) suggest that H/L_s must therefore be a function of the form $(u'/S_L)^{\alpha} R_L^{-\beta} (L_s/\delta)^{\kappa}$, in which α, β and κ are numerical exponents to be optimised experimentally.

Because L_s will be proportional to the pipe diameter *(d)*, and with the assumptions that the rms turbulent gas velocity *(u')* is proportional to the pipe flow mean velocity *(V)*, and that the turbulent Reynolds number (R_L) is proportional to the Reynolds number for the pressurized pipe flow *(Re)*, it follows that the jet flame height normalized by the pipe diameter *(H/d)* will be a function of the dimensionless grouping $(V/S_L)^{\alpha}\ Re^{-\beta} (d/\delta)^{\kappa}$

The value of *V* is taken to be that for sonic flow at the pipe exit plane, that of S_L is the maximum laminar burning velocity of the fuel-air mixture under atmospheric conditions, with the laminar flame thickness, δ, given by ν/S_L. Both ν and S_L are also those for atmospheric conditions. The value of *Re* is that existing at the nozzle exit plane.

It is important to note that the theory allowed the identification of the most appropriate dimensionless groups $\left((V/S_L)^{\alpha}, Re^{-\beta} \text{and} (d/\delta)^{\kappa}\right)$, that then were calibrated by the experimental data, optimizing experimentally the values of the numerical exponents α, β and κ, so as to get the present correlation.

3.7.3. Assessment of an empirical correlation

The correlation of the sonic jet flame length, measured from the pipe exit to the flame tip, normalised by the pipe outlet diameter *(H/d)* involved the sonic gas velocity at the pipe exit and accounted for the non-ideal behaviour of the gas.

To evaluate the aforementioned dimensionless grouping it was necessary to evaluate the following properties at the jet exit: the sonic gas velocity *(V)*, the Reynolds number for the pressurized pipe flow *(Re)* and the pipe diameter *(d)*, assuming isentropic flow and accounting for the non-ideal behaviour of the gas, using the Abel-Noble equation of state (already shown in Eq. (3.3)), as in the studies of Schefer *et al.* (2007) and Molkov (2009) concerning sonic hydrogen jet flames. It was also necessary to evaluate the following properties at ambient conditions: the laminar flame thickness *(δ)* given by the ratio of the gaseous mixture kinematic viscosity to the maximum laminar burning velocity of the fuel-air mixture; and the ratio of specific heats.

The use of ideal gas isentropic flow relationships is valid at low pressures. For example, the sonic gas velocity resulting from the expansion of propane from 0.3 MPa, assuming ideal gas behaviour is 246 $m \cdot s^{-1}$, while for non-ideal gas behaviour it is 244.2 $m \cdot s^{-1}$. However, the differences are greatest at the highest pressures; for example, at high pressures, such as in the present study when hydrogen flames reach 40 MPa, the behaviour of the gas increasingly departs from that of an ideal gas; for example, the expansion of H_2 from 40.1 MPa, considering ideal behaviour gave V = 1327 $m \cdot s^{-1}$, whereas for non-ideal behaviour V = 1190 $m \cdot s^{-1}$.

3.7.3.1. Final correlation

Shown in Fig. 3.20 are the experimental values obtained from the six previously mentioned experimental studies, listed in Table 3.8.

The hydrogen, methane and propane turbulent sonic jet flame heights, measured over all the present experimental conditions for sonic flow, were normalized by the pipe diameter; then these dimensionless jet flame heights *(H/d)* have been expressed in terms of the dimensionless grouping (ζ) with optimised exponents, for the experimental conditions indicated in Table 3.8, indicated by the best fit relationship:

$$\zeta = \left(V/S_L\right) Re^{-0.3} \left(d/\delta\right)^{0.25} \qquad (3.13)$$

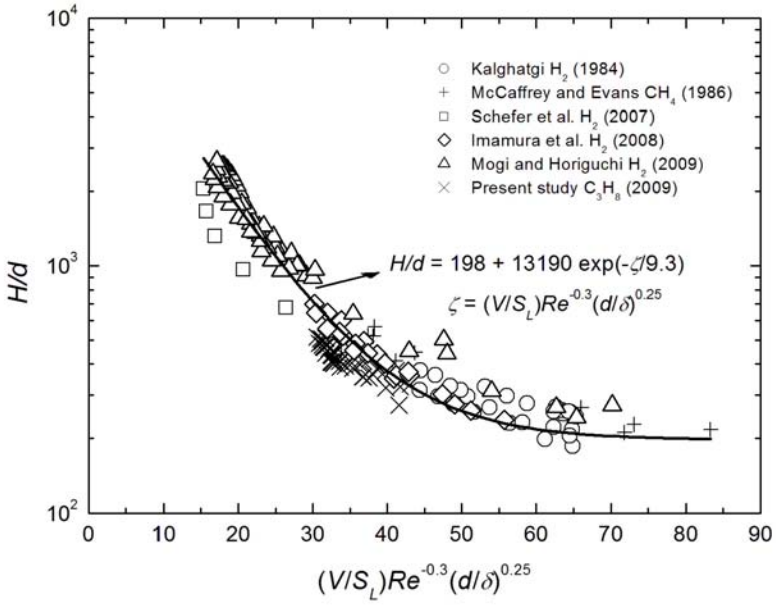

Figure 3.20. Variation in the sonic jet flame heights normalized by the pipe diameter (*H/d*) as a function of the dimensionless grouping (ζ) for various fuels. Eq. 3.14 is also shown.

It can also be seen that the *H/d* data shown in Fig. 3.20 are well correlated by the following expression (Eq. (3.14)), with a correlation coefficient (R^2) equal to 0.92:

$$\frac{H}{d} = 198 + 13190 \ \exp\left(\left(V/S_L\right)Re^{-0.3}\left(d/\delta\right)^{0.25}/9.3\right) \qquad (3.14)$$

Thus, this expression is suggested to estimate the height of turbulent sonic jet hydrocarbon (CH_4 and C_3H_8) and hydrogen flames, based on dimensional analysis of turbulent flames and non-ideal gaseous expansion.

3.8. Comparison with the expressions from other authors

3.8.1. Sonic and subsonic jet flame lengths and lift-off distances

The radiant jet flame heights (L_{IR}) were compared with previous models, concerning published experimental studies where expressions for predicting jet flame height for several fuels have been suggested. The first model concerns Hawthorne's *et al.* (1949) expression, published as the first study used for assessment of turbulent jet flame lengths. The other two models concern the few proposed correlations for predicting jet flame height under sonic and subsonic conditions for several fuels (Becker and Liang, 1978; Kalghatgi, 1984).

Fig. 3.21 shows the comparisons of the present experimental radiant jet flame heights, considered from the base of the flame to the flame tip, with the expression suggested by Hawthorne *et al.* (1949).

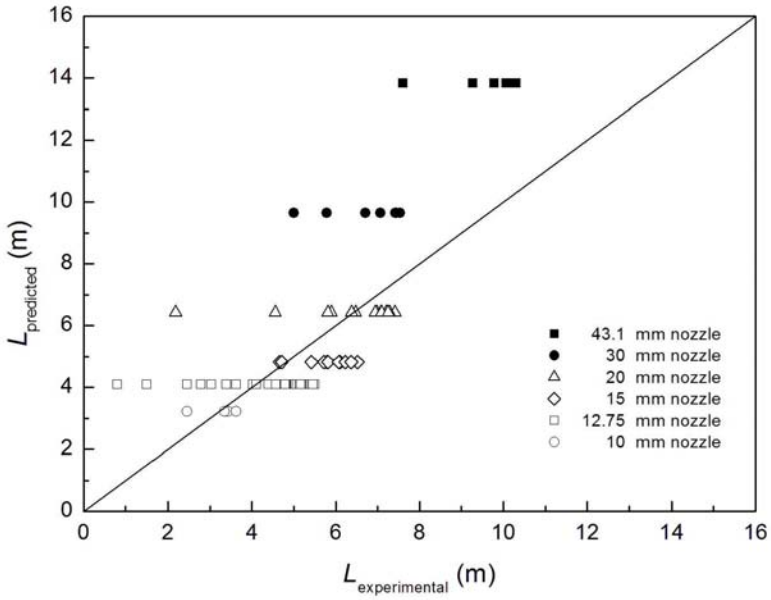

Figure 3.21. Radiant jet flame length predicted by Hawthorne's *et al.* (1949) equation plotted against experimental data.

From Fig. 3.21 it can be seen that for a given pipe diameter, only one jet flame height value is predicted, since the jet flame height is suggested by Hawthorne *et al.* (1949) as a function of *d*, but not as a function of the mass flow rate. This result is in conflict with the present experimental values, as well as with the findings of other authors, where the jet flame height has been found to be a function of both variables: pipe diameter and fuel mass flow rate (Steward, 1970; Kalghatgi, 1984; Schefer *et al.*, 2004; Schefer *et al.*, 2006 and Molkov, 2009).

The jet flame heights predicted by the models proposed by Becker and Liang (1978) and Kalghatgi (1984) are shown in Fig. 3.23. It is important to note that these expressions predict the total jet flame height, considered from the pipe exit plane to the flame tip. Thus, the lift-off distance was added to the radiant jet flame height to obtain a total jet flame height, and then compared with both models, respectively. The predictions are shown in Fig. 3.22.

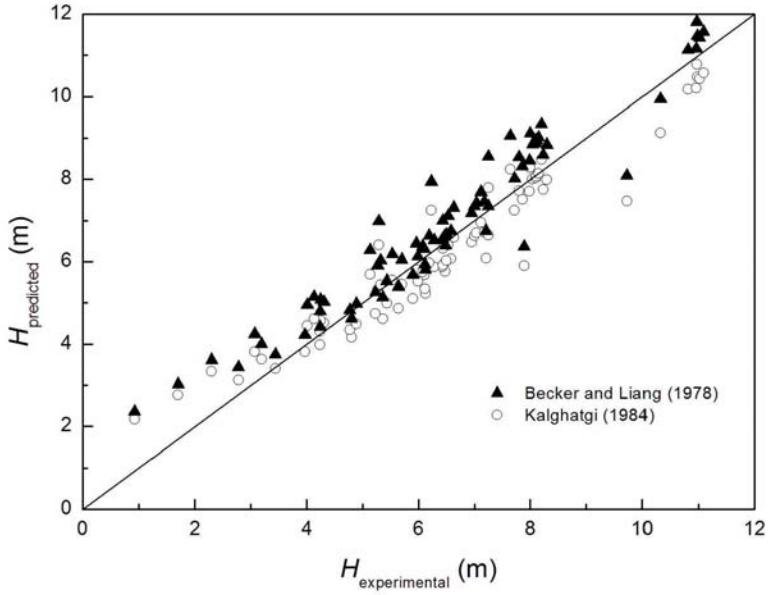

Figure 3.22. Total jet flame height, considered from the pipe exit plane to the flame tip, predicted by Becker and Liang (1978) and Kalghatgi (1984) equations, plotted against experimental data.

It can be seen from Fig. 3.22 that the values predicted by Kalghatgi's (1984) expression (open symbols) agree fairly well with the present experimental jet flame heights, except for a few values concerning some of the lower and higher experimental jet flame heights. It was also found that the jet flame heights predicted by Becker and Liang (1978) (filled symbols) are higher than those predicted by Kalghtagi (1984). Similar results were found by Kalghatgi (1984).

It is also important to note that both correlations (Becker and Liang, 1978; Kalghtagi, 1984) required a vast number of calculations to obtain the parameters involved in the iterative equations. Instead, the expressions suggested in the present study for predicting jet flame height and lift-off distance at sonic and subsonic conditions as a function of *Re* (Eqs. (3.11) and (3.12), respectively) do not need any iterative procedure.

Concerning lift-off distances, the present sonic and subsonic lift-off data were compared with previously suggested models. The selected models concern the few studies that proposed an expression for estimating lift-off height under sonic and subsonic regimes, according to our findings. The studies were carried out by Kalghagi (1984), Miake-Lye and Hammer (1988) and Wu and colleagues (2007 and 2009).

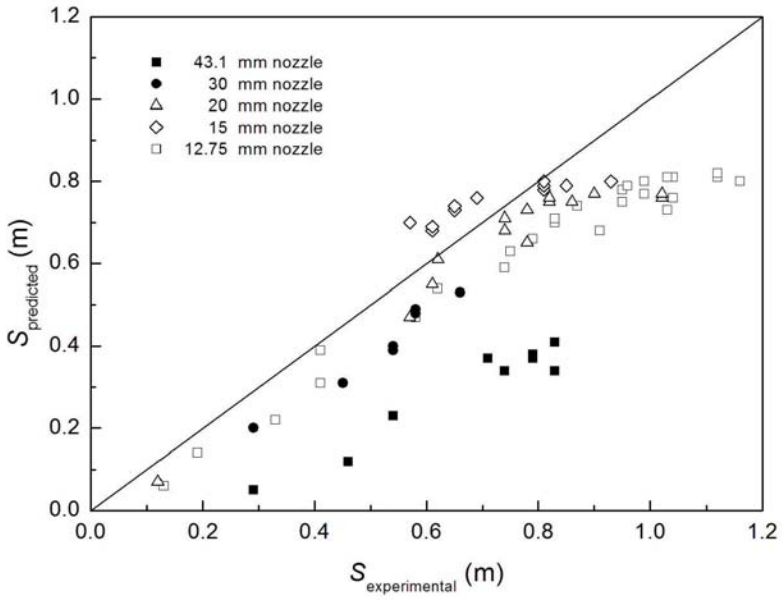

Figure 3.23. Sonic and subsonic lift-off distances predicted by Kalghatgi's (1984) equation and experimental data.

Fig. 3.23 shows the present experimental lift-off distances, under sonic and subsonic conditions, compared with the expression suggested by Kalghatgi (1984).

It can be seen from Fig. 3.23 that the lift-off distance is generally underestimated by this equation, specially the data obtained with the 43.1 mm orifice diameter. It can also be seen that except for the data obtained with d = 43.1 mm, the predictions at low and middle values of S agree with the suggested expression; while at higher lift-off distances –around lift-off distances of 0.9 m in length– more scattering is found. Hydrogen lift-off heights measured by Wu *et al.* (2007 and 2009), were also underestimated, when predicted by Kalghagti's (1984) expression.

Figs. 3.24 and 3.25 show the comparison between the present lift-off data, and the prediction from the expression proposed by Miake-Lye and Hammer's (1988). Due to uncertainties in the jet exit velocity used in this correlation, two plots concerning either the jet exit velocity at the outlet orifice or the velocity when the gas expands fully to atmospheric pressure are shown.

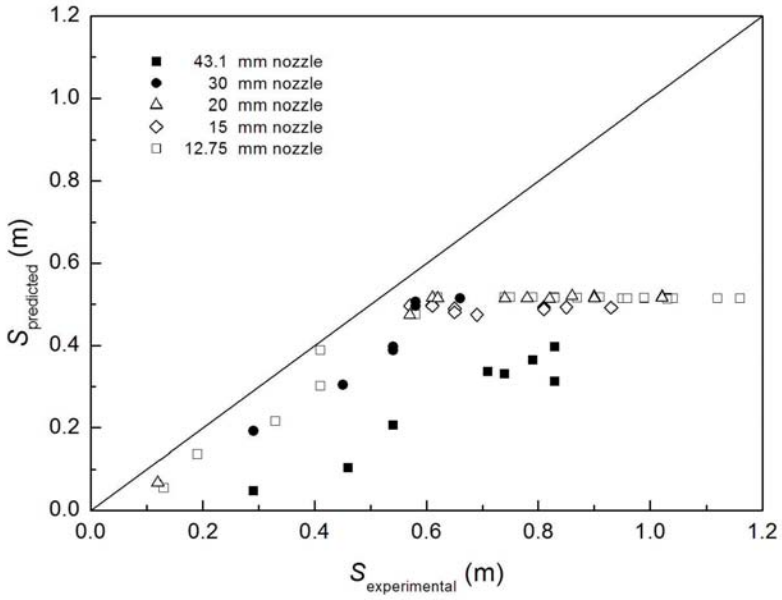

Figure 3.24. Comparison between the sonic and subsonic lift-off distances predicted by Miake-Lye and Hammer's (1988) equation and experimental data.

Fig. 3.24 shows that when the jet exit velocity at the outlet orifice is used in the correlation suggested by Miake-Lye and Hammer (1988), this expression can only be applied to subsonic conditions, since in the sonic regime, a constant lift-off height value is predicted for all the pipe diameters, since the velocity remains constant at the speed of sound in that gas. From Fig. 3.24, it can also be seen that most of the experimental values are underestimated.

The predictions of the measured lift-off data using the Miake-Lye and Hammer's (1988) correlation, involving the velocity when the gas expands fully to atmospheric pressure, are shown in Fig. 3.25. Although it can be seen that most of the data are correctly predicted, the subsonic data obtained with the larger orifice pipe diameter (43.1 mm) are underestimated and scatter is found for the highest lift-off distance values.

It is also important to note that Rokke *et al.* (1994) found that the Miake-Lye and Hammer's (1988) correlation underpredict methane lift-off heights.

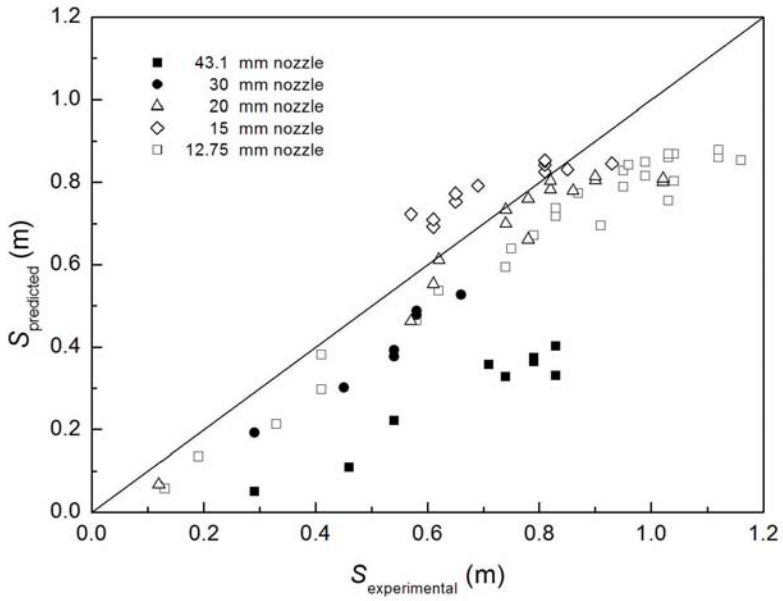

Figure 3.25. Comparisons between the sonic and subsonic lift-off distances predicted by the Miake-Lye and Hammer's (1988) equation, involving the velocity when the gas expands fully to atmospheric pressure, and experimental data.

The lift-off distances under sonic and subsonic regimes predicted by the expression proposed by Wu *et al.* (2007) are plotted in Fig. 3.26. This expression is based on the previous equation proposed by Kalghatgi (1984).

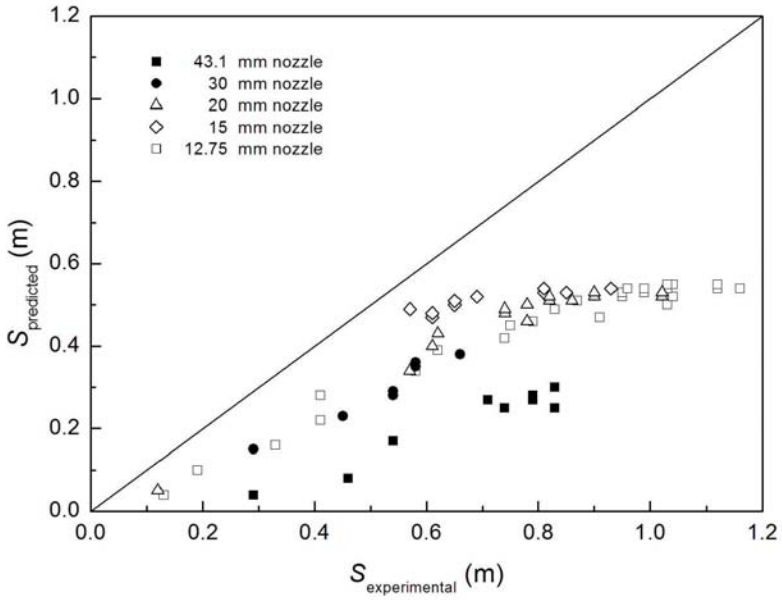

Figure 3.26. Sonic and subsonic lift-off distances predicted by Wu's *et al.* (2007) equation versus the present experimental data.

From Fig 3.26 it can be seen that the present experimental lift-off distances are underestimated by the expression suggested by Wu *et al.* (2007).

In 2009, Wu and co-authors obtained new data on hydrogen-methane mixtures jet flames, modifying the numerical constant involved in their previously suggested expression (Wu *et al.*, 2007). The numerical constant slightly changed from 46 (Wu *et al.*, 2007) to 48 (Wu *et al.*, 2009). Fig. 3.27 shows the comparison between the present experimental lift-off heights and the values obtained by using Wu's *et al.* (2009) correlation.

Finally, Fig. 3.27 shows that the present experimental lift-off distances are again underestimated when using the expression suggested by Wu *et al.* (2009).

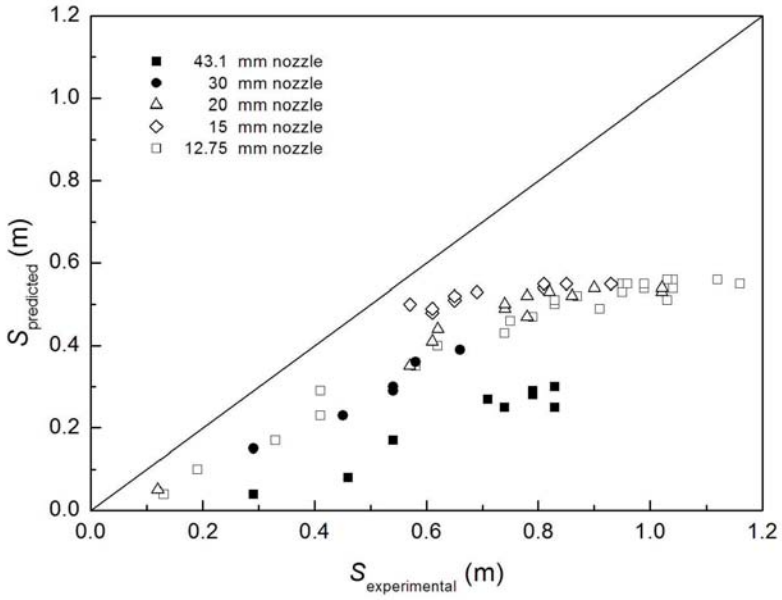

Figure 3.27. Sonic and subsonic lift-off distances predicted by Wu's *et al.* (2009) equation, and experimental data.

3.8.2. Sonic total jet flame height

The jet flame data used in the present suggested correlation for sonic total jet flame height (Eq. (3.14)), obtained from several authors (Kalghatgi, 1984; McCaffrey and Evans, 1986; Schefer *et al.*, 2007; Imamura *et al.*, 2008; Mogi and Horiguchi, 2009), including the present study, have been compared with the values obtained from the expression suggested by Kalghatgi (1984). This expression was selected since, according to Kalghatgi it can be applied to diverse fuels. The models of Hawthorne *et al.* (1949) and Becker and Liang (1978) have not been used since the predictions of the present propane jet fires by Hawthorne's *et al.* (1949) expression gave for a specific pipe diameter, a unique value for the jet flame height. Becker and Liang's (1978) expression, involving iterative procedures, overestimated the present experimental jet flame heights of propane (Fig. 3.22), and also the experimental measurements of Kalghagti (1984). The sonic jet flame data used in the present suggested correlation (Eq. (3.14)) for sonic total jet flame height being predicted by the expression proposed by Kalghatgi (1984) are shown in Fig. 3.28.

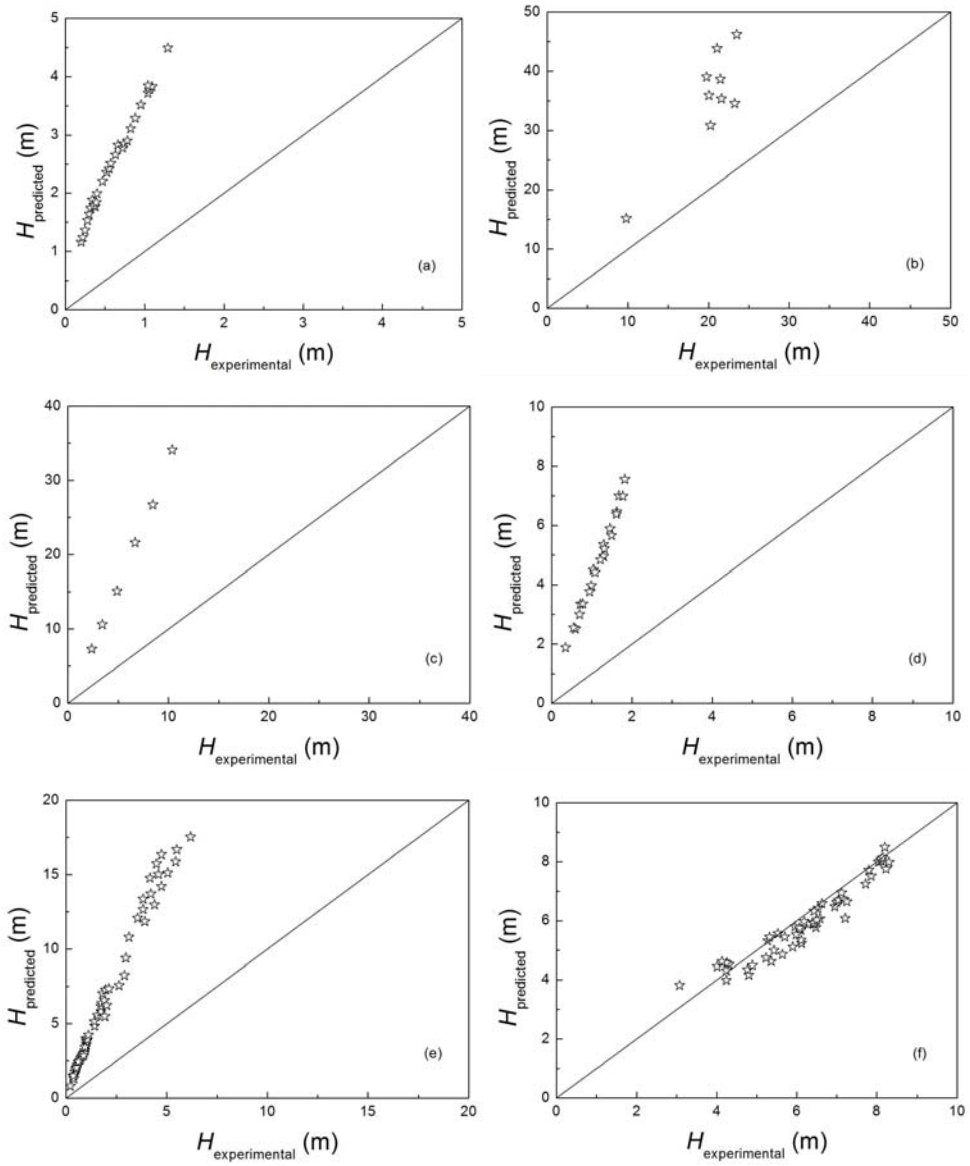

Figure 3.28. Comparisons between the sonic jet flame lengths predicted by Kalghatgi's (1984) equation and experimental data: (a) Kalghatgi (1984), H_2 flames; (b) McCaffrey and Evans (1986), CH_4 flames; (c) Schefer *et al.* (2007), H_2 flames; (d) Imamura *et al.* (2008), H_2 flames; (e) Mogi *et al.* (2009), H_2 flames; (f) present study, C_3H_8 flames.

It can be seen from Fig. 3.28 that the sonic hydrogen data obtained by Kalghatgi (1984), Schefer *et al.* (2007), Imamura *et al.* (2008) and Mogi *et al.* (2009), together with the sonic jet flames of methane obtained by McCaffrey and Evans (1986), are overestimated by Kalghatgi's (1984) expression (Figs. 3.28 (a)-(e)); instead, as already noted in Fig. 3.22 concerning the present sonic data, the expression suggested by Kalghatgi (1984), involving iterative equations, gave good predictions for the present sonic jet flames of propane, with a slight underestimation of some of the data (Fig. 3.28 (f)).

4. FLAME SHAPE

In a risk analysis of an accident scenario involving a jet flame, the size and geometry of the jet flame can be used to determine the separation distances required between structures and equipment and a potential fuel source, in order to avoid flame impingement, which could lead to a further accident. For this reason, a better understanding of jet flame geometry is required to be able to predict the shape and dimension of jet fires and to increase the accuracy in the prediction of their effects. This is of great interest in compact settings, such as those often found in process plants or offshore oil platforms, where a jet fire will often impinge on pipes or equipment, leading to a dangerous situation.

4.1. Literature review

The jet flame geometry has been addressed by several authors through experimental and theoretical approaches. These are discussed in the next sections and compared with our results.

4.1.1. Flame shape

Burke and Schumann (1928) described the surface of laminar jet flames by two types of shape, those of over-ventilated and under-ventilated flames (Fig. 4.1), from a study on the structure of circular and flat confined laminar flames, obtained with gas velocities of less than 0.61 m/s and heights of less than 0.25 m.

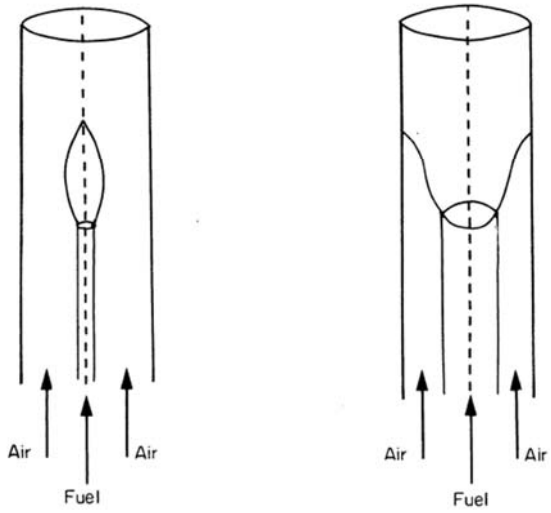

Figure 4.1. The structure of laminar flames: (left) over-ventilated flame, and (right) under-ventilated flame in a concentric duct (taken from Drysdale, 1994).

Concerning turbulent flames, Hawthorne *et al.* (1949), based on an experimental study on turbulent vertical flames of a wide variety of fuels with lengths of up to 1 m, issuing into still air, suggested an inverted circular cone, with the apex located approximately at the orifice exit to define the shape of jet flames (Fig. 4.2(a)). This conical shape has been also proposed by other later authors (Odggard, 1983; Turns, 1991; Schefer *et al.*, 2004; Schefer *et al.*, 2007).

For the jet flame surface of turbulent vertical flames with negligible buoyant force, Baron (1954) proposed a shape resembling a vertical ellipse (Fig. 4.2 (b)). The suggested elliptical shape was compared with the tracing of a photograph of a subsonic small-scale city-gas flame, taken during the experimental work on city-gas and butane flames of up to 1.35 m in length developed by Whol *et al.* (1949(a)). However, once more the features of this flame were very different from those of real accidental jet fires, which are usually larger and are associated to sonic exit velocities.

Another shape proposed to define jet flames has been a cylinder. Several authors have suggested this shape based on both experimental and theoretical studies on subsonic jet fires (Odggard, 1983; Schuller *et al.*, 1983; Sonju and Hustad, 1984; Hustad and Sonju, 1986 and Bagster; Schubach, 1996).

A frustum of a cone (Fig. 4.2 (c)) has been suggested as another proposal for flame shape (Kalghatgi, 1983; Chamberlain, 1987; Johnson *et al.*, 1994). However, although this figure can be used to define the form of a turbulent diffusion flame in a cross-wind (Brzustowski *et al.*, 1975; Gollahalli *et al.*, 1975; Kalghatgi, 1983; Cook *et al.*, 1990), a horizontally released jet fire (Becker and Liang, 1981; Gore and Jian, 1991; Johnson *et al.*, 1994) or a flare under the influence of wind (Brzustowski *et al.*, 1975; APIRP521, 1982; McMurray, 1982; Chamberlain, 1987; APIRP521, 1997), it does not correspond to the contour of a real accidental vertical jet fire in still air. It is important to note that from Kalghatgi's (1983) experimental data on flames of a wide variety of fuels of up to 2.7 m in length, obtained at cross-wind speeds ranging between 2.7 and 8.1 m/s, it can be deduced that at relatively high wind speeds the diffusion flame described as a frustum of a cone becomes almost cylindrical in shape (Mudan and Croce, 1990).

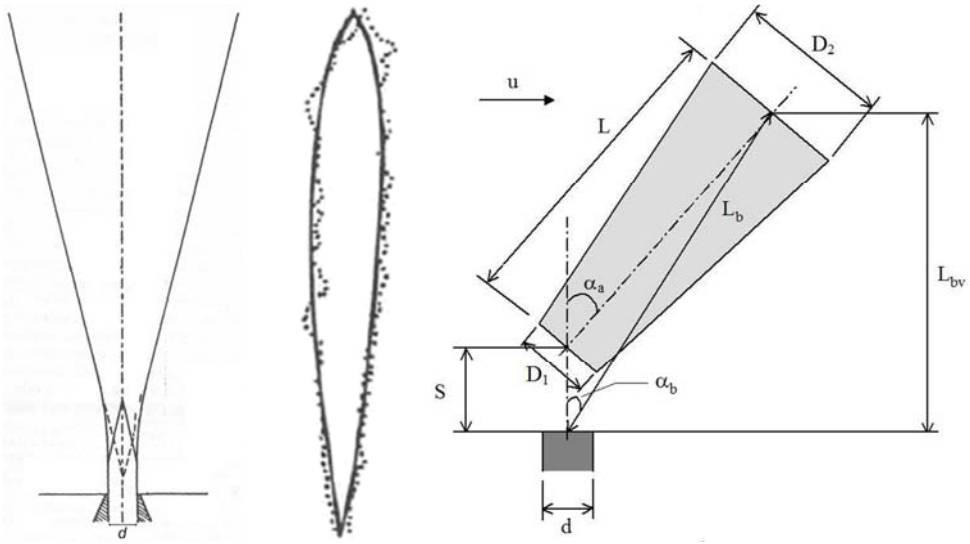

Figure 4.2. Suggested flame shapes: (a) An inverted circular cone (Hawthorne *et al.*, 1949; Odggard, 1983; Turns, 1991; Schefer *et al.*, 2004 and Schefer *et al.*, 2007); (b) A kind of ellipse, proposed by Baron (1954); full line corresponds to the theoretical prediction and dotted line is the tracing of a photograph by Wohl *et al.* (1949(a)); (c) A frustum of a cone (Kalghatgi, 1983; Chamberlain, 1987; Johnson *et al.*, 1994) illustrating the influence of cross-winds.

It can be seen that most of these studies concern either flares or subsonic jet fires, the conditions of which significantly differ from those found in accidental jet fires. This lack of research on the shape of large-scale sonic hydrocarbon jet fires means that they are still poorly understood.

4.1.2. Jet flame width correlations

The jet flame width has been found to be a function of several variables, such as the mass flow rate (Imamura *et al.*, 2008), the dimensionless heat released by combustion (Sugawa and Sakai, 1997), the stagnation pressure (Iwasaka *et al.*, 1979; Imamura *et al.*, 2008; Mogi and Horiguchi, 2009) and the Froude number (Iwasaka *et al.*, 1979; Schuller *et al.*, 1983; Sonju and Hustad, 1984; Hustad and Sonju, 1986; Bagster and Schubach, 1996).

Most models defining flames by their centreline trajectory do not have expressions to address jet flame width. Furthermore, most of the few suggested expressions for jet flame width are related to either hydrogen flames or jet fires with a subsonic exit velocity.

4.1.3. Flame trajectory and displacements

Several expressions for estimating the trajectory and vertical and horizontal displacement of a jet flame have been suggested. These studies concern horizontal jet flames (Becker and Liang, 1981; Gore and Jian, 1991; Johnson *et al.*, 1994), jet flames in the presence of cross winds (Brzustowski *et al.*, 1975; Gollahalli *et al.*, 1975; Kalghatgi, 1983; Cook *et al.*, 1990) and flares (Brzustowski *et al.*, 1975; APIRP521, 1982; McMurray, 1982; Cook *et al.*, 1987b; Cook *et al.*, 1987c; Chamberlain, 1987; APIRP521, 1997).

4.1.4. The relationship between jet flame length and width

From both experimental and theoretical studies, the relationship between jet flame length and width has been proposed by several authors (Hawthorne *et al.*, 1949; Baron, 1954; Schuller *et al.*, 1983; Sonju and Hustad, 1984; Hustad and Sonju, 1986; Turns and Myhr, 1991; Schefer *et al.*, 2004; Schefer *et al.*, 2007; Brennan *et al.*, 2009; Mogi and Horiguchi, 2009); the values proposed have been summarized in Table 4.1.

Table 4.1 Relationship between flame length and flame width based on experimental data

Authors	*L/D*	Flame type	Fuel	Notes
Hawthorne *et al.* (1949)	5.3[a]	Vertical turbulent small-scale flames, up to 1 m in length, obtained with circular nozzles ranging between 3 and 8 mm[b]	Acetylene, carbon monoxide, city gas, hydrogen, propane, mixtures of CO_2-city gas and H_2-propane	—
Baron (1954)[c]	8.3[a,d]	Vertical turbulent flames with negligible buoyant force, obtained with a 10.16 mm circular exit	City gas	Suggested theoretical shape resembling a vertical ellipse (Fig. 4.2 (b)), compared with a subsonic small-scale city gas flame (Wohl *et al.*, 1949(a)). Maximum flame width found at 61% of jet flame length.
Schuller *et al.* (1983)	6.3[e,f]	Vertical turbulent subsonic jet flames, obtained with circular and rectangular nozzles[g,h]	Methane and propane	—
Sonju and	8.4[e,f]	Vertical turbulent	Methane	—

Hustad (1984)	6.75[e,f]	subsonic jet flames, up to 8 m in length, obtained with circular nozzles ranging between 10 and 80 mm[g]	Propane	
Hustad and Sonju (1986)[i]	8.4[e,f]	Vertical turbulent subsonic jet flames, up to 8 m in length, obtained with circular and rectangular nozzles[g,h,j]	Methane	*L/D*: flames from circular and rectangular nozzles.
	6.75[e,f]		Propane	*L/D*: flames from circular and rectangular nozzles.
	6.75[e,f]		Propane/oil mixtures	*L/D*: flames from circular nozzles.
Turns and Myhr (1991)	5.9[a,d,e]	Vertical turbulent jet flames stabilized with hydrogen, obtained with circular exits ranging between 2.18 and 6.17 mm[b]	Ethylene, methane, propane and a mixture of CO-H_2	—
Schefer *et al.* (2004)	5.9[a,d,e]	Vertical high-pressure (up to 172 bar) jet fires, up to 5.8 m in length, obtained through a 7.94 mm circular exit[b]	Hydrogen	—
Schefer *et al.* (2007)	5.9[a,d,e]	Vertical high-pressure (up to 413 bar) jet flames, up to 10.7 m in length, obtained with a 5.08 mm circular exit[b]	Hydrogen	—

Brennan *et al.* (2009)[c]	4–9[a,d,e]	A vertical jet fire at 296 bar (Schefer *et al.*, 2007), obtained through a 5.08 mm circular exit[b]	Hydrogen	CFD large eddy simulation approach of the experimental work carried out by Schefer *et al.* (2007).
Mogi and Horiguchi (2009)	5.6[a,d,e]	Horizontal high-pressure (up to 400 bar) jet flames, up to 6.2 m in length, obtained with circular nozzles ranging between 0.4 and 4 mm	Hydrogen	Flames of up to 1.4 m length were also obtained through slit nozzles with a cross-sectional area equal to that of a circular nozzle d = 1 mm. L/D: 0.25 times the value of the ratio obtained with circular nozzles.

[a] D corresponds to the maximum flame width.

[b] A conical shape has been assumed to describe the jet flame.

[c] Based on either a theoretical study or simulations.

[d] The L/D ratio was calculated as the inverse of the proposed value of D/L.

[e] L is defined as the distance from the gas release point to the tip of the visible flame.

[f] D is the average over the visible flame height.

[g] The jet flame has been modeled as a cylinder.

[h] Circular nozzles ranging between 10 and 80 mm; while the ratios length/width of the rectangular slots have been ranged up to 8000.

[i] Some of the results had already been published in Sonju and Hustad (1984) .

[j] Horizontal propane flames were also obtained, but no L/D ratio was established.

Table 4.1 shows the relationship between jet flame length and width varied from 5.3 to 8.4 (based on experimental jet fires obtained from circular exits). It should be noted that this L/D ratio dependence on the type of fuel is still uncertain, since the results of published studies are rather contradictory (Hawthorne *et al.*, 1949; Schuller *et al.*, 1983; Sonju and Hustad, 1984; Hustad and Sonju, 1986; Turns and Myhr, 1991). Thus, although the described literature improves our understanding of jet flames, there is a lack of experimental research into large-scale hydrocarbon sonic jet flames and methods that could be used to estimate the flame length and width of jet fires.

4.2. Experimental data

The flame width of the present jet flames, at both sonic and subsonic exit velocities, were assessed using the infrared thermographic video recordings, corresponding to the stationary state. The jet flame width has been obtained from the jet flame surface, defined by the previously mentioned temperature criterion (Chapter 3, Fig. 3.19), considering the existence of flame over the region where a minimum given temperature (800 K) had been reached. The length of such a flame is defined as the *radiant jet flame length* (L_{IR}).

The jet flame width ($D_{p\ exp}$) was measured from the registered images, according to this criterion, at five heights: 10%, 30%, 50%, 70%, and 90% of the radiant jet flame length (Fig. 4.3).

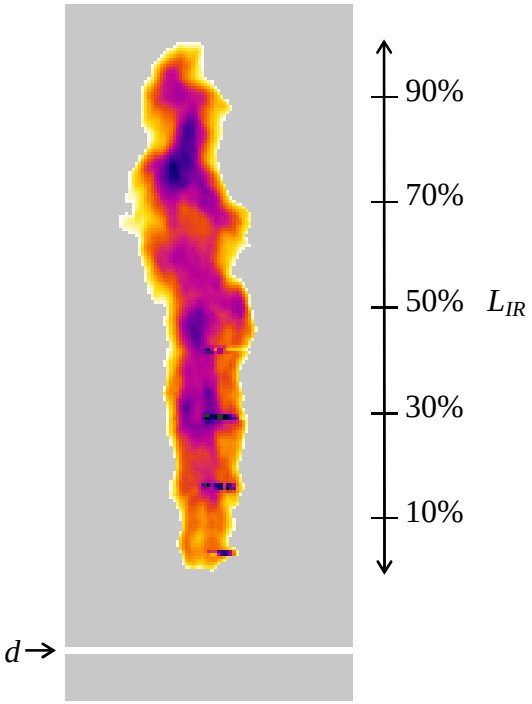

Figure 4.3. An infrared image showing the heights at which the widths ($D_{p\ exp}$) along the radiant jet flame length (L_{IR}) were measured ($D_{p\ exp}$ at 10%, 30%, 50%, 70%, and 90% of L_{IR}). The height at which the outlet orifice diameter was located is shown by the bottom horizontal white line. The isotherm of 800 K (approximately the Draper temperature) was used to define the jet flame contour.

4.3. Data processing

During testing, jet flames generally remained stabilized in a lifted configuration, in which lift-off height increased with the mass flow rate. Nevertheless, the blow-out phenomenon (self-extinction of jet flame immediately after ignition) did occur during the experiments in which an outlet orifice diameter of 10 mm was used (Fig. 1.11). These data were not considered because the conditions with which these flame shapes were obtained do not correspond to those found in real and stable accidental jet fires.

4.3.1. Jet flame width

Several approaches have been analyzed in the present study; however, as later discussed, the approach characterizing the shape of jet flames based on a radiating cylinder, defining the flame length by a radiant flame length (L_{IR}) and a jet flame "equivalent diameter" (D_{eq}), with a volume equal to that surrounded by the jet fire surface corresponding to the isotherm of 800 K, has been proposed to represent the shape of sonic and subsonic jet flames, vertically released into still air. Table 4.2 shows the values of L_{IR}, D_{eq} and the L_{IR}/D_{eq} ratios.

Table 4.2. Experimental data concerning radiant jet flame length (L_{IR}), jet flame equivalent diameter (D_{eq}) and the L_{IR}/D_{eq} ratio

d (m)	L_{IR} (m)	D_{eq} (m)	L_{IR}/D_{eq} (-)
0.01275	0.80	0.24	3.3
0.01275	1.51	0.26	5.8
0.01275	2.45	0.28	8.8
0.01275	3.03	0.29	10.4
0.01275	2.78	0.38	7.3
0.01275	3.39	0.41	8.3
0.01275	3.62	0.47	7.7
0.01275	4.06	0.52	7.8

0.01275	4.02	0.58	6.9
0.01275	4.10	0.60	6.8
0.01275	4.45	0.57	7.8
0.01275	4.40	0.60	7.3
0.01275	4.81	0.62	7.8
0.01275	4.40	0.67	6.6
0.01275	5.03	0.63	8.0
0.01275	5.17	0.66	7.8
0.01275	5.07	0.65	7.8
0.01275	4.71	0.72	6.5
0.01275	4.58	0.75	6.1
0.01275	5.14	0.74	6.9
0.01275	5.49	0.73	7.5
0.01275	4.80	0.84	5.7
0.01275	5.39	0.75	7.2
0.01275	5.16	0.85	6.1
0.01275	5.43	0.78	7.0
0.01275	5.16	0.78	6.6
0.01275	5.46	0.82	6.7
0.015	4.66	0.71	6.6
0.015	4.71	0.81	5.8
0.015	5.42	0.76	7.1
0.015	5.42	0.78	6.9
0.015	5.78	0.86	6.7
0.015	6.52	0.90	7.2
0.015	5.72	0.99	5.8
0.015	6.10	1.03	5.9

0.015	5.82	1.02	5.7
0.015	6.07	1.03	5.9
0.015	6.23	1.02	6.1
0.015	6.37	1.01	6.3
0.02	2.18	0.35	6.2
0.02	4.56	0.71	6.4
0.02	5.89	0.73	8.1
0.02	5.81	0.81	7.2
0.02	6.47	0.84	7.7
0.02	6.38	0.96	6.6
0.02	6.98	0.95	7.3
0.02	7.08	0.98	7.2
0.02	6.94	1.00	6.9
0.02	7.41	1.05	7.1
0.02	7.28	1.08	6.7
0.02	7.22	1.08	6.7
0.02	7.20	1.06	6.8
0.02	7.09	1.11	6.4
0.02	7.25	1.14	6.4
0.03	5.00	0.59	8.5
0.03	5.78	0.79	7.3
0.03	7.45	1.03	7.2
0.03	6.71	0.89	7.5
0.03	7.06	0.95	7.4
0.03	7.42	1.00	7.4
0.03	7.54	1.02	7.4
0.0431	7.60	1.18	6.4

0.0431	9.27	1.34	6.9
0.0431	9.78	1.40	7.0
0.0431	10.07	1.35	7.5
0.0431	10.13	1.43	7.1
0.0431	10.19	1.46	7.0
0.0431	10.31	1.40	7.4
0.0431	10.30	1.35	7.6
0.0431	10.14	1.44	7.0

From Table 4.2 it can be seen that the present data concern relatively large jet fires of up to 10.3 m in length and 1.5 m in width.

4.4. Results

The observations of the infrared images, defining the flame boundary as that corresponding to a temperature of 800 K, were analyzed and compared with the shapes proposed in previous research projects.

4.4.1. Vertical elliptical shape

As a first stage, the shape of sonic and subsonic exit velocity jet flames was analyzed using the theoretical shape suggested by Baron (1954), which resembles a type of vertical ellipse (Fig. 4.2 (b)), defined by the following expression:

$$D_p = b \cdot p \cdot \left(\ln\left(\frac{L}{p} \right) \right)^{1/2} \tag{4.1}$$

In Baron's (1954) theoretical study, the constant *b* shown in Eq. (4.1) was found to be 0.29; this expression was used by Baron (1954) to predict an experimental subsonic exit velocity small-scale jet flame obtained by Wohl *et al.* (1949(a)), concerning a study into butane and city-gas jet fires

with flames of up to 1.35 m in length. However, additional research has been required to test Eq. (4.1), since the conditions created in the experimental study (Wohl *et al*., 1949(a)) significantly differed from those found in real accidental jet fires (larger flame lengths and sonic exit velocities).

By using the jet flame widths ($D_{p\ exp}$) measured at 10%, 30%, 50%, 70%, and 90% of L_{IR}, an attempt to check the expression proposed by Baron (Eq. (4.1)), trying to find a resemblance between Baron's theoretical shape and the one shown by the present experimental sonic and subsonic exit velocity jet flames, has been carried out.

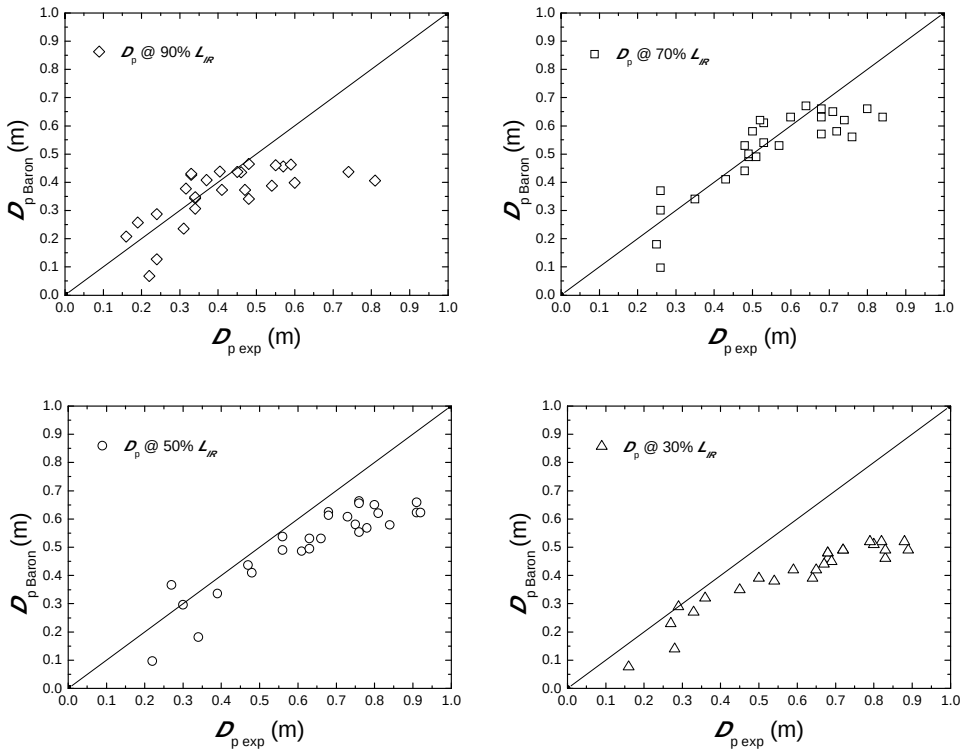

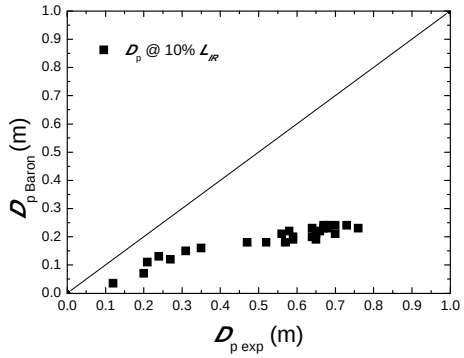

Figure 4.4. Measurements ($D_{p\ exp}$) and predictions ($D_{p\ Baron}$) of sonic and subsonic exit velocity jet flame widths at 10%, 30%, 50%, 70% and 90% of the radiant flame length (L_{IR}), using a 12.75 mm outlet orifice.

Fig. 4.4 shows that although the predictions obtained for $D_{p\ exp}$ at 50% and 70% of L_{IR} are fairly accurate, the results of the predictions and measurements at 90% of L_{IR} are quite different, particularly for larger flames. Finally, the values corresponding to 10% and 30% of L_{IR} show the predicted values for D_p ($D_{p\ Baron}$) to be smaller than the experimental values ($D_{p\ exp}$). Therefore, according to these data, the expression suggested by Baron does not accurately predict the flame shape in the bottom zone.

An analysis of the sonic and subsonic exit velocity jet flames obtained with d = 20 mm was then carried out. It was found that most of the predicted jet flame widths ($D_{p\ Baron}$) were lower than the experimental flame widths (except for two values obtained at 70% of L_{IR}), again indicating the bottom of the flame to be similar to the base of a cylinder. Among all the jet flame width predictions along L_{IR}, those obtained at 10% most significantly illustrated this trend (Fig. 4.5).

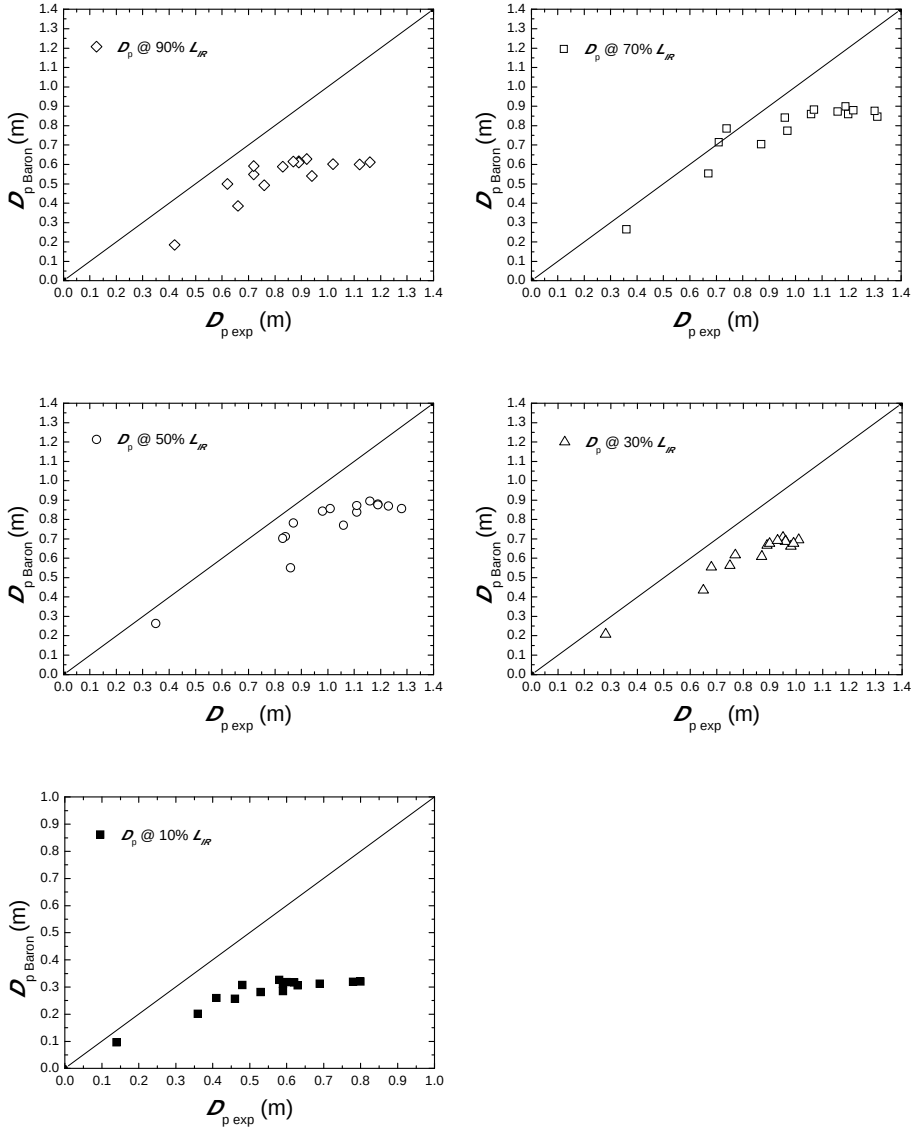

Figure 4.5. Measurements ($D_{p\ \mathrm{exp}}$) and predictions ($D_{p\ \mathrm{Baron}}$) of sonic and subsonic exit velocity jet flame widths at 10%, 30%, 50%, 70% and 90% of the radiant flame length (L_{IR}), using a 20 mm outlet orifice.

As a later stage, the analysis of the sonic and subsonic exit velocity jet flames obtained with the 30 mm outlet orifice was carried out. The results for the comparisons between predicted and measured flame widths were relatively consistent for most data. However, the results for 90% of L_{IR} showed the experimental flame widths ($D_{p\ exp}$) at the highest part of the jet flame to be higher than those predicted by the elliptical shape ($D_{p\ Baron}$). For the bottom of the flame, the experimental measurements at 10% of L_{IR} were again higher than the predicted ones.

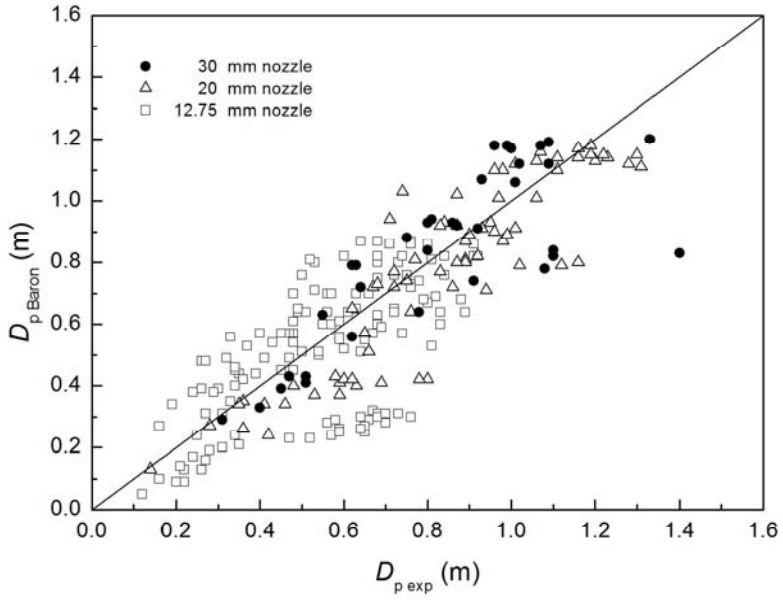

Figure 4.6. Predictions of the sonic and subsonic jet flame widths ($D_{p\ exp}$), obtained with various orifice outlet diameters, using Eq. (4.1) with b = 0.38, and experimental data. The used b constant has been obtained from the correlation of the present experimental data, obtained with d = 12.75 mm, 20 mm and 30 mm.

The constant (b) in Eq. (4.1) has been then determined using the present early mentioned experimental data. By using the 12.75 mm and 30 mm outlet orifices, respectively, b was found to be 0.37 in both cases. When the 20 mm outlet orifice was used and all the data obtained with all three outlet orifices were used (i.e. 12.75, 20 and 30 mm), the b constant was 0.4 and 0.38, respectively. The predictions of the present experimental sonic and

subsonic jet flame widths using b = 0.38 and the theoretical value of b = 0.29, suggested by Baron (1954), are shown in Figs. 4.6 and 4.7, respectively.

It should be noted that the use of the empirical constant b = 0.38 (Eq. (4.1)), resulted in significant scattering of the present experimental data (R^2 = 0.62).

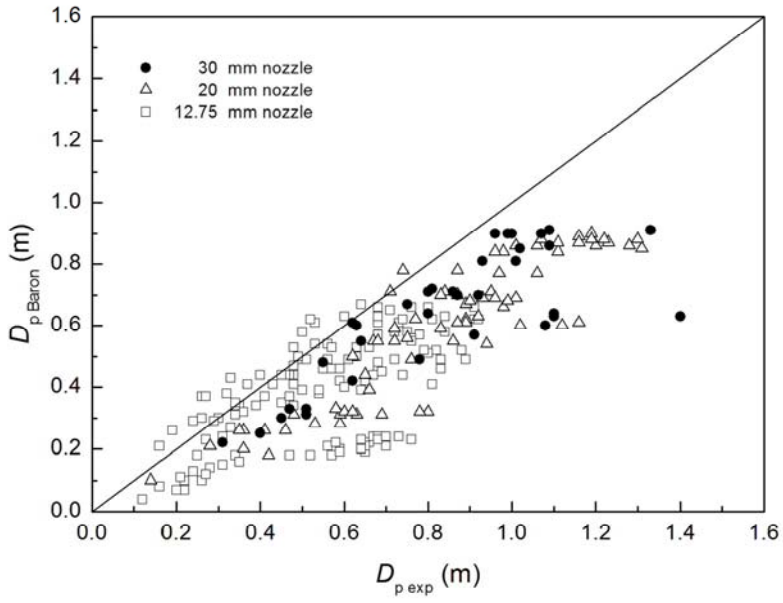

Figure 4.7. Predictions of the sonic and subsonic jet flame widths ($D_{p\,exp}$), obtained with various outlet diameters, using Eq. (4.1) with b = 0.29, and experimental data. The used b constant has been suggested by the theoretical study of Baron (1954).

From Fig. 4.7 it can be seen that most of the data predicted by the expression suggested by Baron (1954) are underestimated.

It should also be mentioned that in Baron's (1954) study, the maximum flame width ($D_{p\,max}$) has been found to appear at 61% of the flame length; while the results obtained with the three analyzed outlet orifice diameters (i.e. 12.75, 20 and 30 mm) have shown the maximum flame width occurring at 55% of the radiant flame length.

Therefore, the theoretical shape suggested by Baron (1954) seems to predict sonic and subsonic exit velocity jet flames relatively well at the middle part of the flame (i.e. at 50% and 70% of L_{IR}). However, the trend shown by the present experimental widths at both the bottom and tip of the flame (e.g. at 10%, 30%, and 90% of L_{IR}) differed from the one predicted by the elliptical shape. Thus, further research on the shape of sonic and subsonic exit velocity jet fires was performed.

4.4.2. Average jet flame diameter (D_{ave})

A jet flame diameter averaged over the jet flame length has also been used in several experimental studies on subsonic exit velocity jet flames (Schuller *et al.*, 1983; Sonju and Hustad, 1984; Hustad and Sonju, 1986). Following this approach, assuming a two-dimensional plane flame, the present sonic and subsonic exit velocity jet flames were considered as a rectangle of height L (the height of the radiant jet flame, L_{IR}) and diameter D_{ave}, corresponding to an average jet flame width value obtained along L_{IR}.

D_{ave} is the arithmetic mean value of the jet flame widths $D_{p\ exp}$ measured at 10%, 30%, 50%, 70% and 90% of the radiant flame length (L_{IR}). The orifice exit diameters considered in this analysis were 12.75 mm, 20 mm and 30 mm.

The use of D_{ave} underestimates the width of jet fires, since the flame widths measured at the bottom and tip flame zones (i.e. at 10% and 90% of L_{IR}) have been found to be smaller than the rest of the flame widths measured along L_{IR}. This trend was observed using the data obtained with a 12.75 mm orifice exit diameter, in which the $D_{p\ exp}$ values for flame tip measured at 90% of L_{IR} were generally the smallest flame diameters measured along L_{IR} (Fig. 4.8). Similar results were obtained with the orifice outlet diameters of 20 mm and 30 mm, where the smallest flame widths ($D_{p\ exp}$) were obtained at 10% of L_{IR}.

From Fig. 4.8 it can be seen that the lines shown at the top of the plot concern those jet flame widths obtained with the highest mass flow rates; since, the jet flame width has been found to increase with m.

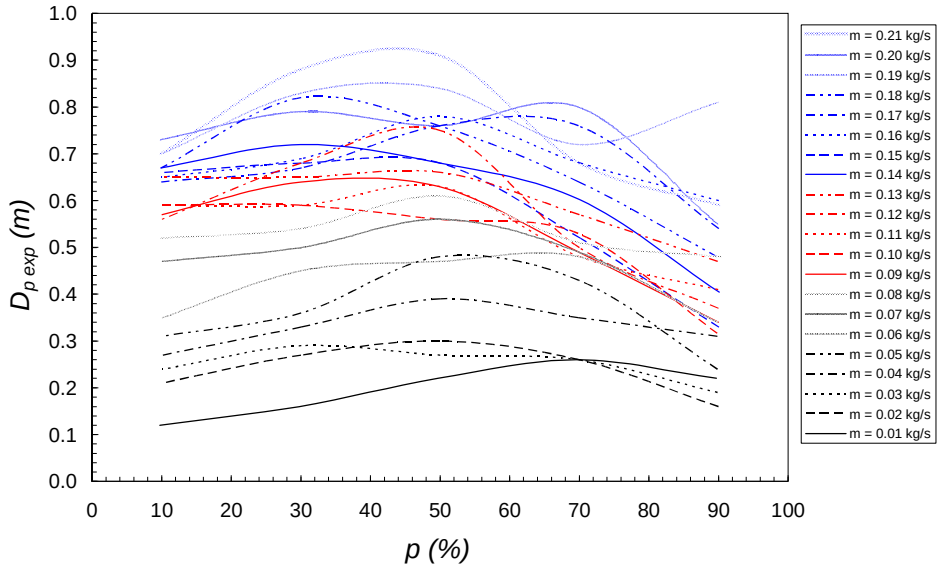

Figure 4.8. Experimental sonic and subsonic exit velocity jet flame widths ($D_{p\ exp}$), measured at different percentages of axial flame position (p): 10%, 30%, 50%, 70% and 90% of radiant jet flame length, for a 12.75 mm orifice outlet diameter. The trend of the experimental data is shown by the lines.

Due to the influence of the smallest diameters measured at the bottom and tip of the flame, D_{ave} gives a slightly smaller value than that found in practice. Consequently, a third approach was applied.

4.4.3. Cylindrical shape: equivalent flame diameter (D_{eq})

The shape of the sonic and subsonic exit velocity jet flames was also characterized based on a radiating cylinder, defining the flame length by the radiant flame length (L_{IR}), and a jet flame "equivalent diameter" (D_{eq}), with a volume equal to that surrounded by the jet fire surface corresponding to the isotherm of 800 K. The two-dimensional area of the corresponding rectangle (A_{IR}) was determined by applying an algorithm developed in MATLAB R2007b®, through which each infrared image was treated to obtain A_{IR}. The small area covered by the thermocouples located along the jet axis, used to measure the axial temperature distribution, was eliminated by applying the same algorithm to each image (Fig. 4.9).

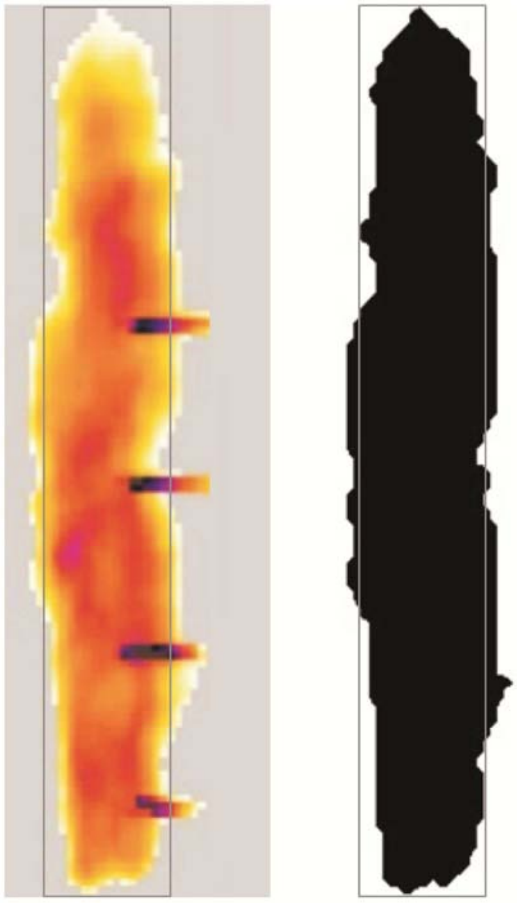

Figure 4.9. An infrared image of the jet flame contour defined by the isotherm of 800 K (left). Example of the transformation of the instantaneous infrared image with the algorithm developed in MatlabR2007b ®, where the area covered by the thermocouples has been removed (right). The suggested rectangular shape, based on the radiant flame length and the equivalent flame diameter, has been drawn in both figures.

For all the data, D_{eq} was calculated as the ratio of A_{IR} to the radiant flame length (L_{IR}):

$$D_{eq} = \frac{A_{IR}}{L_{IR}} \tag{4.2}$$

It should be noted that the D_{ave} values were similar to the D_{eq} values (lightly smaller), showing a difference no greater than 14%. However, since there was a trend in the present data for D_{ave} to underestimate lightly the flame width, the equivalent flame diameter (D_{eq}) is considered the best approach for estimating the jet fire size and shape.

Thus, finally the radiating cylindrical shape defined by the radiant flame length and the equivalent flame diameter is proposed to represent the shape of jet flames at sonic and subsonic exit velocities, vertically released into still air.

4.5. Assessment of empirical correlations

In the present study, the jet flame width has been found to be a function of several variables and dimensionless numbers, such as the mass flow rate, the pipe diameter, the stagnation pressure (related to the mass flow rate), the dimensionless heat released by combustion, involving buoyancy forces, and following the dimensional analysis a function of the orifice's Froude number and the orifice's Reynolds number.

As for the jet flame length and lift-off distance, the jet flame width has been found to increase both with the mass flow rate and the orifice outlet diameter, and to be a function of *Fr* only in the buoyancy-dominated jet regime, regime that does not apply for sonic jet exit velocities.

Thus, the equivalent jet flame diameter, normalized by the pipe diameter, at sonic and subsonic conditions, has been correlated as a function of the orifice's Reynolds number (*Re*). The dimensionless D_{eq}/d ratio was plotted against *Re* in a log-log plot for all data (Fig. 4.10), showing that D_{eq}/d increases with the value of *Re*. The relationship between D_{eq}/d and *Re* can be given by the following expression ($R^2 = 0.7$):

$$\frac{D_{eq}}{d} = 0.14 \cdot Re^{0.4} \tag{4.3}$$

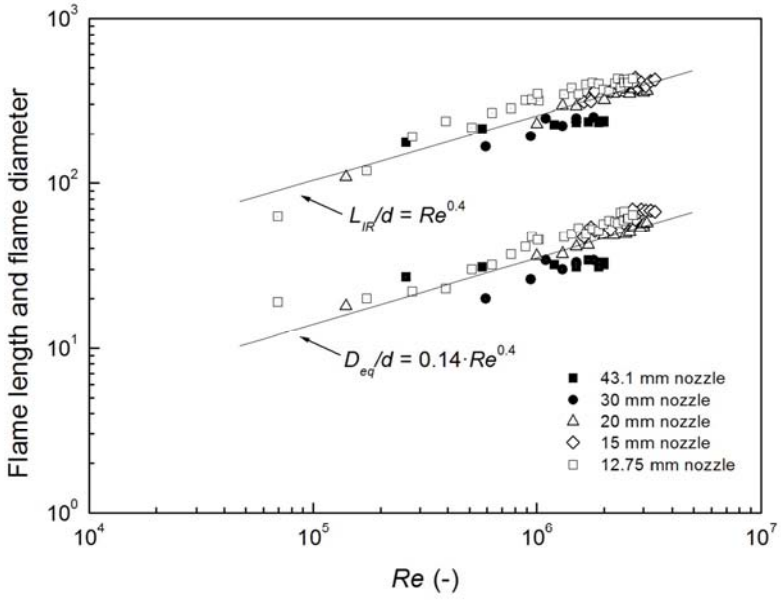

Figure 4.10. Variation of the radiant flame lengths (sonic and subsonic exit velocity) and equivalent jet flame diameters (D_{eq}) as a function of the orifice's exit Reynolds number, for various orifice outlet diameters. Eqs. (3.12) and (4.3) are also shown.

It should be noted that Eqs. (3.12) and (4.3) show that a constant flame-length-to-diameter ratio of 7 (Eq. (4.4)) can be established for all the present subsonic and sonic exit velocity flames ($R^2 = 0.9$):

$$L_{IR} = 7 \cdot D_{eq} \tag{4.4}$$

This can be clearly seen in Fig. 4.11. This ratio is consistent with the experimental values of approximately 7 found for hydrocarbon jet flames, as cited by Turns (1996).

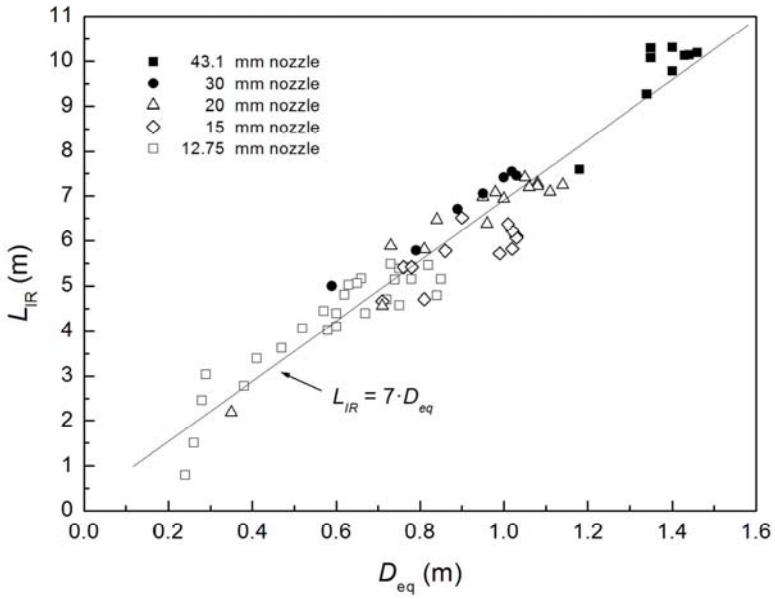

Figure 4.11. Ratio of the radiant flame lengths to the equivalent flame diameters, for various orifice outlet diameters (sonic and subsonic exit velocity). Eq. (4.4) is also plotted.

Fig. 4.12 shows the L_{IR}/D_{eq} ratio plotted against the outlet orifice diameter. It can be observed that almost all L_{IR}/D_{eq} ratios fall within the range 5.7–8.8 (consistent with the previously established range 5.3–8.4, as listed in Table 4.1, based on the experimental results regarding jet flames obtained with circular nozzles), except for the L_{IR}/D_{eq} values of 4.61 and 10.45, which were obtained with the 12.75 mm orifice outlet diameter at subsonic exit velocities.

From Fig. 4.12 it can be seen that the results from the outlet orifices of 15, 20, 30, and 43.1 mm follow the same trend, whereby the L_{IR}/D_{eq} ratio ranges from 5.7 to 7.2, 6.2 to 8.1, 7.2 to 8.5, and 6.4 to 7.6, respectively. The L_{IR}/D_{eq} results for the 12.75 mm outlet orifice vary from 5.7 to 8.8 except for the two aforesaid values. Nevertheless, a constant L_{IR}/D_{eq} ratio of approximately 7 can be established for most of the data.

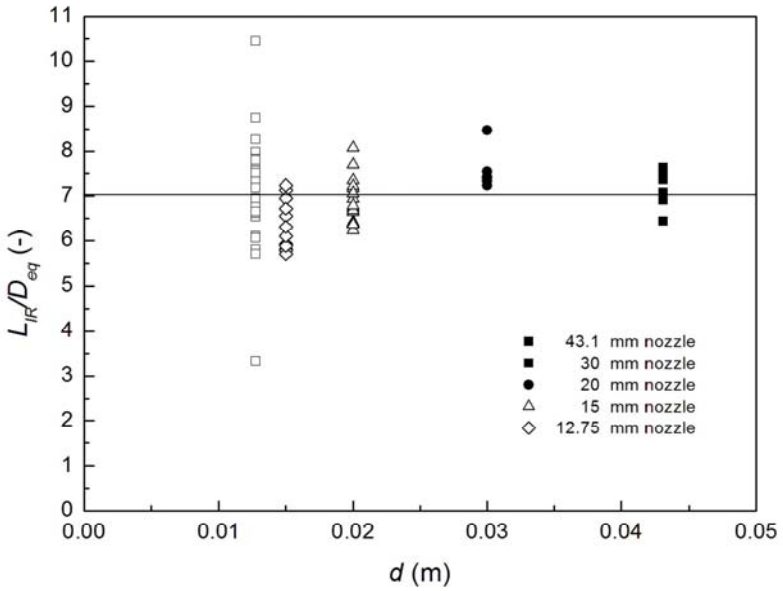

Figure 4.12. Variation of the L_{IR}/D_{eq} ratio as a function of the orifice exit diameter in both sonic and subsonic exit velocity jet flames (standard deviation for all data = 0.85).

5. FLAME RADIATION FEATURES

5.1. Introduction

The area affected by the thermal effects of fires is relatively small as compared to those covered by other major accidents such as explosions or toxic clouds. However, the thermal effects in this area can affect other equipment (a pipe, a tank), leading to a significant increase in the scale, the severity and the consequences of the accident due to the eventual occurrence of a domino effect.

Concerning jet fires, although they are often smaller than pool fires, the heat released by jet flames can be very high and, although the affected area will probably be relatively reduced, the effects on equipment or people over short distances can be very severe. Thus, the knowledge of the radiative properties of jet fires is essential to evaluate their thermal hazards, enabling the setting up of safety distances and measures. However, the data available in the literature on the thermal features of both gas and two-phase jet fires is rather reduced. In this chapter the main thermal features of these fires (thermal radiation at a given distance, surface emissive power and emissivity of the flames) are analyzed.

Several experimental and theoretical studies on the radiative features of jet flames have been carried out by diverse authors. However, once more, most of them concern either subsonic jet fires or flares. The features of such flames differ from those of real accidental jet fires, which usually reach a sonic exit velocity.

Concerning experimental studies on jet flames (Brzustowski *et al*., 1975; API RP521, 1982; McMurray, 1982; Galant and Grouset, 1984; Sonju *et al*.,

1984; Hustad and Sonju, 1985; Gore *et al*., 1986; McCaffrey and Evans, 1986; Cook *et al*., 1987(a); Cook *et al*., 1987(c); Chamberlain, 1987; McCaffrey, 1988; Gore *et al*., 1989; McCaffrey, 1989; Cowley and Pritchard, 1990; API RP521, 1997; Lowesmith *et al*., 2007), it should be noted that natural gas has been the most commonly used fuel. Thus, there is still little information about the radiative characteristics of jet flames from other fuels such as propane or butane.

5.1.1. Estimation of flame radiation intensity

The radiative heat intensity from flames at a given distance depends essentially on the radiative power and the flame's size and shape. The solid flame radiation model is the most commonly used model to estimate the thermal radiation from fires. It is fairly more accurate than the point source model, specially at short distances from the flame, even being rather simple.

According to the solid flame model, the thermal radiation intensity from flames reaching a given target can be estimated by the following expression:

$$I = \tau \cdot F \cdot E \tag{5.1}$$

where τ is the atmospheric transmissivity (-)

F is the view factor between the flame and the target (-) and

E is the surface emissive power ($kW \cdot m^{-2}$).

5.1.1.1. Surface emissive power

The surface emissive power of the flames is the heat emitted by radiation per unit surface of the flame and per unit time; it can be expressed as a function of flame's emissivity and temperature:

$$E = \varepsilon \cdot \sigma \cdot T_f^{\,4} \tag{5.2}$$

where ε is the flame's emissivity (-)

σ is Stefan-Boltzmann constant (5.67 x 10^{-11} kW$\cdot$m$^{-2}\cdot$K^{-4}) and

T_f is the flame temperature (K).

5.1.1.2. Atmospheric transmissivity

Several expressions to estimate the atmospheric transmissivity (τ) can be found in the literature. Some of them (Brzustowski and Sommer, 1973; Yellow Book, 1979; Lihou and Maund, 1982; Jones, 1988; Bagster and Pitblado, 1989; Wayne, 1991; Committee for the Prevention of Disasters, 1997) have been analyzed in the present study.

It has been found that the range of application of some of the above-mentioned expressions do not correspond to the present experimental data. It was also found that some of these expressions are either suitable for flames producing carbon soot or can be only appropriate to certain weather conditions, not taking into account the variation in atmospheric factors such as temperature and humidity. Since the present experimental data differ from the aforesaid features, the literature review led the atmospheric transmissivity to be estimated by the expression suggested by Brzustowski and Sommer (1973), based on a study on the prediction of radiant heating from flares:

$$\tau = 1.304 \cdot (rh \cdot x)^{(-1/16)} \tag{5.3}$$

where rh is the relative humidity (%) and

x is the radial distance from the jet flame axis (m).

5.1.1.3. View factor

The geometric view factor, a parameter which appears in practically all thermal radiation calculations, is the ratio between the amount of thermal radiation emitted by a flame and the amount of thermal radiation received by an object not in contact with the flame. This ratio depends on the shape and size of the fire, the distance between the fire and the receiving element and the relative orientation of both surfaces. It can be represented by the following general equation:

$$F_{dA_{R2}\to A_{R1}} = \oint_{A_{R_1}} \frac{\cos\varphi_1 \cos\varphi_2}{\pi r^2} dA_{R1} \tag{5.4}$$

where A_R is the surface of the solid flame through which heat is radiated (m^2)

r is the distance between the flame surface and the receiving element (m) and

φ_1 and φ_2 are the angles made by the normals and dA_{R1} on the flame and dA_{R2} on the receiving element (º).

Several expressions for calculating view factors can be found in the literature (Hankinson, 1986; Mudan, 1990; Siegel and Howell, 1992; Casal, 2008). In the present study, the view factor between the flame and a receiving target (the heat flux sensors) has been estimated by an area integral method applicable to any solid geometrical shape. This method for calculating the view factor between a flame and a receiving target has been suggested by Hankinson (1986) for a wide range of flame geometries relevant to large-scale fires. The method is accomplished by dividing the whole surface of the solid shape used to represent the flame into small triangular elements. In the present study, the view factor was calculated assuming the flame to be a radiating cylinder with a given length and diameter, including no lift-off distance.

5.2. Experimental results and data treatment

The radiative heat intensity emitted from relatively large-scale sonic and subsonic propane jet flames, vertically released into still air, affecting certain targets was analyzed. The temperatures of the flame surface and the surface emissive power of the flame were also analysed.

The radiative heat intensity (I) was measured through three heat flow sensors located at different x radial distances from the jet flame axis and z distances above the ground. The solid flame model has also been used for estimating the thermal radiation from jet fires by the treatment of infrared images of the flame. The comparisons between experimental and estimated I values led to the determination of the emissivity of the flames.

As mentioned in previous sections, the three heat flow sensors used in this study were Schmidt-Boelter thermopile type sensors, involving two transducers measuring the total heat (convection plus radiation), and a heat radiometer/transducer, measuring total heat and radiation apart. The measured range of the heat flow sensors used was 0-23 kW/m^2 for the transducers and 0-227 kW/m^2 for the radiometer/transducer; they were located at different distances from the jet fire outlet.

Concerning the infrared images, they were obtained from a commercial high-speed thermographic camera (IR), which filmed recordings allowed obtaining four infrared images per second. The infrared thermographic camera used has a focal plane array (FPA) detector of 320 x 240 pixels, which is sensitive to radiation at a certain wavelength. The spectral range of the model used in this study was 7.5-13 μm, and the field of vision was 24º horizontal x 18º vertical.

5.3. Influence of flow condition

Both the tests in which the jet flame was fed by a gas flow and by two-phase flow were considered in this study. The features of jet flames fed by gas or by two-phase flow were found to be significantly different, both from the point of view of size and of radiative features. The flames fed by gas were almost transparent, while the flames fed by a gas-liquid mixture flow were yellow and very luminous, due to a poorer combustion (Figs. 2.16 and 5.1, respectively). The decrease in combustion efficiency must be attributed to the release of liquid droplets, which originates a poorer mixture with the entrained air.

It was also found that the jet flame length and size significantly increased when the flow changed from gas to gas-liquid mixture (Figs. 2.17 and 5.2, respectively), due to the increase in the fuel mass flow rate for a given pressure at the fuel source and a given outlet orifice diameter. Fig. 5.2 shows the images taken by the thermographic camera, for the same test: the left one corresponds to the gas jet fire (stationary state) and the right one was taken at the end of the test, when, due to the cooling of the pipe, the liquefied propane from the storage tank was no longer evaporated and two-phase flow was released through the outlet orifice.

Figure 5.1. Visible images of vertical jet flames of propane obtained with gas phase and d = 20 mm (left), and two-phase flow and d = 43.1 mm (right).

The thermal radiation intensity from the flames was also found to significantly increase when the flow changes from gas to two-phase flow. This change must be attributed to the higher value of both the surface emissive power and the geometric view factor for the most luminous and larger flames (two-phase flow). Fig. 5.3 clearly shows how the thermal radiation intensity received by the radiometer (located at 2.8 m from the flame axis) increases from that corresponding to the gas jet fire at stationary state when two-phase flow begins to be released. The value of I increases abruptly as a result of the change in the flame nature and size. The oscillation in the values of thermal radiation intensity measured by the heat flux sensor for the two-phase flow is due to the increased turbulence of the flames.

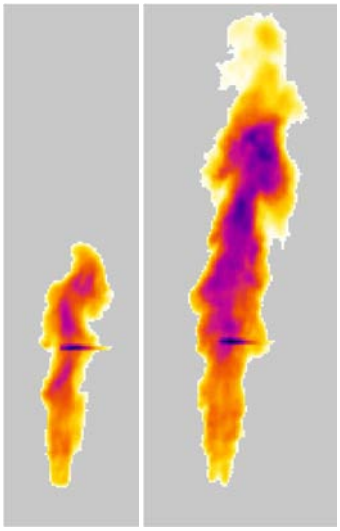

Figure. 5.2. Infrared images of jet flames obtained with a 15 mm outlet diameter: (left) gas flow, total flame height (*H*) 5 m; (right) two-phase flow, *H* = 8.9 m. The flame length (*H*) was measured from the fuel source to the flame tip along the centreline of the jet flame. The position of outlet orifice is shown by the bottom of the figure. The isotherm of 800 K defines the jet flame contour.

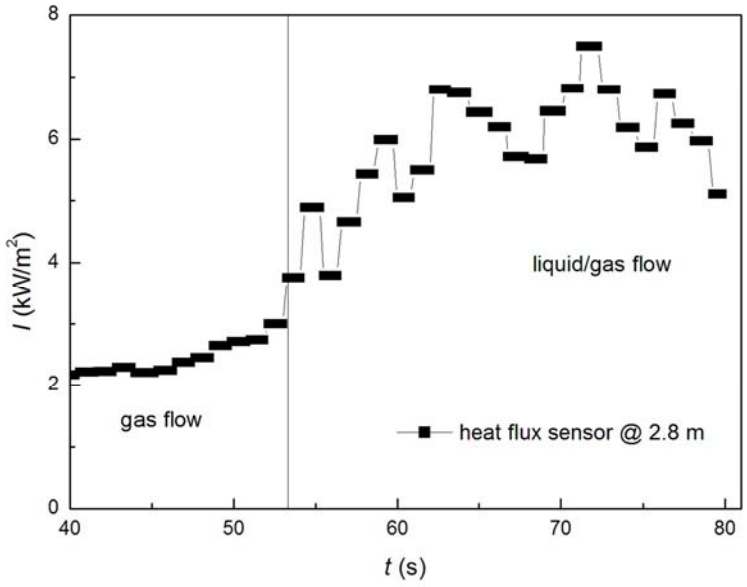

Figure. 5.3. Variation of the radiation intensity received by a target when changing the fuel from gas to two-phase flow. A 15 mm orifice outlet diameter and a 2.8 m radial position from the flame axis and 1 m above the ground heat flux sensor have been used.

5.4. Thermal radiation from flames

The thermal radiation heat emitted from jet flames was measured through three heat flow sensors located at different radial distances from the flame axis (x) and at different distances above ground level (z). The different x and z distances used during the tests were: x = 1.1 m, z = 0.9 m; x = 2.8 m, z = 1 m; x = 3 m, z = 1.5 m; x = 5 m, z = 1.5 m; x = 5.1 m, z = 1.5 m; and x = 10 m, z = 1.5 m. The positions of the heat flux sensors used in each test are listed in Table 2.8.

The variation of the radiant heat intensity (I) of jet fires affecting the three heat flux sensors as a function of target's radial distances from the flame axis, is shown in Fig. 5.4 for a given outlet orifice diameter.

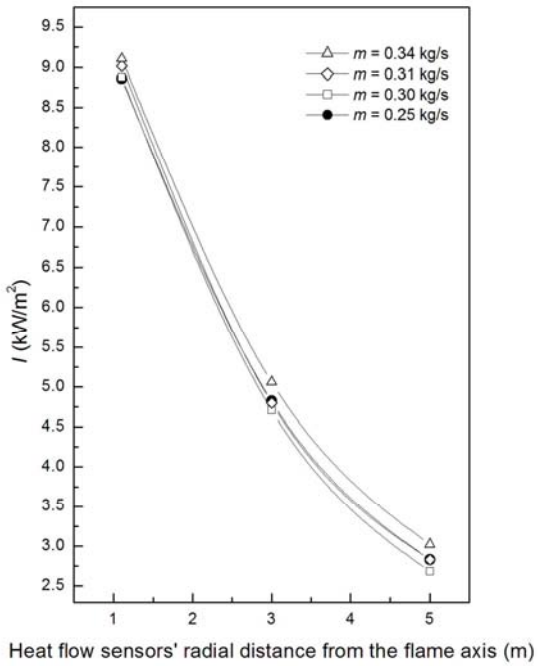

Figure. 5.4. Variation in the incident thermal radiation heat as a function of the different heat flow sensors' radial positions from the jet flame axis, for a 30 mm orifice outlet diameter (gas flow).

The results show that as the radial distance from the jet flame axis increases, I decreases. This logical behavior is due to two facts: as the

distance from the flame axis increases, a bigger amount of heat is absorbed by the atmosphere, leading to a smaller incident heat received by a target; furthermore, as the distance increases the geometrical view factor between the jet fire and the heat flux sensor decreases significantly. The decrease of *I* as a function of the distance is very strong at short distances. This indicates that the hazard associated to the thermal radiation from a jet fire has a rather short reach.

From Fig. 5.4 it can also be seen that for a given distance, *I* increases with the mass flow rate (*m*). As the fuel mass flow rate increases, the size of the flames increases as well and the amount of heat irradiated becomes larger; consequently, the radiation intensity reaching the surface of the sensor increases.

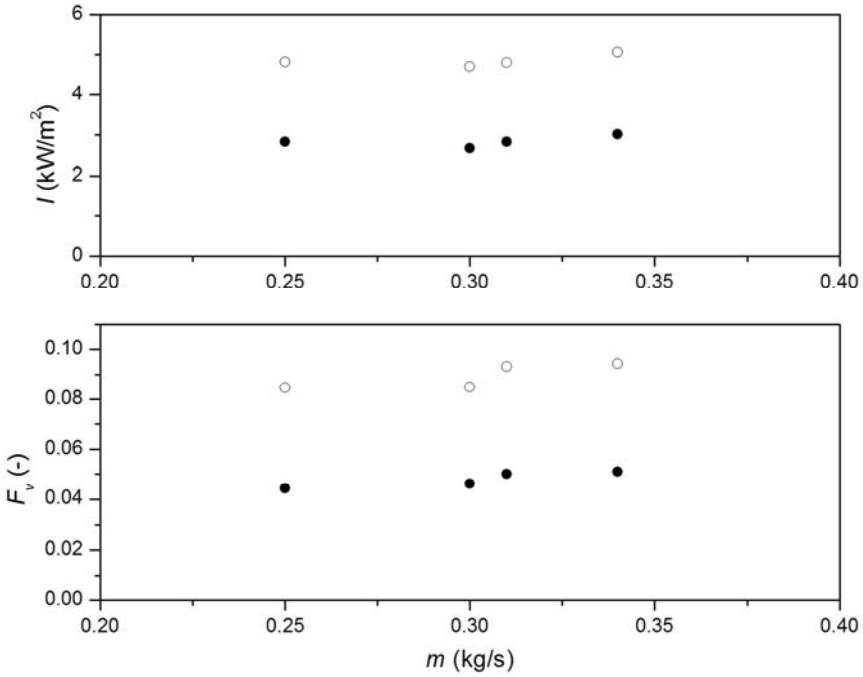

Figure. 5.5. Variation in the geometric view factor and the incident thermal radiation heat as a function of the fuel mass flow rate, for a 30 mm orifice outlet diameter. Different heat flow sensors' radial positions from the flame axis are plotted (open symbols: 3 m; filled symbols: 5 m). Both heat flux sensors have been located at 1.5 above the ground.

The variation of both the geometric view factor and the radiant heat intensity as a function of fuel mass flow rate for a given case has been plotted in Fig. 5.5. The data corresponding to two heat flux sensors (at 3 m and 5 m) can be seen. The trend observed in both plots is similar, clearly showing the significant influence of the view factor on the intensity received by the target. As *m* increases *F* and consequently *I* increase as well. It can also be seen that as the radial distance from the flame axis and the target decreases *F* increases and as a result the thermal radiation intensity received by the surface of the target increases.

The influence of the fuel mass flow rate on the radiation intensity can be observed in more detail in Fig. 5.6 according to the data from the three heat flux sensors. The increase of *I* is very important at low values of the fuel mass flow rate, and becomes less significant at higher values of *m*. This variation is due to the variation of the view factor as a function of the flames length and size; the influence of the distance between the flames and the target is also evident. The influence is stronger for short distances.

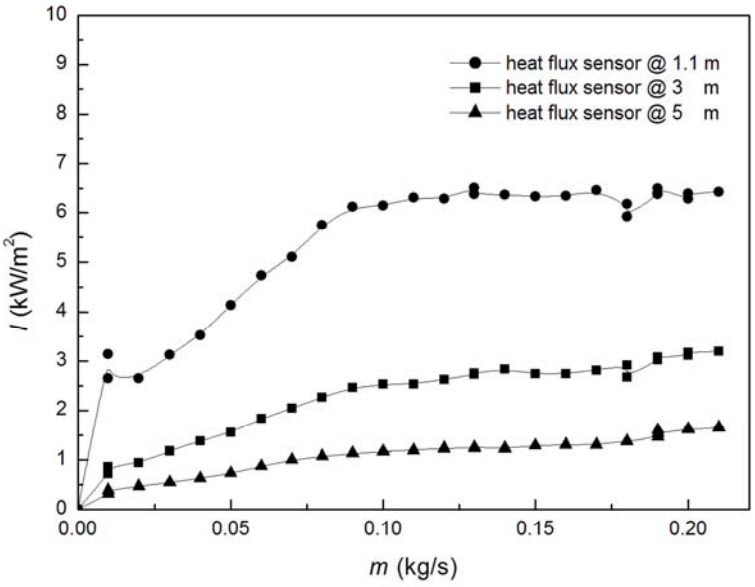

Figure. 5.6. Variation in the incident radiation heat as a function of the fuel mass flow rate, for a 12.75 mm orifice outlet diameter. Different heat flow sensors' radial positions from the flame axis are plotted.

5.5. Infrared images

The analysis of infrared images of propane jet flames enabled the estimation of the radiative heat intensity from flames by a completely different procedure from that described in the previous sections. To calculate I the solid flame model was used. These I values were then compared with the measurements obtained from the heat flow sensors.

5.5.1. Flame temperatures

The infrared camera operates as a radiometer made by a two-dimensional array of sensors. The signal at each sensor is proportional to the radiative heat intensity emitted by a small part of the viewed object (in this case the flame). The infrared camera transforms the signals from the sensors into temperatures by specifying the following four variables: the ambient temperature, the distance between the viewed object and the camera, the emissivity of the viewed object and the relative humidity.

In the present study, the infrared images of jet flames during the stationary state of the tests were exported to Matlab files as matrices of temperature, using the software provided with the thermographic camera and ad-hoc algorithms developed in Matlab R2009b®. The resulting matrix had 240 rows and 320 columns.

In each test, the ambient temperature, the distance between the camera and the flame, and the relative humidity were measured. However, the emissivity of the flame had to be estimated. This variable is a complex function which depends on the extinction coefficient of the flame and on the path length.

Fig. 5.7 shows an example of the matrix of temperatures for an infrared image of a jet flame obtained with a 43.1 mm orifice outlet diameter, exported to and plotted in Matlab.

5.5.2. Flames emissive power

The resulting images of temperature distribution were then transformed to surface emissive power distributions using Eq. (5.2) and ad-hoc algorithms developed in Matlab.

The transformation of the matrix of temperatures shown in Fig. 5.7 to a matrix of surface emissive power values is shown in Fig. 5.8.

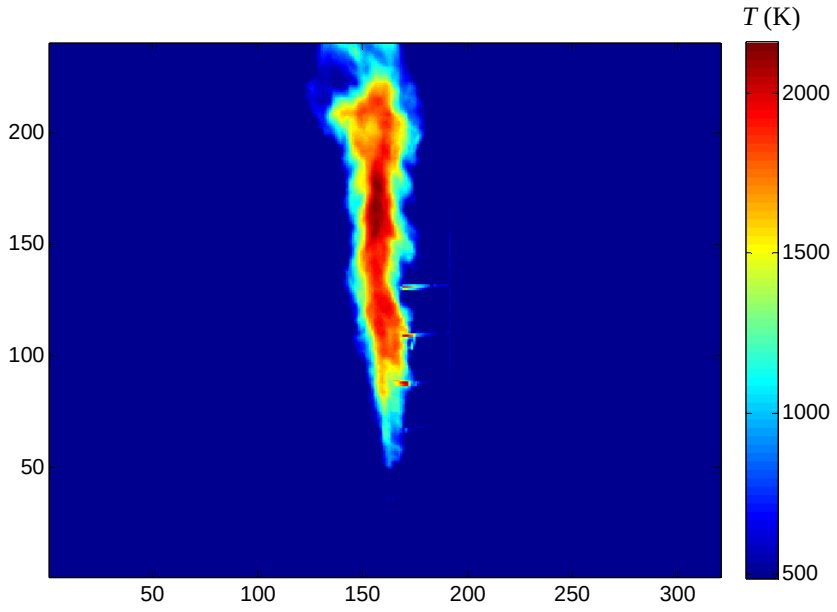

Figure 5.7. Infrared image of a jet fire issuing from a 43.1 mm orifice outlet diameter: temperature distribution over the flame (K). Ad-hoc algorithms developed in Matlab R2009b® and a flame's emissivity of 0.35 have been used.

Fig. 5.8 clearly shows that the emissive power does not have a uniform value over the whole surface of the flame. The highest values are located in the central zone of the flame, the boundaries radiating with a lower intensity. Furthermore, it can be observed that over the lower half of the flame the emissive power is much lower than in the upper half, the maximum values being measured approximately over the third quarter from the bottom. Therefore, the usual use of an average value for the whole jet fire, although being a practical solution, implies a certain error. This error could be significantly decreased by using a two or three zone model, with different values of E for each zone; of course, this would increase somewhat the complexity of the calculation of the view factor (three different values should be determined) and of I.

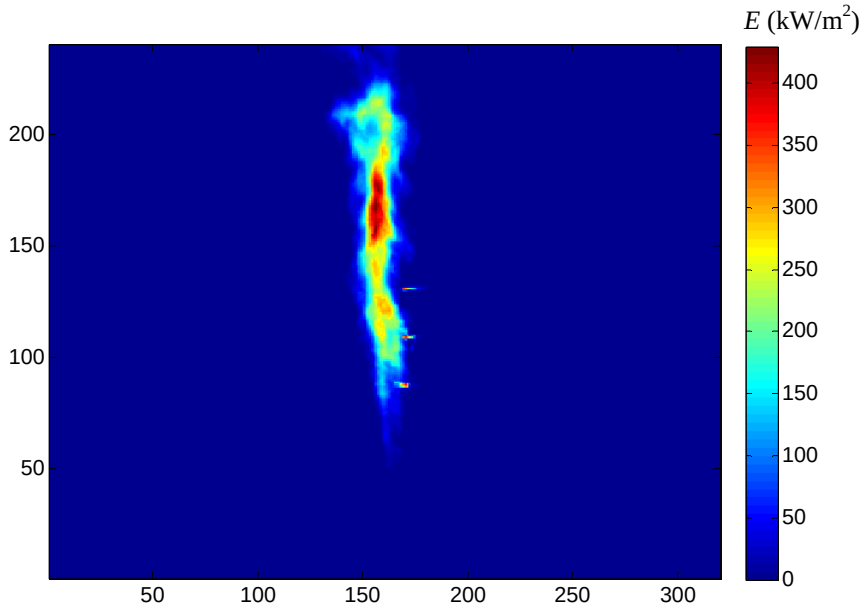

Figure 5.8. Infrared image of a jet fire issuing from a 43.1 mm orifice outlet diameter: transformation of the flame temperature distribution (Fig. 5.7) to a surface emissive power distribution ($kW \cdot m^{-2}$). Ad-hoc algorithms developed in Matlab R2009b® and a flame's emissivity of 0.35 have been used.

5.6. Thermal radiation intensity

Besides measuring it directly with the heat flux sensors, the radiative heat intensity (I) from jet flames was also estimated by applying the solid flame model (Eq. (5.1)). Thus, by using the above-mentioned treatment of the infrared images, enabling the surface emissive power distribution of the flame to be obtained, and by estimating the view factor and the atmospheric transmissivity, I has been calculated.

The energy radiated from the jet flame over a certain target (a heat flux sensor) located at a certain distance, was calculated by assuming a two-dimensional flame and evaluating the heat radiated by each pixel of the flame plane. The heat flux sensor was located in a vertical position at an x distance from the flame axis and a z distance above ground level; thus, the total heat radiated over this target was the sum of the heat radiated from all the pixels on the flame plane.

In an attempt to obtain the emissivity of the flame, the ε value was changed until the minimum difference between the measured and the calculated values of the radiant heat intensity from the jet flames (I) was reached. This difference concerned the heat flux sensors measurements and the values obtained from the infrared images.

An initial value of $\varepsilon = 0.11$ was used. This value had been reported by Straitz and Altube (1977) for propane flames, based on a study performed on flares. Fig. 5.9 shows the comparison between the experimental measurements of radiant heat intensity from jet flames, obtained with a 20 mm orifice outlet diameter, and the predicted values obtained with the treatment of the infrared images, involving the solid flame model, with $\varepsilon = 0.11$. This figure concerns a test where the radiant heat intensity from jet flames reaches a heat flux sensor located at 3 m from the jet flame axis and 1.5 m above the ground.

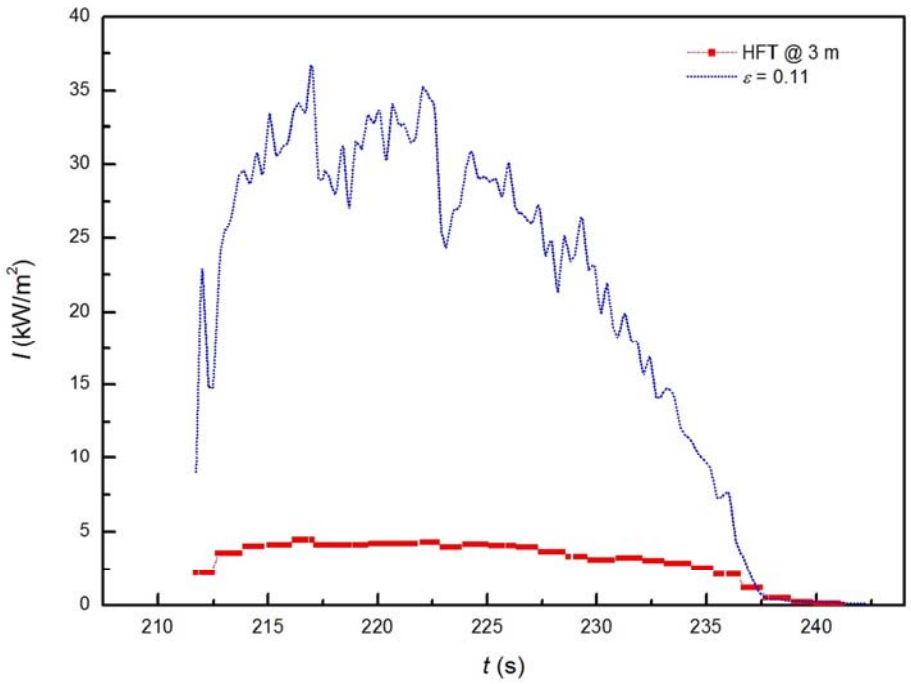

Figure 5.9. Radiant heat intensity from jet flames obtained with a 20 mm orifice outlet diameter, as a function of time. A flame's emissivity of 0.11 has been used. The radiant heat intensity measured from the heat flux sensor located at 3 m radial position from the flame axis and 1.5 m above the ground is also plotted (red line).

From Fig. 5.9 it can be seen that by using $\varepsilon = 0.11$, the radiation heat emitted from jet flames is significantly overestimated. Similar results were obtained with the heat flux sensors located at other distances and with other orifice outlet diameters.

As a later stage, a wider range of flame's emissivity values was tested, according to the results published by Lowesmith *et al*. (2007), based on data on jet fires obtained by other authors (much of which remains unpublished). Lowesmith *et al*. (2007) obtained values of ε ranging between 0.25 and 0.7, concerning gas jet fires. In the present study, as seen in Fig. 5.10, a range of ε values between 0.25 and 0.5 was tested.

The values of the thermal radiation intensity for the different emissivities have been plotted as a function of time in Fig. 5.10 (same orifice diameter and heat flux sensor than in Fig. 5.9).

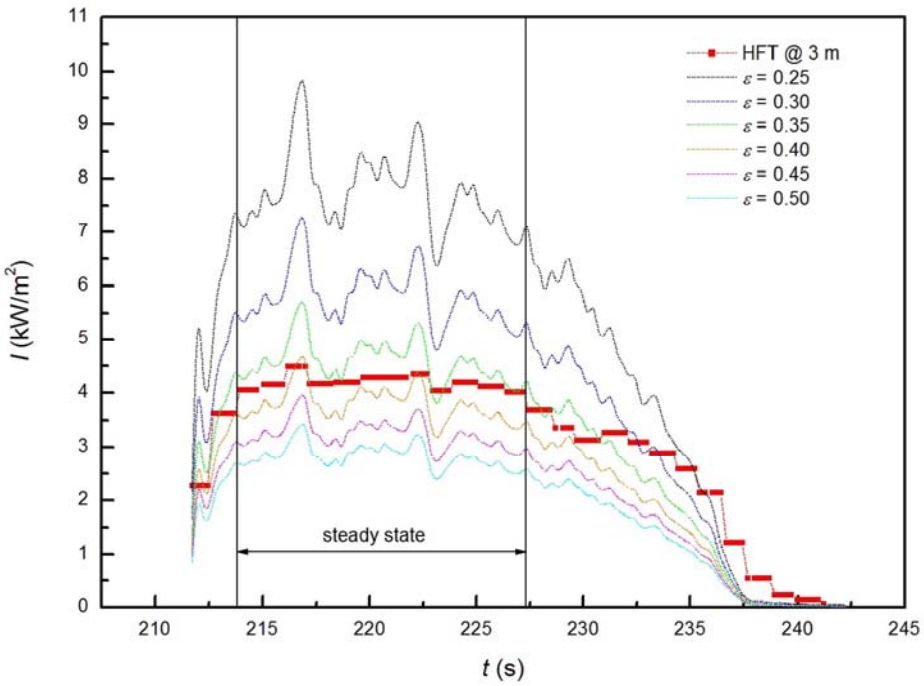

Figure 5.10. Radiant heat intensity from jet flames obtained with a 20 mm orifice outlet diameter, using the infrared images treatment, as a function of time. Diverse flame's emissivity values have been used. The radiant heat intensity measured from the heat flux sensor located at 3 m radial position from the flame axis and 1.5 m above the ground is also plotted (red line).

From Fig. 5.10 it can be seen that the radiation intensity obtained from the heat flux sensor measurements and those obtained by the treatment of infrared images significantly differ depending on the selected flame's emissivity (ε) value. For the lower ε values, I is overestimated while higher ε values underestimate I. As the ε value decreases, the radiant heat intensity resulting from the calculations involving the infrared images increases. This is due to the fact that as ε decreases the temperatures of the flame surface increase, leading to a higher surface emissive power and as a result to higher values of the thermal radiation intensity.

Similar results were found for the radiant heat intensity measurements obtained with the heat flux sensors located at other distances, and with other orifice outlet diameters. Fig. 5.11 shows the results obtained with flame's emissivity values ranging between 0.3 and 0.4, for a 12.75 mm orifice outlet diameter. The heat flux sensor was located at 5 m from the jet flame axis and 1.5 m above the ground.

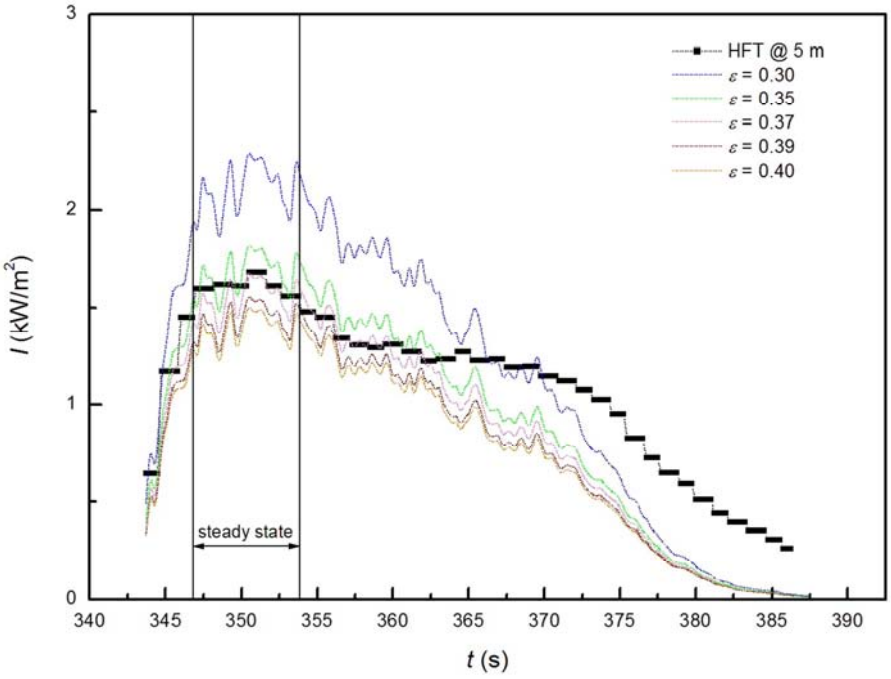

Figure 5.11. Radiant heat intensity from jet flames obtained with a 12.75 mm orifice outlet diameter (infrared images) as a function of time. The radiant heat intensity measured by a heat flux sensor located at 5 m radial position from the flame axis and 1.5 m above the ground is also plotted (black line).

Both in Figs. 5.10 and 5.11 the most representative data are those corresponding to the steady-state period (during which the fuel mass flow rate was constant); during this period the average value of I was constant as well (even though significant oscillations were registered due to the turbulence of the phenomenon). Later on, when the valve of the feeding pipe was closed, the size of the flame gradually decreased. During this non-stationary period, the response time of the heat flux sensor was clearly slower than that of the IR camera, and this is why the registered values are higher than the calculated ones.

The calculations obtained with the heat flux sensor located at 1.1 m from the jet flame axis were not considered in this analysis; there was probably some experimental error in these measurements, as completely anomalous values of ε were required to achieve a good agreement between the calculated and experimental I values. This fact can be attributed to the small distance between the flame and the heat flux sensor located at this nearest position from the jet flame axis. It should also be noted that the data obtained with a 10 mm orifice outlet diameter were not considered in this analysis, since to maintain the flame a permanent ignition source was required to prevent the blow-out phenomenon to occur.

The flame's emissivity for all the data, concerning the stationary state of the tests, was found to be 0.38, 0.4, 0.38, 0.3 and 0.35 for the orifice outlet diameters of 12.75 mm, 15 mm, 20 mm, 30 mm and 43.1 mm, respectively. Thus, the present experimental data lead to an average flame's emissivity value of 0.36.

5.7. Surface emissive power

For each test, and for the data corresponding to the stationary state, the mean surface emissive power was obtained by averaging the infrared images sequence. From each infrared image, using the corresponding flame's emissivity values for each outlet orifice diameter, an emissive power distribution of the flame was obtained by applying Eq. (5.2). Then, this average surface emissive power (E_{IR}) was compared with the average surface emissive power obtained directly from Eq. (5.1), by using the radiant heat intensity registered by the heat flux sensors, the geometric view factor and the atmospheric transmissivity; this average surface emissive power was defined as E_{HFT}.

The comparison between the values of E_{IR} and E_{HFT} is shown in Fig. 5.12. For the tests analyzed the average surface emissive power ranged between 33 and 142 kW·m^{-2} for E_{IR}, and between 36 and 127 kW·m^{-2} for E_{HFT}.

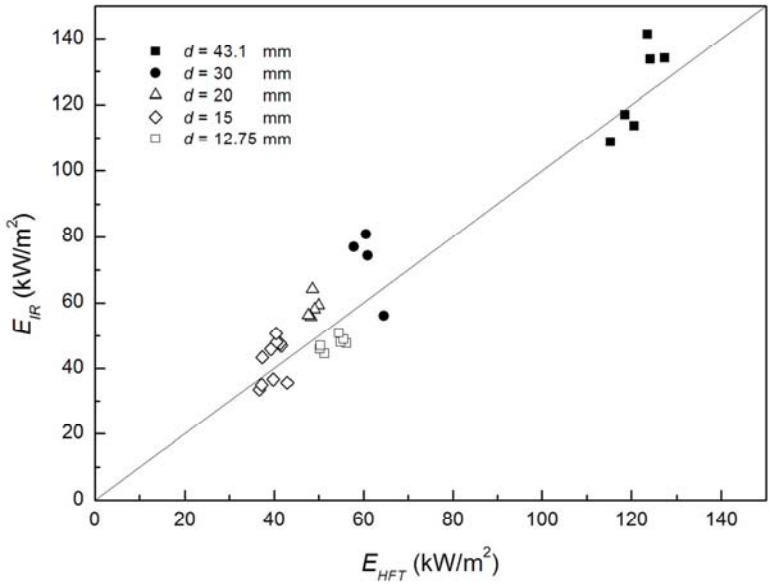

Figure 5.12. Comparison between the average surface emissive power E_{IR} and E_{HFT} for the different orifice outlet diameters.

From this figure it can be seen that the E_{IR} and E_{HFT} values are generally fairly similar, showing a difference no greater than 14%. This indicates that the applied values of ε are essentially correct.

The average surface emissive power was found to increase with the jet flame length. Figs. 5.13 and 5.14 show the variation of the average values of E_{IR} and E_{HFT}, as a function of the radiant jet flame length, respectively. The experimental data obtained by Sonju and Hustad (1984), concerning large-scale turbulent subsonic jet fires of propane (up to 8 m in length), obtained with orifice exit diameters ranging between 2 mm and 80 mm, have also been plotted in both figures. It can be seen that all data (except for those obtained with d = 43.1 mm) follow the same trend, clearly represented by the increase of the average surface emissive power as the jet flame length is increased. It can be also seen from these figures that most of the present data

agree with the values obtained by Sonju and Hustad (1984), following the same common trend.

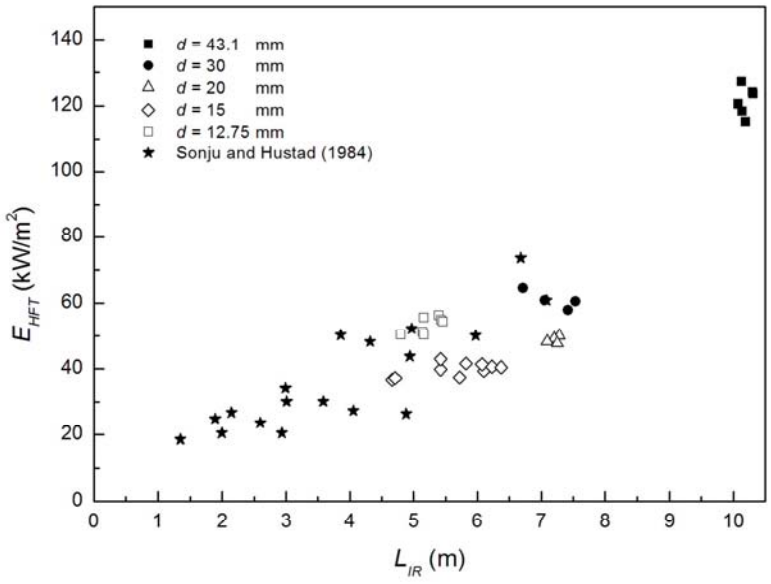

Figure 5.13. Average surface emissive power E_{HFT} as a function of the radiant jet flame length. The experimental data on turbulent subsonic jet fires of propane obtained by Sonju and Hustad (1984) are also shown.

Correspondingly, the average surface emissive power was also found to increase with the fuel mass flow rate (m). Figs. 5.15 and 5.16 show the variation of the average values of E_{HFT} and E_{IR} as a function of m, respectively. Fig. 5.15 shows for most of the data an increase in the average surface emissive power as the fuel mass flow rate is increased. Similar results are shown in Fig. 5.16; however, a larger scattering is shown in Fig. 5.15. It should be noted again that the scattering in the tests analyzed is very difficult to avoid when performing open field large-scale experiments.

In Fig. 5.17 the variation of the average surface emissive power E_{HFT} as a function of the radiant jet flame length, for both gas phase and two-phase flows (orifice outlet diameter: 15 mm) has been plotted. It can be seen that the significantly larger E values are obtained for the two-phase flow jet flames. The differences found can be attributed to the obtention of larger heat intensities and larger geometric view factors for gas-liquid mixture flames.

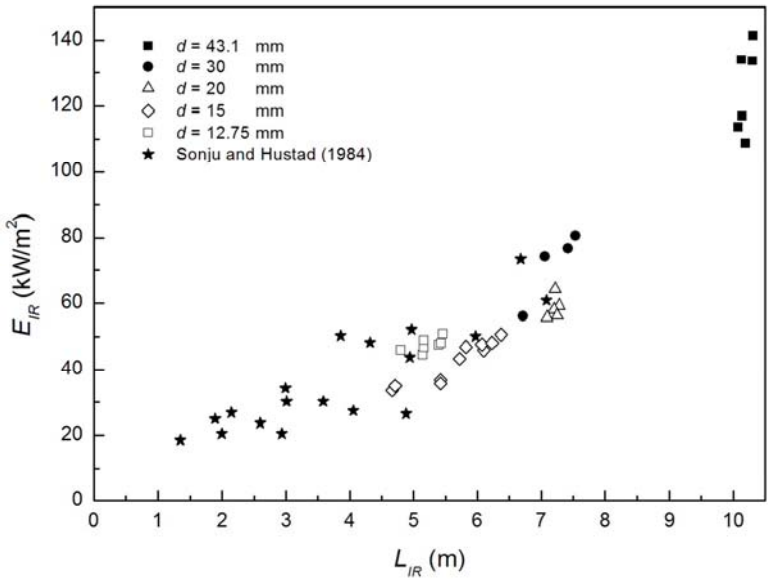

Figure 5.14. Average surface emissive power E_{IR} as a function of the radiant jet flame length. The experimental data on turbulent subsonic jet fires of propane obtained by Sonju and Hustad (1984) are also shown.

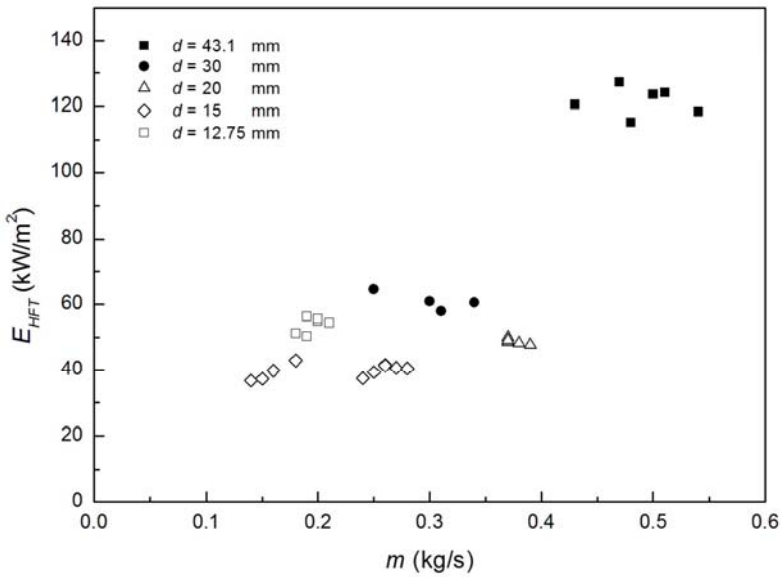

Figure 5.15. Average surface emissive power E_{HFT} as a function of the fuel mass flow rate.

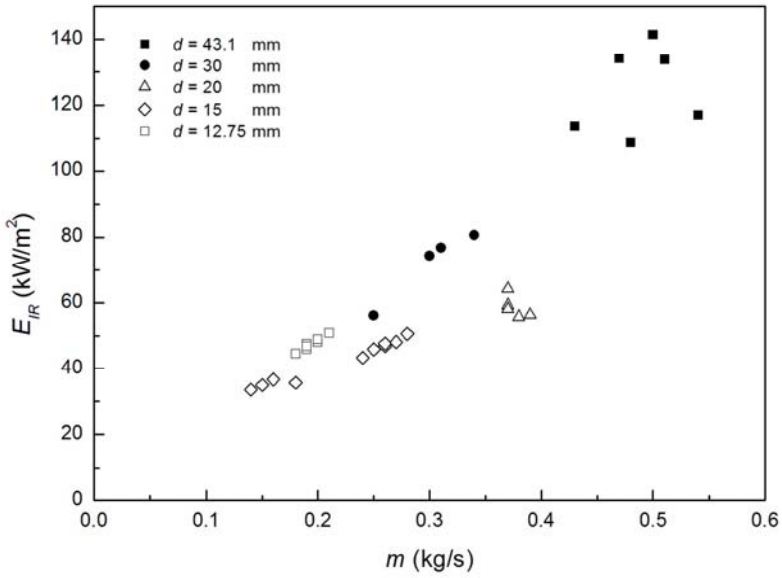

Figure 5.16. Average surface emissive power E_{IR} as a function of the fuel mass flow rate.

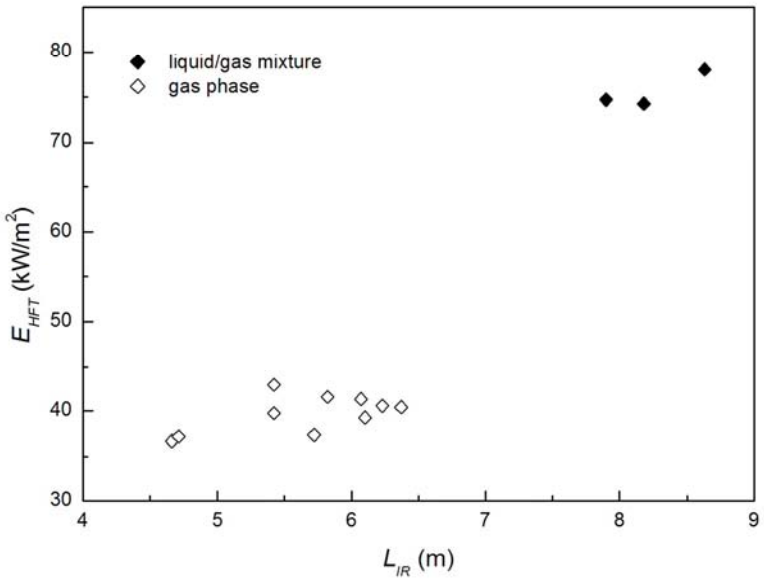

Figure 5.17. Average surface emissive power E_{HFT} as a function of the radiant jet flame length (orifice outlet diameter: 15 mm).

5.8. Three zone model versus one zone model

The existence of three different regions over the whole surface of the jet flame, concerning the temperature distribution of the flame along the jet fire centreline, was identified in most of the infrared images analyzed. Due to the fact that the surface emissive power of the flames is a function of the flame's temperature, these three regions were also identified in the images analyzed, concerning the surface power emission distribution of the flames.

As already mentioned in Chapter 2 ("Experimental Set-Up"), a set of thermocouples allowed the analysis of the temperature profile of the jet flames along the jet fire centreline. The results obtained have shown that the centreline temperature varies considerably. Three regions have been identified: Region I, considered from the bottom of the flame up to 40% of the jet flame length, where the temperature increased with the axial position reaching values of approximately 1800 K; Region II, considered from the 40% to the 70% of the flame length, where the temperature profile showed a smooth variation with an average value of the temperature close to 1800 K and maximum values of 1900 K; and Region III, considered from the 70% of the flame length to the flame tip, where the temperature decreased; however, the values measured at this region were considerably higher than those measured at Region I (Gómez-Mares *et al*., 2009). This behaviour can be attributed to the improvement in air/fuel mixing along the jet fire, with a relatively low concentration of oxygen in Region I and a much better ratio in Region II; and the low fuel concentration (due to fuel consumption) in Region III. The progressive increase in gas temperature along the jet also influenced the behaviour, since the gas entering Region I was cold, whereas most of the gas entering Regions II and III was hot.

These three regions were considered over the whole surface of the flame to obtain an average surface emissive power of the flames for each one of them. The aforementioned treatment of infrared images and ad-hoc algorithms developed in Matlab led to the obtention of these average values, and by applying the solid flame model the radiant heat intensity originated from each region and the total radiant heat intensity from the whole surface of the flame were also obtained.

Figure 5.18 shows the temperature distribution of a jet flame obtained with a 30 mm orifice outlet diameter and the transformation of its matrix of temperatures to a matrix of surface emissive power values.

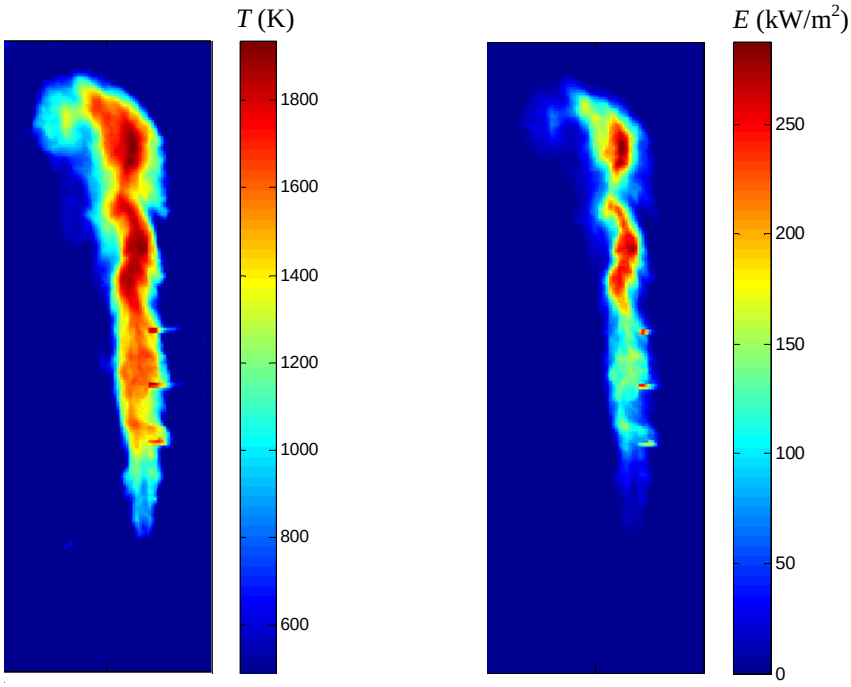

Figure 5.18. Infrared image of a jet fire issuing from a 30 mm orifice outlet diameter. Left: temperature distribution over the flame (K). Right: Transformation of the flame temperature distribution to a surface emissive power distribution ($kW \cdot m^{-2}$). Ad-hoc algorithms developed in Matlab R2009b® and a flame's emissivity of 0.3 have been used.

From Fig. 5.18 it can be seen that the emissive power does not have a uniform value over the whole surface of the flame, showing the highest values at the tip of the flame.

As a later stage, the radiant heat intensity was estimated by applying the solid flame model, using both the average surface emissive power for the whole surface of the flame and the average surface emissive power of the flames for each region.

Fig 5.19 shows the surface power distribution of a jet flame (already shown in Fig. 5.18), and the three regions previously identified by the temperature analysis: Region I (0% - 40% of the radiant jet flame length), Region II (40% - 70% of L_{IR}) and Region III (70% - 100% of L_{IR}).

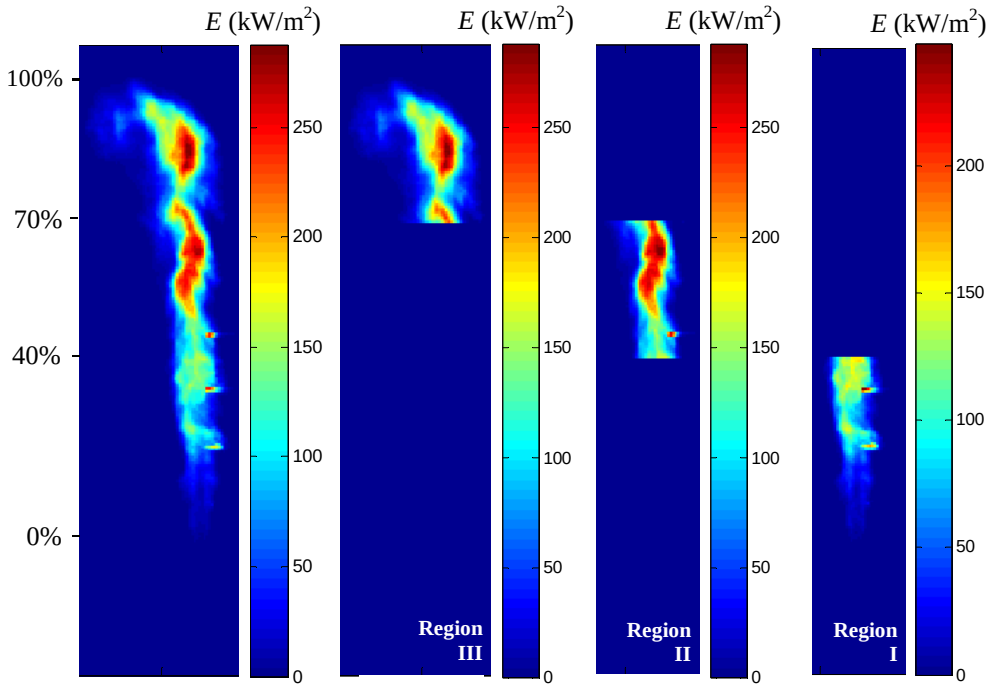

Figure 5.19. Infrared image of a jet fire issuing from a 30 mm orifice outlet diameter. Surface emissive power distribution ($kW \cdot m^{-2}$) over the whole surface of the flame and in each analyzed region, respectively. Ad-hoc algorithms developed in Matlab R2009b® and a flame's emissivity of 0.3 have been used.

Table 5.1 shows the average surface emissive power for the whole surface of the jet flame, the average surface emissive power for each region and the arithmetic average value obtained from these three regions. The estimated radiant heat intensities calculated using the one zone model and the three zone model are also shown in this table.

From Table 5.1 it can be seen that the surface power distribution of the flames follows the same behavior of the temperature distribution, since the maximum surface emissive power values were obtained at the middle of the flame (Region II), being followed by the tip of the flame (Region III) and finally the lowest values obtained at the bottom of the flame (Region I). It can also be observed that the average surface emissive power involving the whole surface of the jet flame and the arithmetic average value obtained from the average surface emissive power for each region are very similar (with a small difference of 1.4%). Thus, the radiant heat intensity estimated

by both models is very similar (with a difference of 2.7%), and agree fairly well with the experimental radiant heat intensity value. It is important to note that the radiant heat intensity obtained by the three zone model is the accumulative value of the radiant heat intensity of each region, involving an average surface emissive power of the flames and a view factor for each region, respectively.

Table 5.1. Comparison of calculated radiant heat intensity and surface emissive power of the flames using the one zone and the three zone model. A jet flame obtained with a 30 mm orifice outlet diameter and a heat flux sensor located at 3 m from the jet flame axis and 1.5 m above ground is analysed.

	d = 30 mm; HFT [3, 1.5] (m)					
	Exp.	Pred. 1Z	Pred. 3Z	Pred. RI	Pred. RII	Pred. RIII
I (kW/m^2)	3.8	3.7	3.8	1.9	1.3	0.58
E_{HFT} (kW/m^2)	-	70.4	71.4	56.1	91.7	66.4

It should be noted that this analysis concerns a heat flux sensor located at 3 m from the jet flame axis and 1.5 m above ground. As a later stage, the same analysis was carried out for the same flame, obtained with a 30 mm orifice outlet diameter, with the heat flux sensor located at 5 m from the jet flame axis and 1.5 m above ground. The results obtained are shown in Table 5.2.

Table 5.2. Comparison of calculated radiant heat intensity and surface emissive power of the flames using the one zone and the three zone model. A jet flame obtained with a 30 mm orifice outlet diameter and a heat flux sensor located at 5 m from the jet flame axis and 1.5 m above ground is analysed.

	d = 30 mm; HFT [5, 1.5] (m)					
	Exp.	Pred. 1Z	Pred. 3Z	Pred. RI	Pred. RII	Pred. RIII
I (kW/m^2)	2.1	2.3	2.4	0.82	0.9	0.64
E_{HFT} (kW/m^2)	-	70.4	71.4	56.1	91.7	66.4

From Table 5.2 it can be seen that the experimental radiant heat intensity value was again estimated fairly accurately by both models, showing a difference of 4.3% between the models. Thus, it can be deduced that the use of a three zone model does not improve the estimation of the radiant heat

intensity values obtained from the usual model using an average surface emissive power value for the whole surface of the jet flame.

The same analysis was carried out using a 20 mm orifice outlet diameter. Fig. 5.3 shows the temperature distribution of a jet flame and the transformation of its matrix of temperatures to a matrix of surface emissive power values.

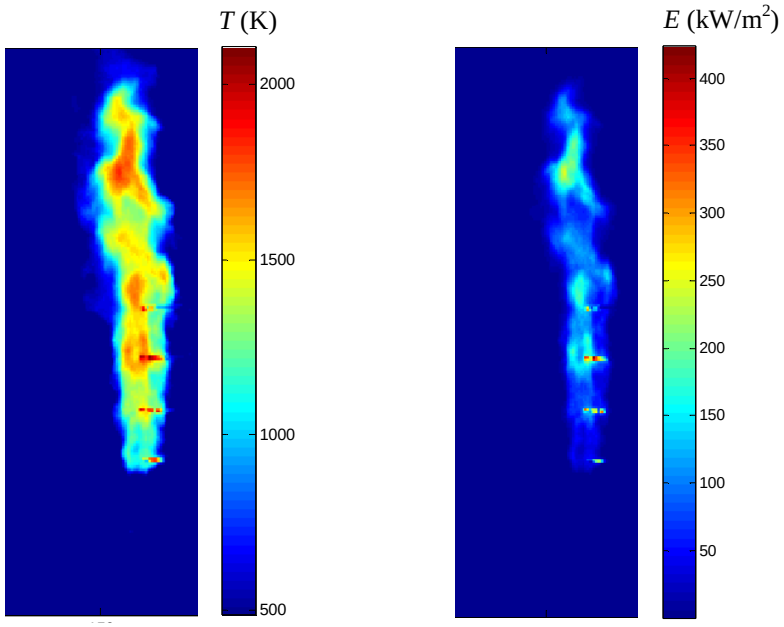

Figure 5.20. Infrared image of a jet fire issuing from a 20 mm orifice outlet diameter. Left: temperature distribution over the flame (K). Right: Transformation of the flame temperature distribution to a surface emissive power distribution ($kW \cdot m^{-2}$). Ad-hoc algorithms developed in Matlab R2009b® and a flame's emissivity of 0.38 have been used.

From Fig. 5.20 it can be seen that the surface emissive power does not show significantly differences over the whole surface of the flame, showing the highest *E* values at tip and centre of the flame.

The radiant heat intensity was again estimated by the aforementioned analysis applying the solid flame model, using the average surface emissive power for the whole surface of the flame and the average surface emissive power for each of the three regions. The results obtained are shown in Table 5.3.

Table 5.3. Comparison of calculated radiant heat intensity and surface emissive power of the flames using the one zone and the three zone model. A jet flame obtained with a 20 mm orifice outlet diameter and a heat flux sensor located at 3 m from the jet flame axis and 1.5 m above ground is analysed.

	d = 20 mm; HFT [3, 1.5] (m)					
	Exp.	Pred. 1Z	Pred. 3Z	Pred. RI	Pred. RII	Pred. RIII
I (kW/m^2)	4.2	4.0	4.1	2.6	1.1	0.4
E_{HFT} (kW/m^2)	-	60.9	61.0	62.2	60.0	60.8

Table 5.3 shows that the surface power distribution of the flames has almost the same value for each of the three regions over the whole surface of the jet flame, with an E average value around 60 kW.m^{-2}. It can also be seen that the average surface emissive power involving the whole surface of the jet flame and the arithmetic E average value obtained from the E values obtained from each region are very similar (with a difference of 0.16%). Due to the similar E average values obtained using both models, Table 5.3 also shows the radiant heat intensity estimated by both models to have practically the same value (with a difference of 2.5%), and to agree fairly well with the experimental radiant heat intensity value. These results concern a heat flux sensor located at 3 m from the jet flame axis and 1.5 m above ground. Finally, an analysis involving the same flame and the heat flux sensor located this time at 5 m from the jet flame axis and 1.5 m above ground was carried out. Table 5.4. shows the results obtained.

Table 5.4. Comparison of calculated radiant heat intensity and surface emissive power of the flames using the one zone and the three zone model. A jet flame obtained with a 20 mm orifice outlet diameter and a heat flux sensor located at 5 m from the jet flame axis and 1.5 m above ground is analysed.

	d = 20 mm; HFT [5, 1.5] (m)					
	Exp.	Pred. 1Z	Pred. 3Z	Pred. RI	Pred. RII	Pred. RIII
I (kW/m^2)	2.2	2.3	2.3	1.1	0.8	0.38
E_{HFT} (kW/m^2)	-	60.9	61.0	62.2	60.0	60.8

From Table 5.4 it can be seen that the experimental radiant heat intensity value was again estimated fairly accurately by both models, obtaining the

same I estimated value, with a difference of 4.5% from the experimental value.

Thus, again it can be deduced that the use of a three zone model does not improve the estimation of the radiant heat intensity value obtained from the usual model using an average surface emissive power value for the whole surface of the jet flame. Then, due to the increase in the complexity involved in the three zone model to estimate the radiant heat intensity (three different values should be determined), a model of one zone is finally suggested.

5.9. Comparison of predicted radiative heat intensity with measured values

The calculated radiative heat intensity and flame parameters have been compared with measured values. The selected model to predict the flame shape and radiation levels has been the well known and widely used model proposed by the Committee for the Prevention of Disasters (1997), based on the model previously developed by Chamberlain (1987). The involved procedure is briefly commented.

5.9.1. Calculation of flame dimensions

The model proposed by the Committee for the Prevention of Disasters (CPR model) represents the flame as a frustum of a cone. For this analysis, the geometrical features of the flame obtained from this model involved jet flame length, flame width at frustum base and tip, respectively, and lift-off distance. It should be noted that for jet flames in still air, such as in the present analysis, the jet flame length is calculated by the CPR model, using the expression suggested by Kalghatgi (1984).

For the calculation of the suggested flame surface area, two shapes are taken into account: the surface area of a frustum of a cone and, as an alternative for the calculation of the frustum surface area, a cylinder (without including the two end discs) is applied.

5.9.1.1. Calculation of the view factor

The geometrical view factor is calculated by using the surface area for a cylinder (without including end discs) with a given average width. The

flame average width is calculated as the average value of the width values at the flame tip and flame base, assuming a frustum of a cone to define the flame shape.

5.9.2. Calculation of the surface emissive power

The surface emissive power is calculated by the CPR model using the net heat released from combustion of the flammable gas, the fraction of that part of the heat which is radiated and the early mentioned surface area of a cylinder (now including end discs), representing the flame as a radiating solid body with a uniform surface emissive power.

5.9.3. Radiative heat intensity

The measured and calculated radiative heat intensity and flame parameters, using the CPR model, by applying the solid flame model, are listed in Table 5.5. This analysis concerns propane jet flames vertically released into still air, issuing from an orifice outlet diameter of 12.75 mm and affecting certain targets located at a distance of 3 m and 5 m, respectively.

Table 5.5. Comparison of calculated radiation levels and flame parameters with measured values

	1		2		3		4	
	Exp.	Pred.	Exp.	Pred.	Exp.	Pred.	Exp.	Pred.
I (kW·m^{-2})	3.1	4.4	1.6	2.6	3.2	4.5	1.7	2.7
E (kW·m^{-2})	55.0	69.4	54.4	69.4	54.3	70.1	52.8	70.1
F_v (-)	0.06	0.07	0.03	0.04	0.06	0.07	0.03	0.04
L (m)	5.4	5.6	5.4	5.6	5.5	5.8	5.5	5.8
S (m)	1.0	1.4	1.0	1.4	1.1	1.4	1.1	1.4
D (m)[a]	0.8	1.1	0.8	1.1	0.8	1.1	0.8	1.1
HFT [x, z] (m)	(3, 1.5)		(5, 1.5)		(3, 1.5)		(5, 1.5)	

[a] For the experimental values (Exp), D corresponds to the equivalent flame diameter values (D_{eq}); while for the predicted values (Pred), D concerns the flame average width of the width values at the flame tip and flame base, assuming the flame shape as a frustum of a cone.

Fig. 5.21 shows the calculated radiative heat intensity, using the CPR model, applying the solid flame model, against the measured values obtained from the heat flux sensors.

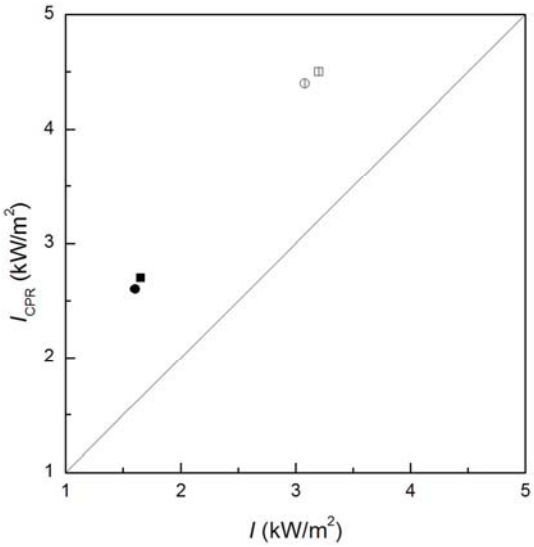

Figure 5.21. Radiant heat intensity from jet flames predicted by the Committee for the Prevention of Disasters (CPR model, 1997) against experimental data (orifice outlet diameter: 12.75 mm). Different heat flow sensors' radial positions from the flame axis are plotted (open symbols: 3 m; filled symbols: 5 m). Both heat flux sensors have been located at 1.5 above the ground.

From Fig. 5.21 it can be seen that the radiative heat intensity resulting from calculations is overestimated, having an average error of about 52%. This difference must be attributed to the higher value of both the surface emissive power and the geometric view factor for the calculated values.

Comparisons of surface emissive power values calculated with the CPR model, using the net heat released from combustion of the flammable gas, the fraction of that part of the heat radiated and the surface area of a cylinder, and those E values, calculated from the experimental measurements by applying the solid flame model and concerning the E_{HTF} early mentioned values, are shown in Fig. 5.22.

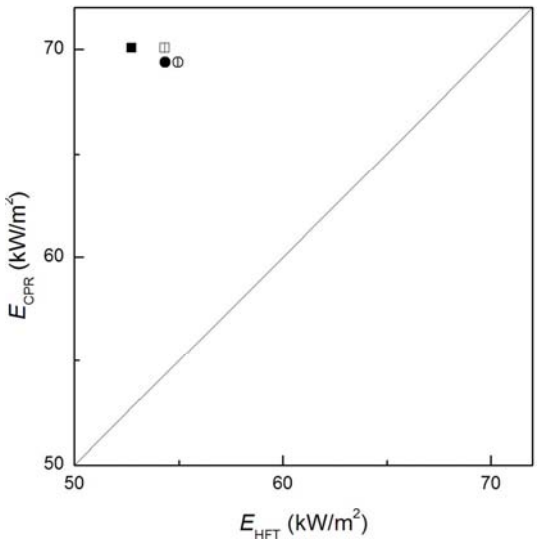

Figure 5.22. Average surface emissive power predicted by the CPR model, E_{CPR}, against that calculated from experimental measurements, E_{HFT} (orifice outlet diameter: 12.75 mm). Different heat flow sensors' radial positions from the flame axis are plotted (open symbols: 3 m; filled symbols: 5 m). Both heat flux sensors have been located at 1.5 above the ground.

From Fig. 5.22 it can be observed that the average surface emissive power obtained from CPR model's calculations is overestimated, having an average difference of about 29%. This difference must be attributed to the higher values of the flame geometrical parameters for the calculated values: the jet flame height, flame width and lift-off distance have been overestimated by the CPR model, having an average overestimation of about 14%, 94% and 66%, respectively. As the CPR model involves the flame surface area in its calculations, it can be deduced that the surface emissive power calculated by the CPR model involves a significantly overestimated flame surface area, leading to higher *E* values.

The differences between the calculated and observed geometrical features of the flame are also the reason to explain why the values for the geometrical view factor obtained from the calculations and the experimental measurements differ in about 22% (Fig. 5.23).

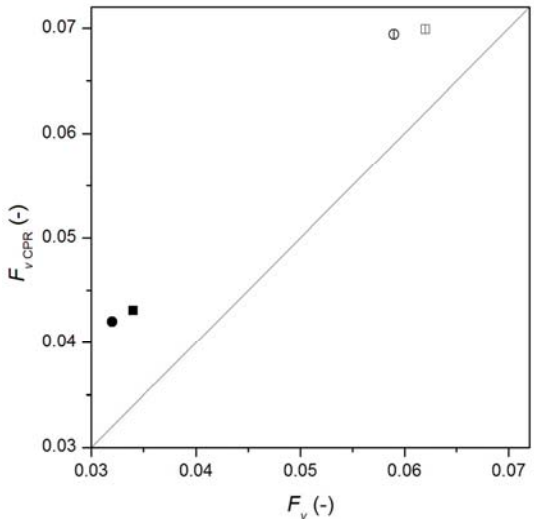

Figure 5.23. Vertical geometrical view factor predicted by the CPR model against that obtained from experimental measurements (orifice outlet diameter: 12.75 mm). Different heat flow sensors' radial positions from the flame axis are plotted (open symbols: 3 m; filled symbols: 5 m). Both heat flux sensors have been located at 1.5 above the ground.

It is important to note that the heat flux sensors involved in this analysis concern vertical receivers, this is why the geometrical view factor involved in the calculations, as shown in Fig. 5.23, is the vertical one.

Finally, it should also be noted that the atmospheric transmissivity values used by the CPR model and those used in this analysis (Brzustowski and Sommer, 1973) only differed in about 4%, thus slightly affecting the radiative heat intensity values resulting from calculations. Thus, as early mentioned, the differences (average overestimation of about 52%) between the radiative heat intensity resulting from calculations using the CPR model and the experimental values can be attributable to higher values of both the surface emissive power and the geometric view factor for the calculated values. Furthermore, the suggested cylinder obtained by the CPR model to define the flame surface area, involved in the calculation of the radiative heat intensity by using the solid flame model, has also been found to be over-sized; both jet flame length (14%) and flame width (94%) have been found to be overestimated, finding a higher difference for the jet flame width. This leads to higher surface emissive power and view factor calculated values than those calculated from the experimental measurements.

6. CONCLUSIONS

The work done in this thesis has allowed drawing the following summarized conclusions:

1. Among the major fire accidents, jet fires are important because they have been reported as often being the first stage of a domino effect sequence, leading to severe accidents involving explosions, large fires, and serious damage to equipment.
2. Although jet flames have been studied both experimentally and theoretically, most of the research performed up to now had been focused on relatively small-scale jet flames, subsonic jet fires and flares, which features are quite different from those of real accidental jet flames. Thus, expressions enabling the accurate prediction of jet fires reach were still lacking.
3. The features of jet flames originated by gas releases were found to be significantly different from those originated from a gas-liquid mixture. The flames fed by a gas phase were smaller, less luminous (almost transparent some times) and found to emit a thermal radiation significantly smaller than the flames originated by two-phase releases. These latter were found to be more luminous (yellow), due to a poorer combustion, and with a higher surface emissive power than gas jet fires.
4. The results obtained have shown that jet flame height, flame width and lift-off distance increase with the fuel mass flow rate and the outlet orifice diameter.

5. The sonic and subsonic data were correlated with the most appropriate dimensionless groups obtained by dimensional analysis. New expressions (Eqs. (3.11), (3.12) and (4.3)) have been proposed to estimate lift-off distance, jet flame length and flame width, respectively, as a function of the orifice's Reynolds number, for both sonic and subsonic jet exit velocities.
6. A single correlation (Eq. (3.14)) for the height of sonic exit velocity jet flames, measured from the pipe exit plane to the flame tip, for C_3H_8, CH_4 and H_2 over wide ranges of pressures and pipe diameters and accounting for the non-ideal behaviour of the gas was obtained. It was found that, whilst a number of existing correlations might be successful for each gas separately, only the one developed in the present study could embrace all three.
7. The jet flame data obtained have revealed that previous suggested shapes such as a vertical ellipse, a frustum of a cone and an inverted circular cone cannot be used to assess vertical jet fires in still air.
8. To solve the difficulty found when trying to define the flame contour, a comparative study of visible images, IR images and diverse isothermal contours was performed. Thus, the 800 K isotherm (corresponding to the Draper point) was found to be the best envelope for the jet flames.
9. To assess the proposal of a cylindrical shape, the average value of the jet flame diameter was obtained from IR images (D_{IR}). In an attempt to find a better approach for defining the shape of vertical jet fires, an "equivalent diameter" (D_{eq}) was obtained by defining a cylinder with a volume equal to that surrounded by the jet fire surface (isotherm of 800 K). The corresponding two-dimensional rectangle, with the same area as that covered by the two-dimensional flame surface both with the radiant flame length L_{IR}, gave the value of D_{eq}. The experimental results have shown that this is the best way to define the shape of a vertical jet fire. Thus, assuming a cylindrical shape with length L_{IR} and equivalent diameter D_{eq}, the resulting ratio was 7.
10. The incident radiant heat over a given target was found to increase as the distance from the flame surface decreases and as the fuel mass flow rate and the jet flame length increase.

11. The measurements obtained from the heat flux sensors and the treatment of infrared images allowed calculating the surface emissive power and the emissivity of the flames. The surface emissive power increases with the fuel mass flow rate and the jet flame length. An average value of 0.36 was obtained for the emissivity of flames.

    E values were applied to the solid flame model to analyze whether a three-zone model would improve significantly the prediction of the thermal radiation intensity. The results obtained are similar to those found with a simpler one-zone model.

12. The results obtained in this study contribute to a better understanding of jet fires, allowing a better prediction of their size and shape. However, due to the lack of data on this subject, it would be useful to check and extend the suggested expressions with other fuels and larger orifice diameters by developing large-scale field tests.

NOMENCLATURE

a	constant in Eq. (3.1) (-)
A	turbulent flame mean cross section area (m^2)
A_{IR}	jet fire surface (m^2)
A_R	surface of the solid flame through which heat is radiated (m^2)
b	constant in Eq. (4.1) (-)
c	constant in Eq. 3.6 (s)
$\bar{c}$	mean reaction progress variable (0-1)
C_D	dimensionless discharge coefficient (-)
C_P	specific heat capacity at constant pressure (kJ/kg·K)
d	orifice exit diameter (m or mm)
d_{ps}	pseudo-orifice exit diameter, originated by the expansion of the jet from the orifice exit to the atmosphere $\left(d\left[C_D \cdot \frac{P_{in}}{P_\infty}\left(\frac{2}{\gamma+1}\right)^{(\gamma+1)/2(\gamma-1)}\right]^{1/2}\right)$ (m)
D	flame width / flame diameter (m)
e	constant in Eq. (4.5) (-)
E	surface emissive power (kW/m^2)
f	number of dimensional physical variables
F	view factor (-)
Fr	Froude number ($V^2/g \cdot d$) (-)
g	acceleration of gravity (m/s^2)
h	co-volume constant in Eq. (3.3) (m^3/kg)
H	flame height, from the top of the burner to the flame tip (m)
i	intermittency (-)
I	thermal radiation intensity (kW/m^2)

I_o	dimensionless factor to allow for the effect of flame stretch rate on S_L
j	number of dimensionless groups
k	constant inversely proportional to integral length scale of turbulence (L_s) (m^{-1})
l	length (m)
L	flame height, from the base of the flame to the flame tip (m)
L_{IR}	radiant jet flame length, from the base of the flame to the flame tip (m), defined by the isotherm of 800 K
L_s	integral length scale of turbulence (m)
m	fuel mass flow rate (kg/s)
M	mass (kg)
M_v	fuel molecular weight (kg/kmole)
n	constant in Eq. (3.1) (-)
p	percentage of axial flame position, ranging between 0% (bottom of the flame) and 100% (tip of the flame) of L_{IR}
P	pressure (Pa, atm or MPa)
q	number of physical dimensions
Q	heat release rate (kW)
Q^*	dimensionless heat release rate $\left(Q/\left(\rho_\infty \cdot C_P \cdot T_\infty \cdot \sqrt{g \cdot W} \cdot W^2\right)\right)$
r	distance between the surface of the flames and the target (m)
rh	relative humidity (%)
R	universal gas constant (8.314 J/K·mol;82.06 atm·cm^3/K·mol)
R^2	correlation coefficient
Re	Reynolds number for the pressurized pipe flow ($d \cdot V \cdot \rho_{or}/\mu_{or}$)
R_L	turbulent Reynolds number ($u' \cdot L_s/\nu_{mix}$) (-)
S	lift-off distance, the centerline distance from the gas release point to the base of the stable detached flame (m)
S_L	laminar burning velocity (m/s)

S_T	turbulent burning velocity (m/s)
t	time (s)
T	temperature (K)
u	wind speed (m/s)
u'	rms turbulent gas velocity (m/s)
U_s	speed of sound of the gas at the jet exit (m/s)
V	velocity in the jet at the gas outlet (m/s)
W	orifice diameter or characteristic dimension of burner or pyrolyzing surface (m)
x	radial distance from the jet flame axis (m)
Y_f	mass fraction fuel (kg fuel/ kg total)
z	distance above ground level (m)
Z	gas compressibility factor (-)

Greek

α	numerical exponent
α_a	tilt angle of the flame (º)
α_b	angle between the axis of the outlet orifice and the line joining the center of the outlet orifice and the tip of the flame (º)
β	numerical exponent
δ	laminar flame thickness, under atmospheric conditions (ν_{mix}/S_L) (m)
Δ	difference
ε	flame emissivity (-)

γ	ratio of specific heats (-)
φ	angle between the plane perpendicular to the receiving surface and the line joining the source point and the target (º)
κ	numerical exponent
μ	dynamic viscosity (kg/m·s)
ν	kinematic viscosity (m^2/s)
ρ	density (kg/m^3)
σ	Stefan-Boltzmann constant (5.67×10^{-11} $kW \cdot m^{-2} \cdot K^{-4}$)
Σ	flame surface density (m^{-1})
$\overline{\Sigma}$	mean flame surface density through the flame brush (m^{-1})
τ	atmospheric transmissivity (-)
ζ	dimensionless grouping for sonic exit velocity $\left((V/S_L)\, Re^{-0.3} (d/\delta)^{0.25}\right)$
ψ	dimensionless factor that depends on the velocity of the gas

Subscripts

1	at the bottom of the flame
2	at the tip of the flame
ave	average
b	distance between the center of the outlet orifice and the tip of the flame
Baron	predicted by Baron's expression Eq. (4.1) with $b = 0.29$
e	conditions at jet exit

eq	equivalent
exp	experimental
f	flame
in	at the fuel source –inside the tank or the pipe, in the pipe just upstream the orifice, considered stagnation conditions
IR	a temperature ≥ 800 K defines the jet flame
max	maximum
mix	gaseous mixture under ambient conditions
or	at the outlet orifice
out	downstream from the outlet orifice
p	percentage of axial flame position, ranging between 0% (bottom of the flame) and 100% (tip of the flame) of L_{IR}
ps	pseudo
s	sound
v	vertical
VIS	visible images
∞	ambient conditions or ambient gas (generally air)

Abbreviations

1Z	One zone model
3Z	Three zone model
CFD	Computational Fluid Dynamics
CPR	Model proposed by the Committee for the Prevention of Disasters

DN	Nominal diameter
Exp.	Experimental
FP	FieldPoint
FPA	Focal Plane Array
HFT	Heat Flux Transducer
HFTR	Heat Flux Transducer and Radiometer
I/O	Input/Output
IR	Infrared
JFT	Jet Fire Test
Max.	Maximum
Min.	Minimum
PN	Nominal pressure
Pred.	Predicted
R	Radiation measurements
R1	Region I (0% - 40% of the radiant jet flame length)
R2	Region II (40% - 70% of the radiant jet flame length)
R3	Region III (70% - 100% of the radiant jet flame length)
RAD	Radiometer
RTD	Resistance temperature detector
T	Total heat (convection plus radiation) measurements
TB	B-Type thermocouple
TK	K-Type thermocouple
TS	S-Type thermocouple
UV	Ultraviolet
VHS	Sequence of visible video images
VIS	Visible

REFERENCES

American Petroleum Institute Recommended Practice 521. (1982) *Guide for Pressure-Relieving and Depressuring Systems*, 2nd ed. Washington, DC: American Petroleum Institute.

American Petroleum Institute Recommended Practice 521. (1997) *Guide for Pressure-Relieving and Depressuring Systems*, 4th ed. Washington, DC: American Petroleum Institute.

Annushkin, Y.M., Sverdlov, E.D. (1979) Stability of Submerged Diffusion Flames in Subsonic and Underexpanded Supersonic Gas-Fuel Streams. *Combustion, Explosion and Shock Waves*, 14(5): 597–605.

Arnaldos, J., Casal, J., Montiel, H., Vílchez, J.A. (1997) *Estudio del Riesgo originado por Fugas Accidentales en Tuberías de Gas Natural*. Final Report for Gas Natural, Barcelona: SDG, S.A.

Baev, V.K., Kuznetsov, P.P., Mogil'nyi, I.A., Tret'yakov, P.K., Yasakov, V.A. (1974) Length of Diffusion Flames. *Fizika Goreniya i Vzryva*, 10(4): 485–492; translation available in *Combustion, Explosion and Shock Waves*, 10: 420–426.

Baev, V.K., Yasakov, V.A. (1974) Influence of Buoyant Forces on the Height of Diffuse Flames. *Fizika Goreniya i Vzryva*, 10(6): 835–841; translation available in *Combustion, Explosion and Shock Waves*, 10: 752–756.

Bagster, D.F., Pitblado, R.M. (1989) Thermal Hazards in the Process Industry. *Chem. Eng. Prog.*, July: 69–75

Bagster, D.F., Schubach, S.A. (1996) The Prediction of Jet-Fire Dimensions. *Journal of Loss Prevention in the Process Industries*, 9(3): 241–245.

Baron, T. (1954) Reaction in Turbulent Free Jets – The Turbulent Diffusion Flame. *Chemical Engineering Progress*, 50(2): 73–76.

Becker, H.A., Liang, D. (1978) Visible Length of Vertical Free Turbulent Diffusion Flames. *Combustion and Flame*, 32: 115–137.

Becker, H.A., Liang, D. (1981) Effect of Burner Orientation and Ambient Airflow on Geometry of Turbulent Free Diffusion Flames. *Eighteenth Symposium (International) on Combustion. The Combustion Institute*, 1061–1070.

Birch, A.D., Hughes, D.J., Swaffield, F. (1987) Velocity Decay of High Pressure Jets. *Combustion Science and Technology*, 52: 161–171.

Blake, T.R., McDonald, M. (1993) An Examination of Flame Length Data from Vertical Turbulent Diffusion Flames. *Combustion and Flame,* 94: 426–432.

Bradley, D., Gaskell, P.H., Gu, X.J. (1998) The Mathematical Modeling of Liftoff and Blowoff of Turbulent Non-Premixed Methane Jet Flames at High Strain Rates. *Twenty-Seventh Symposium (International) on Combustion. The Combustion Institute*, 1199–1206.

Bradley, D., Lawes, M., Kexin L. (2008) Turbulent Flame Speeds in Ducts and the Deflagration/Detonation Transition. *Combustion and Flame*, 154: 96–108.

Bradley, D., Lawes, M., Mansour, M.S. (2009) Flame Surface Densities during Spherical Turbulent Flame Explosions. *Proc. Combust. Inst.*, 32: 1587–1593.

Bradley, D., Casal, J., Palacios, A. (2010) Correlation of the Height of Turbulent Choked Jet Flames. *Sixth International Seminar on Fire and Explosions Hazard*, Leeds, UK. Eds. D. Bradley, G. Makhviladze, V. Molkov. In Press.

Brennan, S.L., Makarov, D.V., Molkov, V. (2009) LES of High Pressure Hydrogen Jet Fire. *Journal of Loss Prevention in the Process Industries*, 22: 353–359.

Broadwell, J.E., Dahm, W.J.A., Mungal M.G., (1984) Blowout of Turbulent Diffusion Flames. *Twentieth Symposium (International) on Combustion. The Combustion Institute,* 303–310.

Brzustowski, T.A. (1973) A New Criterion for the Length of a Gaseous Turbulent Diffusion Flame. *Combustion Science and Technology*. 6: 313–319.

Brzustowski, T.A., Sommer, E.C., Jr., (1973) Predicting Radiant Heating from Flares. *Proc. Division of Refining. American Petroleum Institute.* 53: 865-893.

Brzustowski, T.A., Gollahalli, S.R., Kaptein, M.E., Sullivan, H.F., Gupta, M.P. (1975) *ASME Heat Transfer Conference*, Paper 75-HT-4.

Butler, C.J., Royle, M. (2001) Experimental Data Acquisition of a New Vapour Cloud Fire (VCF) Modelling Approach. HSL Internal Report PS/01/01.

Burke, S.P., Schumann, T.E.W. (1928) Diffusion Flames. *Industrial and Engineering Chemistry*, 20(10): 998–1004.

Casal, J. (2008) *Evaluation of the Effects and Consequences of Major Accidents in Industrial Plants*. Barcelona: Elsevier Science.

Committee for the Prevention of Disasters. (1997) *Methods for the Calculation of Physical Effects (the "Yellow Book")*. 3rd ed. The Hague: SDU.

Cook, D.K., Fairweather, M., Hammonds, J., Hughes, D.J. (1987a) Size and Radiative Characteristics of Natural Gas Flares. Part 1: Field Scale Experiments. *Chemical Engineering Research and Design*, 65: 310–317.

Cook, D.K., Fairweather, M., Hammonds J., Hughes D.J. (1987b) Size and Radiative Characteristics of Natural Gas Flares. Part 2: Empirical Model. *Chemical Engineering Research and Design*, 65:318–325.

Cook, D.K., Fairweather, M., Hankinson, G., O'Brien, K. (1987c) Flaring of Natural Gas from Inclined Vent Stacks. *IChemE Symposium Series*, 102: 289–300.

Cook, J., Bahrami, Z., Whitehouse, R.J. (1990) A Comprehensive Program for Calculation of Flame Radiation Levels. *Journal of Loss Prevention in the Process Industries*, 3: 150–155.

Costa, M., Parente, C., Santos, A. (2004) Nitrogen Oxides Emissions from Buoyancy and Momentum Controlled Turbulent Methane Jet Diffusion Flames. *Experimental Thermal and Fluid Science*, 28: 729–734.

Council Directive 96/82/EC of 9 December 1996 on the Control of Major-Accident Hazards Involving Dangerous Substances. (1997) Official Journal of the European Communities No. 10, 14 January 1997, article 3.

Cowley, L.T., Tam, V.H.Y. (1988) Pressurised LPG Releases. The Isle of Grain Full Scale Experiments. *The 13th International LNG/LPG Conference and Exhibition, Gastech Ltd., Herts., UK.* Gastech 88, Section 4.3.

Cowley, L.T., Pritchard M. J. (1990) Large-Scale Natural Gas and LPG Jet Fires and Thermal Impact on Structures. *The 14th International LNG/LPG Conference and Exhibition, Gastech Ltd., Herts. UK.* Gastech 90.

Crespo, A., Hernandez, J., Servert, J., Garcia, J. and Manuel, F. (1994) Hazard Consequences of Jet Fire Interactions with Vessels Containing Pressurized Liquids. Final Report from UPM to EC, contract STEP-CT90-0098.

Cha, M.S., Chung, S.H. (1996) Characteristics of Lifted Flames in Nonpremixed Turbulent Confined Jet. *Twenty-Sixth International Symposium on Combustion. The Combustion Institute,* 121–128.

Chamberlain, G.A. (1987) Developments in Design Methods for Predicting Thermal Radiation from Flares. *Chemical Engineering Research and Design*, 65: 299–309.

Chatris Riu, J.M. (2001) *Velocitat de combustió i distribució de temperatures en incendis de bassals d'hidrocarburs*. PhD Thesis: Universitat Politècnica de Catalunya, Barcelona.

Chatris, J.M., Quintela, J., Folch, J., Planas, E., Arnaldos, J., Casal, J. (2001) Experimental Study of Burning Rate in Hydrocarbon Pool Fires. *Combustion and Flame*, 126: 1373–1383.

Chen, M., Herrmann, M., Peters N. (2000) Flamelet Modeling of Lifted Turbulent Methane/Air and Propane/Air Jet Diffusion Flames. *Proceedings of the Combustion Institute*, 28: 167–174.

Choi, M.Y., Hamins, A., Rushmeier, H., Kashiwagi, T. (1994) Simultaneous Optical Measurement of Soot Volume Fraction, Temperature, and CO_2 in Heptane Pool Fire. *Proceedings of the Twenty-Fifth International Symposium on combustion, The Combustion Institute*, 1471–1480.

Darbra, R.M., Casal, J. (2004) Historical Analysis of Accidents occurred in Seaports. *Safety Science*. 42: 85–98.

Darbra, R.M., Palacios, A., Casal, J. (2010) Domino Effect in Chemical Accidents: Main Features and Accident Sequences. *Journal of*

Hazardous Materials, 183: 565–573.

Delichatsios, M. (1993) Transition from Momentum to Buoyancy-Controlled Turbulent Jet Diffusion Flames and Flame Height Relationships. *Combustion and Flame,* 92: 349–364.

Donnerhack, S., Peters, N. (1984) Stabilization Heights in Lifted Methane-Air Jet Diffusion Flames Diluted with Nitrogen. *Combustion Science and Technology,* 41: 101–108.

Draper, J.W. (1847) On the Production of Light by Heat. *The London Edinburgh and Dublin Philosophical Magazine and Journal of Science,* 30(3): 345–360.

Driscoll, J.F., Upatnieks, A., Rasmussen, C.C., Ceccio, S.L. (2004) Liftoff of Turbulent Jet Flames–Assessment of Edge Flame and other Concepts using Cinema-PI. *Combustion and Flame,* 138: 259–272.

Drysdale, D. (1994) *An Introduction to Fire Dynamics*. England: Wiley.

Eickhoff, H., Lenza, B., Leuckel, W. (1984) Experimental Investigation on the Stabilization Mechanism of Jet Diffusion Flames. *Twentieth Symposium (International) on Combustion. The Combustion Institute,* 311–318.

Eisenberg, N.A., Lynch, C.J. and Breeding, R.J. (1975) Vulnerability Model: A Simulation System for Assessing Damage resulting from Marine Spills. *Enviro. Control. Inc., Rockville, MD Spills*. Report CG-D-136-75.

Ferrero, F. (2006) *Incendios de Hidrocarburos: Estudio de la Formación y Evolución del Boilover de Capa Fina*. PhD Thesis: Universitat Politècnica de Catalunya, Barcelona.

Forsth, L.R., Odgaard, E. (1982) Beregning av Jetflammer. *Veritas Teknisk Notat.* FDIV 13/10-82.

Galant, S., Grouset, D., Martinez, G. (1984) Comparison between Test Results and the API-Guidelines. *Third International Flare System Seminar,* Trondheim, Norway.

Gollahalli, S.R., Brzustowski, T.A., Sullivan, H.F. (1975) Characteristics of A Turbulent Propane Diffusion Flame in a Cross–Wind. *Transactions of the CSME,* 3(4): 205–214.

Gómez-Mares, M., Zárate, L., Casal, J. (2008) Jet Fires and the Domino Effect. *Fire Safety Journal*, 43(8): 583–588.

Gómez-Mares, M., Muñoz, M., Casal, J. (2009) Axial Temperature Distribution in Vertical Jet Fires. *Journal of Hazardous Materials*, 172: 54–60.

Gore, J.P., Faeth, G.M., Evans, D., Pfenning, D.B. (1986) Structure and Radiation Properties of Large-Scale Natural Gas/Air Diffusion Flames. *Fire and Materials*, 10: 161–169.

Gore, J.P., Skinner, S.M., Stroup, D.W., Madrzykowski, D., Evans, D.D. (1989) Structure and Radiation Properties of Large Two-Phase Flames. *Heat Transfer in Combustion Systems. Winter Annual Meeting of ASME*, San Francisco, California.

Gore, J.P., Jian, C.Q. (1991) Trajectories of Horizontal Buoyant Free Jet Flames. *ASME/JSME Thermal Engineering Proceedings*, 5: 127–138.

Gritzo, L.A., Sivathanu, Y.R., Gill, W. (1998) Transient Measurements of Radiative Properties, Soot Volume Fraction and Soot Temperature in A Large Pool Fire. *Combustion Science and Technology*, 139(1–6): 113–136.

Hankinson, G. (1986) A Method for Calculating the Configuration Factor between a Flame and a Receiving Target for a Wide Range of Flame Geometries Relevant to Large Scale Fires. *Fire Safety Science: Proceedings of the First International Symposium*, 197–209.

Hawthorne, W.R., Weddell, D.S., Hottel, H.C. (1949) Mixing and Combustion in Turbulent Gas Jets. *Proc. Combustion Flame and Explosions Phenomena*, 3: 266–288.

Health and Safety Executive. (1993) Interim Jet Fire Test for Determining the Effectiveness of Passive Fire Protection Materials. OTO Report No. OTO-93-028.

Health and Safety Executive. (1996a) Assessment of the Uniformity of the Interim Jet Fire Test Procedure. Offshore Technology Report No. OTH-95-477.

Health and Safety Executive. (1996b) Jet-Fire Resistance Test of Passive Fire Protection Materials. Offshore Technology Report No. OTI-95-634.

Health and Safety Executive. (1997).Validation of the Jet Fire Resistance Test Procedure-Additional Measurements. Offshore Technology Report No. OTO-96-056.

Health and Safety Executive. (1999) CFD Calculation of Impinging Gas Jet Flames. OTO Report No. OTO 1999 011.

Health and Safety Executive. (2000) Efficacy of Water Spray Protection Against Butane Jet Fires Impinging on Liquefied Petroleum Gas (LPG) Storage Tanks. Contract Research Report 298/2000.

Heskestad, G. (1999) Turbulent Jet Diffusion Flames: Consolidation of Flame Height Data. *Combustion and Flame,* 118: 51–60.

Hess, K. (1964) *Flammenlänge und Flammenstabilität*. PhD Thesis: Technische Hochschule Karlsruhe.

Hirst, W.J.S. (1984) Combustion of Large Scale Jet-Releases of Pressurised Liquid Propane. *The Institute of Gas Engineers. 50th Autumn Meeting*, Communication 1241.

Hustad, J., Sonju, O.K. (1985) Radiation and Size Scaling of Large Gas and Gas/Oil Diffusion Flames. *Interm Colloquium of Explosions and Reactive Systems*, Berkeley.

Hustad, J.E., Sonju, O.K. (1986) Radiation and Size Scaling of Large Gas and Gas/Oil Diffusion Flames. *Dynamics of Flames and Reactive Systems. AAIA Progress in Aeronautics and Aeronautics*, 105: 365–387.

Imamura, T., Hamada, S., Mogi, T., Wada, Y., Horiguchi, S., Miyake, A., Ogawa, T. (2008) Experimental Investigation on the Thermal Properties of Hydrogen Jet Flame and Hot Currents in the Downstream Region. *International Journal of Hydrogen Energy*, 33: 3426–3435.

Iwasaka, M., Urano, Y., Hashiguchi, Y. (1979) Fire Hazard of Compressed Hydrogen by Rapid Leak. *Koatsu Gas. Journal of the High Pressure Gas Safety Institute of Japan,* 16(7): 333–338.

Johnson, A.D., Brightwell, H.M., Carsley, A.J. (1994) A Model for Predicting the Thermal Radiation Hazards from Large-Scale Horizontally Released Natural Gas Jet Fires. *Trans IChemE*, 72(B): 157–166.

Jones, D.A. (1988) Radiation and Fire Hazards. *In Proceedings of Seminar on Risk Assessment Techniques and Management*. Delhi, India.

Kalghatgi, G.T. (1981) Blow-Out Stability of Gaseous Jet Diffusion Flames Part I: In Still Air. *Combustion Science and Technology,* 26: 233–239.

Kalghatgi, G.T. (1983) The Visible Shape and Size of a Turbulent Hydrocarbon Jet Diffusion Flame in a Cross-Wind. *Combustion and Flame,* 52(1): 91–106.

Kalghatgi, G.T. (1984) Lift-Off Heights and Visible Lengths of Vertical Turbulent Jet Diffusion Flames in Still Air. *Combustion Science and Technology,* 41: 17–29.

Kiran, D.Y., Mishra, D.P. (2007) Experimental Studies of Flame Stability and Emission Characteristics of Simple LPG Jet Diffusion Flame. *Fuel*, 86: 1545–1551.

Klassen, M., Sivathanu, Y.R., Gore, J.P. (1992) Simultaneous Emission Absorption Measurements in Toluene-Fueled Pool Flames. *Combustion and Flame*, 90: 34–44.

Komov, V.F., Grishin, V.V., Krivulin, V.N. (1973) *Problems of Combustion and Fire Extinguishing*. In: *VNIIPO* Part I. Moscow: 188–195.

Koseki, H. (1999) Large Scale pool Fires: Results of Recent Experiments. In: *Fire Safety Sciene, Sixth Symposium on Fire Safety Science*, Vol. 6, France, p. 115–132.

Lee, B.J., Kim, J.S., Chung, S.H. (1994) Effect of Dilution on the Liftoff of Non-Premixed Jet Flames. *Twenty-Fifth International Symposium on Combustion. The Combustion Institute*, 1175–1181.

Lihou, D.A., Maund, J.K. (1982) Thermal Radiation Hazard from Fireballs. *I. Chem. E. Symp.,* 71: 191–224.

Lowesmith, B.J., Hankinson, G., Acton, M.R., Chamberlain, G. (2007) An Overview of the Nature of Hydrocarbon Jet Fire Hazards in the Oil and Gas Industry and a Simplified Approach to Assessing the Hazards. Trans IChemE, Part B, *Process Safety and Environmental Protection*, 85(B·): 207–220.

Major Accident Reporting System (MARS). (2009) Major Accident Hazards Bureau. European Comission's Joint Research Centre.

McCaffrey, B.J., Evans, D.D. (1986) Very Large Methane Jet Diffusion Flames. *Twenty-First Symposium (International) on Combustion. The Combustion Institute*, 25–31.

McCaffrey, B.J. (1988) Flame Height. *SFPE Handbook of Fire Protection Engineering*. Section 1/Chapter 18: 298–305.

McCaffrey, B.J. (1989) Momentum Diffusion Flame Characteristics and the Effects of Water Spray. *Combustion Science and Technology*, 63: 315–335.

McMurray, R. (1982) Flare Radiation Estimated. *Hydrocarbon Processing*, 61(11): 175–181.

Meteorological Service of Catalonia. <http://www.meteo.cat/mediamb_xemec/servmet//index.html> [Consulted 11/2010]

Miake-Lye, R.C., Hammer, J. (1988) Lifted Turbulent Jet Flames: A Stability Criterion based on the Jet Large-Scale Structure. *Twenty-Second Symposium (International) on Combustion. The Combustion Institute*, 817–824.

Mizner, G.A., Eyre, J.A. (1983) Radiation from Liquefied Gas Fires on Water. *Combustion Science and Technology*, 35(1–4): 33–57.

Mogi T, Nishida H, Horiguchi S. (2005) Flame Characteristics of High-Pressure Hydrogen Gas Jet. *In: Proceedings of First International Conference on Hydrogen Safety*, Pisa, Italy.

Mogi, T., Horiguchi, S. (2009) Experimental Study on the Hazards of High-Pressure Hydrogen Diffusion Flames. *Journal of Loss Prevention in the Process Industries*, 22: 45–51.

Molkov, V.V. (2009) Hydrogen Non-Reacting Jets and Jet Fires. *Fourth European Summer School on Hydrogen Safety* ESSHS, Corsica, France.

Montiel, H., Vílchez, J.A., Casal, J., Arnaldos, J. (1998) Mathematical Modelling of Accidental Gas Releases. *Journal of Hazardous Materials*, 59: 211–233.

Mudan, K.S., Croce, P.A. (1990) Fire Hazard Calculations for Large Open Hydrocarbon Fires. In: DiNenno, P.J. (Eds.). *The SFPE Handbook of Fire Protection Engineering*, 2nd ed. Massachusetts: National Fire Protection Association and Society of Fire Protection Engineers.

Muñoz, M. (2005) *Estudio de los Parámetros que Intervienen en la Modelización de los Efectos de Grandes Incendios de Hidrocarburo: Geometría y Radiación Térmica de la Llama*. PhD Thesis: Universitat Politècnica de Catalunya, Barcelona.

Müller, C.M., Breitbach, H., Peters N. (1994) Partially Premixed Turbulent Flame Propagation in Jet Flames. *Twenty-Fifth Symposium (International) on Combustion. The Combustion Institute*, 1099–1106.

Niemitz, K.J. (2010) Process Safety Culture or What are the Performance Determining Steps?. *Workshop on Safety Performance Indicators*. Ispra, Italy.

O'KEEFE Controls Co. (2000) *Chocked Flow of Gases*. PDF file, URL <http://www.okcc.com/PDF/Choked%20Flow%20of%20Gases%20pg.48.pdf> [Consulted 11/2010].

Odgaard, E. (1983) Characteristics of Hydrocarbon Fires in Open-Air. Report No. 82-0704. Hoevik, Norway: Det Norske Veritas. Research Division.

Oggero, A., Darbra, R.M., Muñoz, M., Planas, E., Casal, J. (2006) A Survey of Accidents occurring during the Transport of Hazardous Substances by Road and Rail. *Journal of Hazardous Materials*, 133(1–3): 1–7.

Palacios, A., Muñoz, M., Casal, J. (2009) Jet Fires: An experimental Study of the Main Geometrical Features of the Flame in Subsonic and Sonic Regimes. *AIChE Journal*, 55 (1): 256–263.

Palacios, A., Casal, J. (2010) Assessment of the Shape of Vertical Jet Fires. *Fuel*, doi:10.1016/j.fuel.2010.09.048

Peters, N., Williams, F.A. (1983) Liftoff Characteristics of Turbulent Jet Diffusion Flames. *The American Institute of Aeronautics and Astronautics Journal*, 21(3): 423–429.

Peters, N., Göttgens, J. (1991) Scaling of Buoyant Turbulent Jet Diffusion Flames. *Combustion and Flame*, 85: 206–214.

Peters, N. (2000) *Turbulent Combustion*. UK : Cambridge University Press.

Pietersen, C.M., Cendejas, S. (1985) Analysis of the LPG Accident in San Juan Ixhuatepec, Mexico City, TNO, Report 85-0222, The Hague.

Pitts, W.M. (1989) Importance of Isothermal Mixing Processes to the Understanding of Lift-off and Blowout of Turbulent Jet Diffusion Flames. *Combustion and Flame*, 76: 197–212.

Planas, E., Montiel, H., Casal. J. (1997) A Survey of the Origin, Type and Consequences of Fire Accidents in Process Plants and in the Transportation of Hazardous Material. *Trans IChemE*, 75(B): 3–8.

Muñoz, M., Arnaldos, J., Casal, J., Planas, E. (2004) Analysis of the Geometric and Radiative Characteristics of Hydrocarbon Pool Fires. *Combustion and Flame,* 139: 263–277.

Proust, C., Jamois, D., Studer, E. (2009) High Pressure Hydrogen Fires. *Third International Conference on Hydrogen Safety*. Corsica, France.

Raj, P.P.K. and Emmons, H.W. (1975). On the Burning of A Large Flammable Vapour Cloud. *The Joint Technical Meeting of the Western and Central States Section of the Combustion Institute*. San Antonio, TX, USA, April 1975.

Ricou, F.P., Spalding, D.B. (1961) Measurements of Entrainment by Axisymmetrical Turbulent Jets. *Journal of Fluid Mechanics,* 8: 21–32.

Roberts, T., Gosse A., Hawksworth S. (2000) Thermal Radiation from Fireballs on Failure of Liquefied Petroleum Gas Storage Vessels. *Trans IChemE*., 78(B): 184–192.

Rokke, N.A., Hustad, J.E., Sonju, O.K. (1994) A Study of Partially premixed Unconfined Propane Flames. *Combustion and Flame*, 97(1): 88–106.

Ronza, A., Félez, S., Darbra, R.M., Carol, S., Vílchez, J.A., Casal, J. (2003) Predicting the Frequency of Accidents in Ports Areas by Developing Event Trees from Historical Analysis. *Journal of Loss Prevention in the Process Industries*, 16: 551–560.

Santos, A., (2003) *Estudo da Formação de NO em Chamas de Difusão Turbulentas*. Masther Thesis. Lisbon: Facultade de Ciências e Tecnologia da Universidade Nova de Lisboa.

Santos, A., Costa, M. (2005) Reexamination of the Scaling Laws for NOx Emissions from Hydrocarbon Turbulent Jet Diffusion Flames. *Combustion and Flame*, 142: 160–169.

Schefer, R.W., Houf, B., Bourne, B., Colton, J. (2004) Experimental Measurements to Characterize the Thermal and Radiation Properties of An Open-Flame Hydrogen Plume. *The 15th Annual Hydrogen Conference and Hydrogen Expo*. Los Angeles, CA, USA.

Schefer, R.W., Houf, W.G., Bourne, B., Colton, J. (2006) Spatial and Radiative Properties of An Open-Flame Hydrogen Plume. *International Journal of Hydrogen Energy,* 31: 1332–1340.

Schefer, R.W., Houf, W.G., Williams, T.C., Bourne, B., Colton, J. (2007) Characterization of High-Pressure, Underexpanded Hydrogen-Jet Flames. *International Journal of Hydrogen Energy*, 32(12): 2081–2093.

Schuller, R.B., Nylund, J., Sonju, O.K., Hustad, J. (1983) Effect of Nozzle Geometry on Burning Subsonic Hydrocarbon Jets. *The 21st ASME/AIChE National Heat Transfer Conference*. 25: 33–36.

Seeger, P.G., Werthenbach, H.G. (1970) Diffusionsflammen Mit Extreme Niedriger Strömungsgeschwindigkeit. *Chem. Ind. Technol.,* 42(5): 282–286.

SFPE. (1988) *The SFPE Handbook of Fire Protection Engineering*. 2nd Edn., DiNenno, P.J. (ed.) Quincy (MA): National Fire Protection Association (NFPA); Society of Fire Protection Engineers (SFPE).

Shell Shepherd Desktop Technical Guide. (2003) SHEPHERD Version 1.0.4.5 Technical Guide.

Shevyakov, G.G., Komov, V.F. (1977) Effect of Non-Combustible Admixtures on Length of An Axisymmetric On-Port Turbulent Diffusion Flame. *Combustion, Explosion and Shock Waves,* 13: 563–566 (translated from *Fizika Goreniya I Vzryva*, 1977; 13(5): 667–670).

Siegel, R., Howell, J.R. (1992) *Thermal Radiation Heat Transfer*, 3rd ed. USA: Taylor & Francis.

Sonju, O.K., Hustad, J. (1984) An Experimental Study of Turbulent Jet Diffusion Flames. *Norwegian Maritime Research*, 4: 2–11.

Steward, F.R. (1970) Prediction of the Height of Turbulent Diffusion Buoyant Flames. *Combustion Science and Technology,* 2: 203–212.

Straitz, J.F., III., Altube, R.J. (1983) Flares: Design and Operation. *National Air-Oil Burner Company, Inc.* Philadelphia, USA.

Sugawa, O., Sakai, K. (1997) Flame Length and Width Produced by Ejected Propane Gas fuel from a Pipe. *Fire Science and Technology*, 17: 55–63.

Suris, A.L., Flankin, E.V., Shorin, S.N. (1977) Length of Free Diffusion Flames. *Combustion, Explosion, and Shock Waves*, 13(4): 459–462.

Turns, S.R., Myhr, F.H. (1991) Oxides of Nitrogen Emissions from Turbulent Jet Flames: Part I – Fuel Effects and Flame Radiation. *Combustion and Flame,* 87: 319–335.

Turns, S.R. (1996) *An Introduction to Combustion: Concepts and Applications.* New York: Mc. Graw-Hill.

Vanquickenborne, L.,Van Tiggelen, A. (1966) The Stabilization Mechanism of Lifted Diffusion Flames. *Combustion and Flame,* 10: 59–69.

Verheij, J.F., Duijm, N.J. (1991) Windtunnel Modelling of Torch Fires. TNO Report No. 91-422. Apeldoorn, The Netherlands.

Vílchez, J.A., Sevilla, S., Montiel, H., Casal, J. (1995) Historical Analysis of Accidents in Chemical Plants and in the Transportation of Hazardous Materials. *Journal of Loss Prevention in the Process Industries*, 8(2): 87–89.

Wayne, F.D. (1991) An Economical Formula for Calculating Atmospheric Infrared Transmissivites. *Journal of Loss Prevention in the Process Industries,* 4: 86–92.

Wohl, K., Gazley, C., Kapp, N. (1949(a)) Diffusion Flames. *Proc. Combustion Flame and Explosions Phenomena,* 3: 288–300.

Wohl, K., Kapp, N., Gazley C. (1949(b)) The Stability of Open Flames. *Third Symposium on Combustion, Flame and Explosion Phenomen*a, 3–21.

Wu, Y., Al-Rahbi, I.S., Lu, Y., Kalghatgi, G.T. (2007) The Stability of Turbulent Hydrogen Jet Flames with Carbon Dioxide and Propane Addition. *Fuel,* 86: 1840–1848.

Wu, Y., Lu, Y., Al-Rahbi, I.S., Kalghatgi, G.T. (2009) Prediction of the Liftoff, Blowout and Blowoff Stability Limits of Pure Hydrogen and Hydrogen/Hydrocarbon Mixture Jet Flames. *International Journal of Hydrogen Energy*, 34: 5940–5945.

Yellow Book. (1979) *Report of the Committee for the Prevention of Disasters.* The Hague (The Netherlands): Directorate General of Labour, Ministry of Social Affairs.

Zukoski, E.E., Kubota, T., Cetegen, B. (1980/81) Entrainment in Fire Plumes. *Fire Safety Journal,* (3): 107–121.

Zukoski, E.E., Cetegen, B.M., Kubota, T. (1984) Visible Structure of Buoyant Diffusion Flames. *Twentieth Symposium (International) on Combustion. The Combustion Institute,* 361–366.

Zukoski, E.E. (1995) *Properties of Fire Plumes*. In: Cox G, eds. Combustion Fundamentals of Fire. San Diego, Calif: Academic Press, 101–151.

APPENDIX I. FLOW OF GAS/VAPOUR THROUGH AN ORIFICE

When a gas is flowing from a tank or a pipe at a certain pressure (P_{in}) through an orifice in the wall, if P_{in} increases, the velocity of the gas through the orifice increases. This velocity will increase until the velocity of sound in that gas (in exit gas conditions) will be reached (Fig. I.1). Further increase of P_{in} will not increase the fluid velocity since the velocity of sound at the pressure and temperature at the outlet orifice (P_{or} and T_{or}, respectively) is the maximum velocity at which the gas can flow through the orifice. P_{or} is called choked or critical pressure and the velocity at the hole at these conditions is called choked or critical velocity (Casal, 2008).

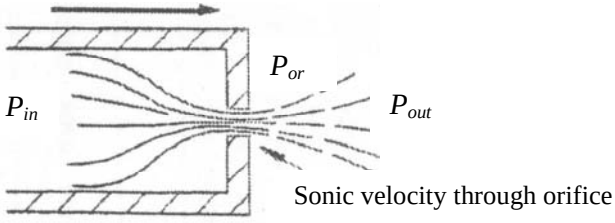

Figure I.1. Flow of gas/vapour through an orifice (modified from O'KEEFE Controls Co., 2000)

However, the density of a gas increases with pressure; thus, once the choked velocity has been reached, if P_{in} is further increased, the release gas velocity will still be the speed of sound, but the density of the gas will be

higher. As a result, the mass flow rate will increase with P_{in}. Choked velocity will be reached if the following condition is fulfilled:

$$\frac{P_{in}}{P_{out}} \geq \left[\frac{\gamma+1}{2}\right]^{\frac{\gamma}{\gamma-1}} \tag{I.1}$$

where P_{in} is the pressure inside the tank or the pipe (Pa)

P_{out} is the pressure downstream the outlet orifice (Pa) and

γ is the ratio of specific heats (-).

For sonic gas velocity, the mass flow rate of gas through an orifice can be calculated with the following expression:

$$m = U_s \cdot \frac{\pi}{4} \cdot d^2 \cdot \rho_{or} \tag{I.2}$$

where m is the mass flow rate (kg/s)

d is the orifice exit diameter (m)

U_s is the speed of sound of the gas at the jet exit (m/s)

ρ_{or} is the gas density at the outlet orifice (at P_{or} and T_{or}) (kg/m^3)

P_{or} is the pressure at the outlet orifice (Pa) and

T_{or} is the temperature at the outlet orifice (K).

The speed of sound in an ideal gas at a certain value of temperature can be calculated with the following expression:

$$U_s = \sqrt{\frac{\gamma \cdot T_{in} \cdot R \cdot 10^3}{M_v}} \tag{I.3}$$

where M_v is the molecular weight of the gas (kg/kmole)

T_{in} is the temperature inside the tank or pipe (K), in the pipe just upstream the orifice, considered as stagnation condition, and

R is the universal gas constant (8.314 kJ/kmole·K).

It should be noted that the same m values are obtained from Eq. (I.2) and from the following Eq. (I.4), obtained from the mechanical energy balance, assuming isentropic expansion, introducing a discharge coefficient (C_D) and using a C_D value of 1:

$$m = \frac{\pi}{4} \cdot d^2 \cdot C_D \cdot P_{in} \cdot \psi \sqrt{\gamma \cdot \left(\frac{2}{\gamma+1} \right)^{\frac{\gamma+1}{\gamma-1}} \frac{M_v}{Z \cdot T_{in} \cdot R \cdot 10^3}} \qquad \text{(I.4)}$$

where C_D is a dimensionless discharge coefficient (-)

Z is the gas compressibility factor at P_{in}, T_{in} (-) (for ideal gas behaviour $Z = 1$) and

ψ is a dimensionless factor that depends on the velocity of the gas (for sonic gas velocity $\psi = 1$).

Assuming isentropic expansion, the properties of the gas in the jet at the orifice exit can be calculated by the following equations:

$$\frac{P_{or}}{P_{in}} = \left(\frac{2}{\gamma+1} \right)^{\left(\frac{\gamma}{\gamma-1} \right)} \qquad \text{(I.5)}$$

$$T_{or} = T_{in} \left(\frac{P_{or}}{P_{in}} \right)^{\left(\frac{\gamma-1}{\gamma} \right)} \qquad \text{(I.6)}$$

If Eq. (I.1) is not fulfilled, P_{or} is assumed to be equal to atmospheric pressure. And for subsonic gas velocity:

$$\psi^2 = \sqrt{\frac{2}{\gamma-1}\cdot\left(\frac{\gamma+1}{2}\right)^{\frac{\gamma+1}{\gamma-1}}\cdot\left(\frac{P_{or}}{P_{in}}\right)^{\frac{2}{\gamma}}\left(1-\left(\frac{P_{or}}{P_{in}}\right)^{\frac{\gamma-1}{\gamma}}\right)} \qquad \text{(I.7)}$$

Thus, for subsonic gas velocity, Eq. (I.4) becomes Eq. (I.8), and the mass flow rate can be calculated by the following expression:

$$m = \frac{\pi}{4}\cdot d^2\cdot C_D\cdot P_{in}\sqrt{\gamma\cdot\left(\frac{2}{\gamma-1}\right)\frac{M_{in}}{Z\cdot T_{in}\cdot R\cdot 10^3}\left[\left(\left(\frac{P_{or}}{P_{in}}\right)^{\frac{2}{\gamma}}-\left(\frac{P_{or}}{P_{in}}\right)^{\frac{\gamma+1}{\gamma}}\right)\right]} \qquad \text{(I.8)}$$

In the present study, the values of γ were obtained from the Aspen-Hysys 2006 ® software, under ambient conditions, Z was assumed to be the unity, and a value of C_D = 1 was used. This value is suggested when C_D is uncertain, maximizing in that way the calculated mass flow rate (m) (Arnaldos *et al.*, 1997; Montiel *et al.*, 1998).

APPENDIX II. DIMENSIONAL ANALYSIS

The dimensional analysis was carried out by applying the Buckingham's pi theorem, which states that a physically meaningful equation involving a certain number of *f* dimensional physical variables, involving *q* independent fundamental physical dimensions, can be expressed in terms of *j* dimensionless groups, obtained from the original variables and fulfilling the following expression: $j = f - q$.

The dimensional analysis of the jet flame length has been carried out by the following procedure.

Regarding the buoyancy-dominated jet regime, the dimensional physical variables considered in the present study are the jet exit velocity (*V)*, the pipe diameter *(d)*, the density at the outlet orifice (ρ_{or}), the acceleration of gravity (*g)*, the dynamic viscosity at the outlet orifice (μ) and the total jet flame length (*H*). These six physical variables were expressed in terms of three physical fundamental dimensions: length (*l*), mass (*M*) and time (*t*). Thus, using the Buckingham's theorem, the number of dimensionless groups was $6 - 3 = 3$.

Table II.1 shows the dimensional matrix, with the values of the physical variables as columns and those for physical dimensions as rows.

Table II.1. Dimensional matrix

	l	*M*	*t*
V	1	0	-1
d	1	0	0

ρ_{or}	-3	1	0
g	1	0	-2
μ	-1	1	-1
H	1	0	0

Then, it was necessary to choose variables to represent the dimensions, and hence V, d and ρ_{or} were selected as the recurring set. As a later stage, the dimensionless groups were obtained by the following procedure. The first dimensionless group was given by:

$$\pi_1 = g^a \cdot V^b \cdot d^c \cdot \rho_{or}^{\ d} \qquad \text{(II.1)}$$

Thus, the following system of equations was obtained:

$$[l]: \quad a + b + c - 3d = 0 \qquad \text{(II.2)}$$

$$[M]: \quad d = 0 \qquad \text{(II.3)}$$

$$[t]: \quad -2a - b = 0 \qquad \text{(II.4)}$$

Solving the system of equations and assuming a = -1, it was found that b = 2, c = -1 and d = 0. Then, substituting the dimensions in terms of variables, it was obtained that:

$$\pi_1 = g^{-1} \cdot V^2 \cdot d^{-1} \cdot \rho_{or}^{\ 0} = \frac{V^2}{g \cdot d} = Fr \qquad \text{(II.5)}$$

Thus, the first dimensionless group was found to be the orifice's Froude number (Fr).

As a second step, the following dimensionless group was given by:

$$\pi_2 = \mu^a \cdot V^b \cdot d^c \cdot \rho_{\text{or}}{}^d \qquad \text{(II.6)}$$

Thus, the system of equations obtained was:

[*l*]: - a + b + c - 3d = 0 (II.7)

[*M*]: a + d = 0 (II.8)

[*t*]: - a - b = 0 (II.9)

Solving the system of equations and assuming a = -1, it was found that b = 1, c = 1 and d = 1. Then, substituting the dimensions in terms of variables, it was obtained that:

$$\pi_2 = \mu^{-1} \cdot V^1 \cdot d^1 \cdot \rho_{or}{}^1 = \frac{V \cdot d \cdot \rho_{or}}{\mu} = Re \qquad \text{(II.10)}$$

Thus, it was found that the second dimensionless group was the orifice's Reynolds number (*Re*).

Then, the third dimensionless group was given by:

$$\pi_3 = H^a \cdot V^b \cdot d^c \cdot \rho_{or}{}^d \qquad \text{(II.11)}$$

Finally, the following system of equations was obtained:

[*l*]: a + b + c - 3d = 0 (II.12)

[*M*]: d = 0 (II.13)

[*t*]: - b = 0 (II.14)

Solving the system of equations and assuming a = 1, it was found that b = 0, c = -1 and d = 0. Then, substituting the dimensions in terms of variables, it was obtained that:

$$\pi_3 = H^1 \cdot V^0 \cdot d^{-1} \cdot \rho_{or}{}^0 = \frac{H}{d} \qquad \text{(II.15)}$$

Thus, the expression obtained for the jet flame length taking into account the gravity or buoyancy forces can be expressed by the following expression:

$$\frac{H}{d} = a \cdot \mathrm{Re}^b \cdot Fr^c \qquad \text{(II.16)}$$

As a later stage, the dimensional analysis for the total jet flame length (*H*) over the momentum-dominated jet regime has been carried out. It involves five of the six previously mentioned physical variables; these are the jet exit velocity (*V)*, the pipe diameter *(d)*, the density at the outlet orifice (ρ_{or}), the dynamic viscosity at the outlet orifice (μ) and the jet flame length (*H*). It can be seen that the acceleration of gravity (*g*) has not been included. These five physical variables were expressed in terms of the three fundamental physical dimensions: length (*l*), mass (*M*) and time (*t*). Thus, using the Buckingham's theorem, the number of dimensionless groups (*j*) was 5 – 3 = 2.

The dimensional matrix, with the values of the physical variables as columns and those for physical dimensions as rows is shown in Table II.2.

Table II.2. Dimensional matrix

	l	*M*	*t*
V	1	0	-1
d	1	0	0
ρ_{or}	-3	1	0

μ	-1	1	-1
H	1	0	0

Then, to obtain the dimensionless groups, three variables were selected to represent the dimensions; the recurring set involved V, d and ρ_{or}. The first dimensionless group was given by:

$$\pi_1 = \mu^a \cdot V^b \cdot d^c \cdot \rho_{or}{}^d \qquad \text{(II.17)}$$

Thus, the following system of equations was obtained:

[l]: - a + b + c - 3d = 0 (II.18)

[M]: a + d = 0 (II.19)

[t]: - a - b = 0 (II.20)

Solving the system of equations and assuming a = -1, it was found that b = 1, c = 1 and d = 1. Then, substituting the dimensions in terms of variables, it was obtained that:

$$\pi_1 = \mu^{-1} \cdot V^1 \cdot d^1 \cdot \rho_{or}{}^1 = \frac{V \cdot d \cdot \rho_{or}}{\mu} = Re \qquad \text{(II.21)}$$

Thus, the first dimensionless group was found to be the orifice's Reynolds number (*Re*).

As a second step, the following dimensionless group was given through:

$$\pi_2 = H^a \cdot V^b \cdot d^c \cdot \rho_{or}{}^d \qquad \text{(II.22)}$$

Thus, the following system of equations was obtained:

[*l*]: $a + b + c - 3d = 0$ (II.23)

[*M*]: $d = 0$ (II.24)

[*t*]: $- b = 0$ (II.25)

Solving the system of equations and assuming a = 1, it was found that b = 0, c = -1 and d = 0. Then, substituting the dimensions in terms of variables, it was obtained that:

$$\pi_2 = H^1 \cdot V^0 \cdot d^{-1} \cdot \rho_{or}{}^0 = \frac{H}{d} \quad \text{(II.26)}$$

Thus, the expression obtained for the jet flame length over the momentum-dominated regime can be expressed by the following expression:

$$\frac{H}{d} = a \cdot \mathrm{Re}^b \quad \text{(II.27)}$$

It should be noted that *H* involves the jet flame length considered as the distance from the base of the lifted jet flame to the flame tip (*L*), plus the lift-off distance (*S*), defined as the centerline distance from the gas release point to the base of the lifted jet flame. Thus, the dimensional physical variable for the flame length can also be expressed by *L* and *S*. Thus, by replacing, respectively, *H* for *L* and *S* in the same procedure, the dimensionless groups *L/d* and *S/d* are obtained.